Stand Alone PV Based Single Phase Power Generating Unit for Rural Household Application

Ritwik Chattopadhyay

(Roll No: 10307042)

Department of Electrical Engineering

Indian Institute of Technology

Mumbai-400076, Maharshtra, India.

July 2012

Stand Alone PV Based Single Phase Power Generating Unit for Rural Household Application

Master of Technology Dissertation

submitted in partial fulfillment of the requirements for degree of

Master of Technology

By

Ritwik Chattopadhyay

(Roll No: 10307042)

Under the guidance

of

Prof. Kishore Chatterjee

Department of Electrical Engineering

Indian Institute of Technology

Mumbai-400076, Maharshtra, India.

July 2012

Dissertation Approval

The dissertation entitled

Stand Alone PV Based Single Phase Power Generating Unit for Rural Household Application

by

Ritwik Chattopadhyay

(Roll no: 10307042)

is approved for the degree of

Master of Technology

_____

Examiner 1

_____

Examiner 2

_____

Project Guide

_____

Chairman

Date:_____

Place:_____

Declaration

I hereby declare that this written thesis work represents ideas of my own and in my own words and where others ideas or words have been included; I have adequately cited and referenced the original sources. I also declare that I have adhered to all principles of academic honesty and integrity and not misrepresented or fabricated or falsified any idea/data/facts/source in my submission. I understand that any violation of the above will cause for disciplinary action by the Institute and can also evoke penal action from the sources which have thus not been properly cited or from whom proper permission has not been taken when needed.

Date: _____ _____

(Signature)

_____

(Name of Student)

_____

(Roll Number)

Acknowledgement

I would like to express my sincere gratitude to my project guide, Prof. Kishore Chatterjee for providing me the opportunity to work on this really interesting project and for his generous guidance and support throughout the time. I would also like to thank NCPRE council members specially Prof. B.G. Fernandes for providing support and financial assistance.

I would like to thank all the faculty members from PEPS group of Electrical Engineering Department, IIT Bombay for their support, encouragement and the priceless knowledge they have been imparting to all the students.

I would also like to thank the PhD students, specially Mr. Sreeraj E.S., Mr. Ajit Ghodke, Mr. Vishal Vekhande, Mr. Dipankar Debnath and all other research scholars for helping me with their helpful and fruitful suggestions. I would also like to thank my batchmates specially Ankush Laddha, Vijay A.S. for their support, help and advices during implementation of hardware prototype.

I would also like to thank Mr. Khanderkar for his helpful advices during the problems faced in building up the hardware. I would also like to thanks all the RAs, Project Staffs, my colleagues and intern students who have been there in the lab.

Place:_____ Ritwik Chattopadhyay

Date: _____

Abstract

The aim of the thesis project is to implement a reliable, efficient and reduced stage PV based single phase power generating unit for household loads with a battery as an energy storage element. In this thesis work, a transformer coupled half-bridge boost converter together with a bidirectional converter and single phase VSI has been proposed for harnessing power from PV, storing and extracting energy from battery and for connecting to ac loads. A control scheme for the system has been proposed for controlling output voltage, inverter dc link voltage, MPPT of PV and battery charging/discharging current. The scheme has been validated by performing detailed simulation studies. A laboratory prototype has been built to validate the control scheme performed in simulation studies. For hardware implementation Agilent E4360 Solar Array Simulator is used as a pseudo PV source along with four 12 volt “Quanta” batteries as energy storage element. The control scheme and hardware operation has been performed using a TMS320F28335 DSP Experimenter Kit.

Contents

List of figures

Chapter 1
Introduction

PV systems meant for acting as a power supply require an auxiliary power source in form of battery, super capacitor, fuel cell, wind generator or maybe grid, if possible. Output power of PV modules vary widely with changes in solar irradiation and temperature. PV systems meant for small or low power applications generally exhibit relatively high power capacity at high level of irradiation and very low power capacity at low level of irradiation. So an economic designing of a PV based power generation system require an energy storage element in the form of battery. For rural household applications where power supply required throughout a varies widely with change in atmospheric conditions thereby choosing battery for energy storage scheme is an effective choice. Rural Household applications generally involve ac power driven appliances while output power of PV or battery is dc in nature. Hence, there is a need for efficient and reliable electrical power conversion system. Several research work has been carried out on this aspect of power electronic application. The scope of the project work involves integration, analysis, simulation and hardware implementation of such a reliable, efficient and reduced topology.

Past research endeavors on stand alone PV based applications possess many different configurations for integrating PV modules with battery and load. For designing a PV system with battery requires an effective battery charging and discharging control so as not to affect battery life and health. Battery life and health deteriorates if unregulated current is drawn from or supplied to the battery. For supplying power to ac loads, there is requirement for an inverter which must be fed with a 400V dc link to give 230V(rms) voltage at the output of inverter. A general block diagram of stand alone PV system is shown in Fig. 1.1. Previous works done on this area of application, exhibit large number of stages of power conversion or unregulated battery configuration. The work included in this thesis proposes a configuration using half-bridge boost inverter with bidirectional dc-dc converter and single phase inverter. Converter analysis of half bridge boost converter and bidirectional dc-dc converter is presented in chapter 2. Modeling of solar array of 36V along with PV and Battery sizing has been presented in chapter 3. Control

scheme employed for the proposed configuration is presented in chapter 4. Details of hardware prototype built, is presented in chapter 5. Detailed simulation and hardware results are presented in chapter 6.

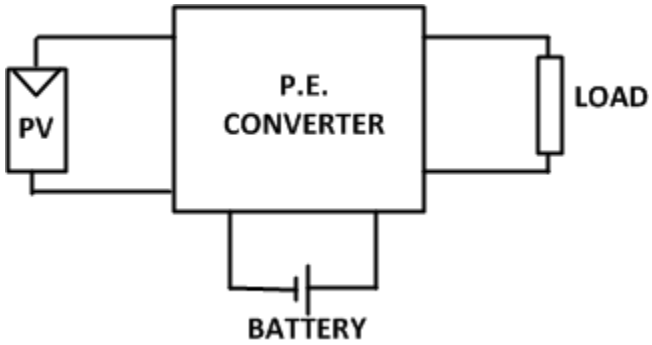

Fig. 1.1. Schematic Block Diagram of Stand Alone PV Based Systems

1.1 Existing Configurations for Stand Alone PV Systems

Stand Alone PV based units require to produce stable single phase dc supply. Conventional VSIs require a large dc link of 400V in order to give good performance. So, the challenges involved are mainly in the dc stage of the configuration to give 400V dc bus. Generally the PV modules are of lower voltage ratings(around 36V) and batteries have typical voltage ratings of 12V, 24V, 48V etc..

1.1.1. Four Stage Conversion System

In Fig. 1.2, the configuration from [1],[3] has four power stage converters with two DC links whose voltages are to be maintained for desirable outputs. This kind of configuration requires at least five controlled switches on the dc side. The input dc stage to inverter is generally having a high step up gain (transformer coupled) converter, due to limitation of voltage boosts of conventional boost converters. Generally transformer coupled boost converters have minimum two controlled switches. Hence at least two controlled switches are required to provide a high voltage dc link to the inverter. The bidirectional battery converter also requires two controlled switches for carrying a bidirectional current. The PV converter, which can be a conventional boost converter, requires one switch. Hence, total of 5 controlled switches are required for dc-dc conversion stage along with 4 switches for the inverter.

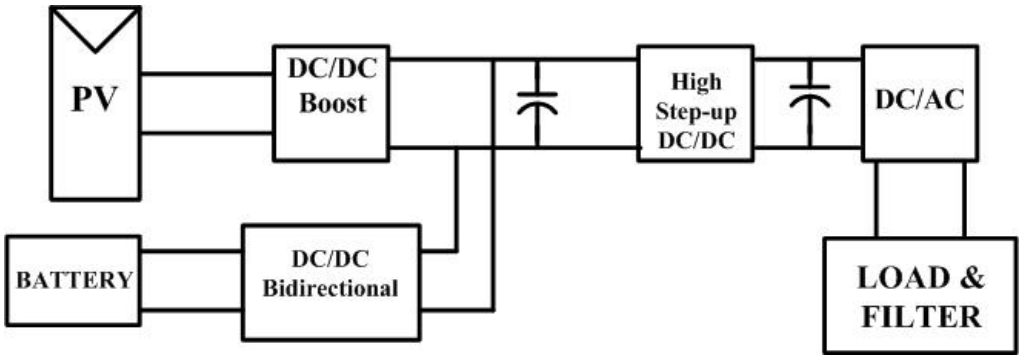

Fig. 1.2. Four Stage Configuration with Two Controlled DC Links

Fig. 1.3 shows a three port transformer based implementation. In this configuration, minimum six switches are required for transformer coupled converters in addition with four inverter switches. The power flow in this system is controlled by controlling the phase angle between the terminal voltages across the three windings of the transformer [4], [5]. This converter allows efficient operation of the system but increases the number of switches as controlling power flow using phase angle shift technique requires controlled switches connected to all the three high frequency converters.

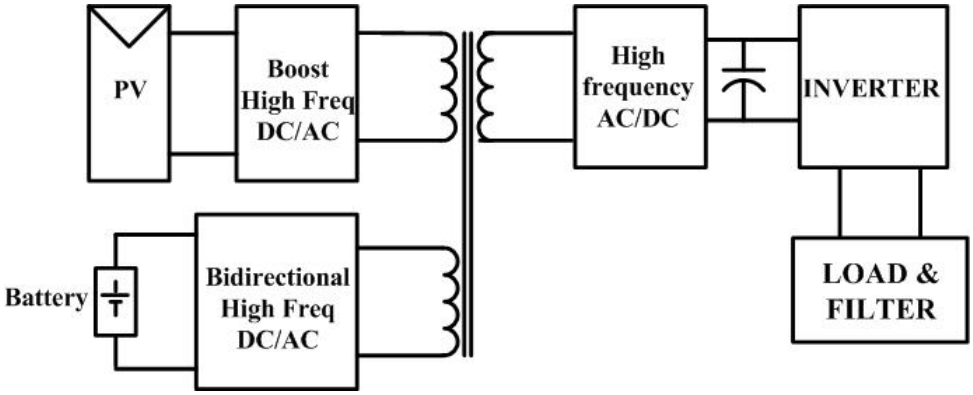

Fig. 1.3. Three-Port High Frequency Transformer with Four Converters

1.1.2. Three Stage Conversion System

The configuration shown in Fig. 1.4 requires a transformer coupled configuration for high step up gain which requires minimum three switches on the dc-dc stage along with four separate switches for the inverter, but this configuration has cascaded battery connection, which is not a preferable solution as for every change in load, the corresponding change in dc link voltage

would disturb the battery charging/discharging current. Frequent disturbances in battery charging/discharging current puts stresses on the battery and reduces battery life[1],[2].

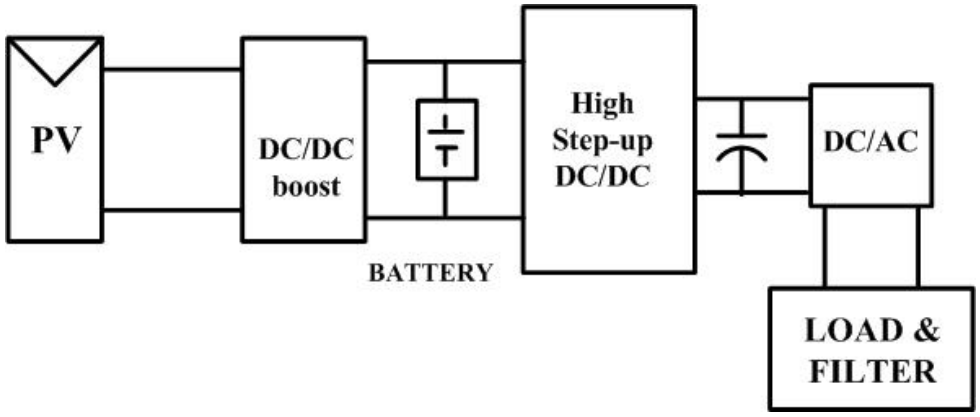

Fig. 1.4. Three Stage Configuration with Cascaded Battery

Fig. 1.5 depicts a three stage configuration, where two high step up transformer coupled dc-dc converters, are required to maintain the 400V dc link[1], [2], [3], [6]. In this case, both the high step up converters, mainly of transformer coupled configuration, requires the battery charger to be bidirectional. Bidirectional high step-up/step-down converters require minimum four controlled switches and high step-up converter for PV requires minimum two controlled switches. In total, it demands six switches for the DC stage along with four inverter switches.

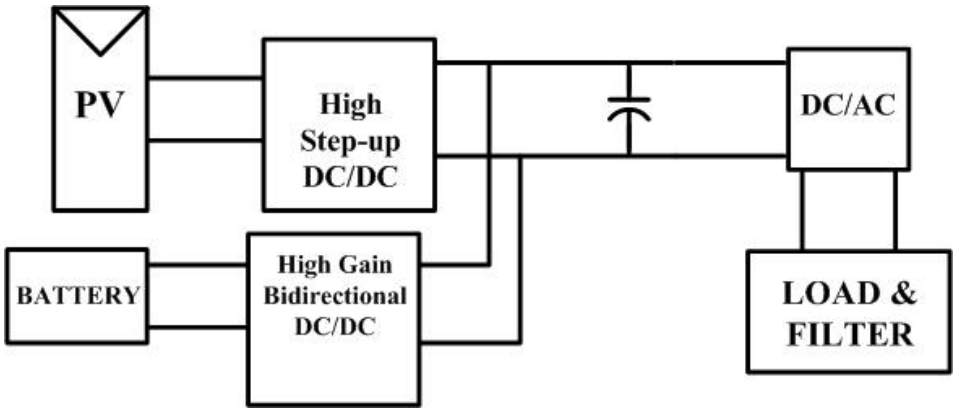

Fig. 1.5. Three Stage Configuration with Six Controlled Switches

1.1.3. Two Stage Conversion System

The configuration presented in Fig.1.6 shows a topology, which requires either PV array to consist of several series connected modules to sustain a high voltage over a wide operating range, together with a high gain bidirectional battery charger, or a boost inverter configuration on

the AC side with lower DC side voltage. Having a high series voltage over a wide operating range can lead to over-sizing of PV modules. The problem associated with boost inverter is that ground connection is not available at the output, so a coupling power transformer is required for providing a ground terminal on the load side [7].

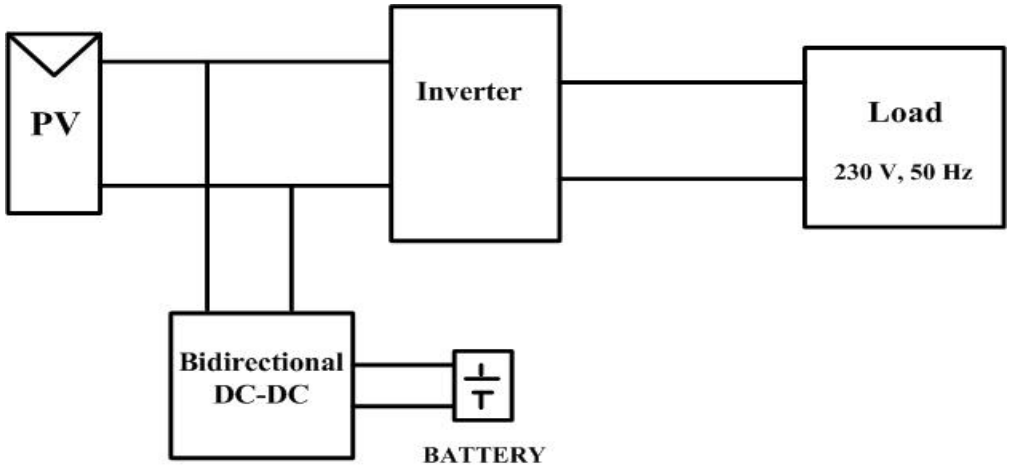

Fig. 1.6. Two Stage Configuration with High Boost Inverter or High PV Voltage

1.2. Summary

From the analysis of the above schematic configurations, it can be inferred that either higher number of converter stages and controlled switches are required for proper operation of a PV based system, or there is an unregulated battery performance with lower number of stages, or there is requirement for higher PV voltage or isolation transformer. Scope of this thesis work looks into bringing a trade-off between the number of controlled switches or converter stages and battery control performance,

Chapter 2

Proposed Converter Configuration

The work of the thesis proposes a converter configuration using a half bridge boost converter([8],[9]) along with a bidirectional buck-boost dc-dc converter for the dc power conversion stage and a single phase VSI for connecting to ac loads. The motivation behind the use of this converter is the high boost that can be obtained using the transformer coupled configuration. In addition, the half bridge boost converter has two dc links on both sides of the high frequency transformer. Controlling the voltage of one dc link ensures controlling the voltage of the other dc link, which makes the control strategy to be lesser complex. Moreover, additional converters can be integrated with any of the two the dc links. The proposed converter configuration is shown in Fig. 2.1. The work of this thesis includes integrating a bidirectional dc-dc boost converter with the primary side dc link. Using this converter configuration, high boost of PV voltage and battery current control can be realized using only four controllable switches.

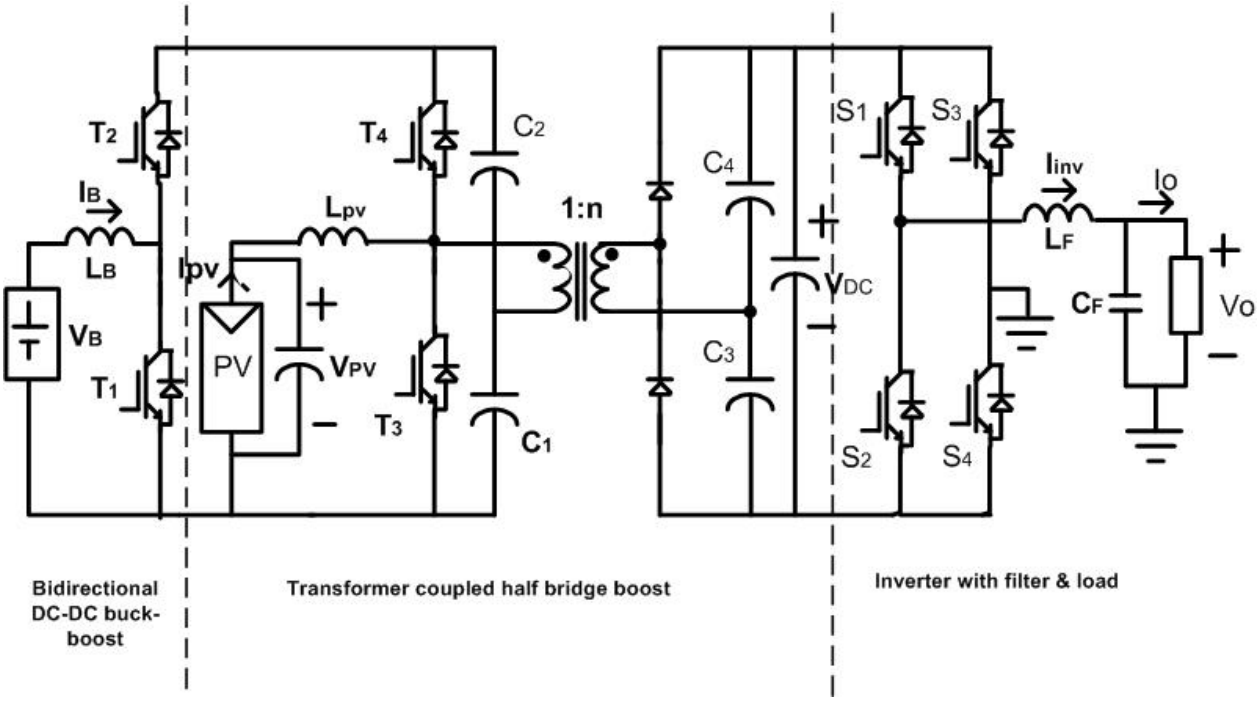

Fig. 2.1. Proposed Converter Configuration with Half-Bridge Boost Converter

2.1. Half Bridge Boost Converter

The power circuit diagram of half bridge boost converter is shown in Fig. 2.2. The switches S1 and S2 are operated in complimentary manner. When switch S1 is ON, the current through the source inductor increases. The bottom capacitor C1 discharges through the transformer primary and switch S1 as shown in Fig.3.3. In secondary side capacitor C3 is charged through transformer secondary and diode D1.

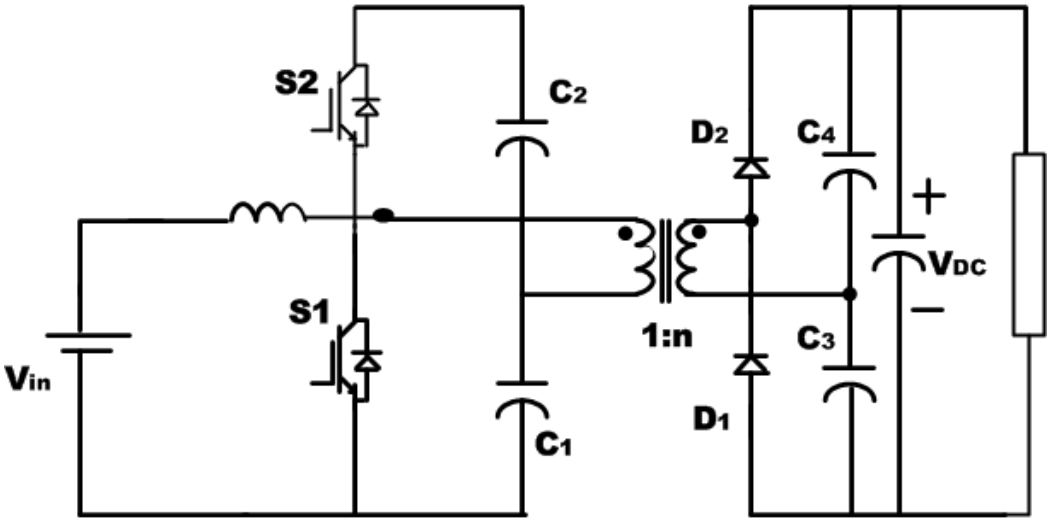

Fig. 2.2. Half-Bridge Boost Converter

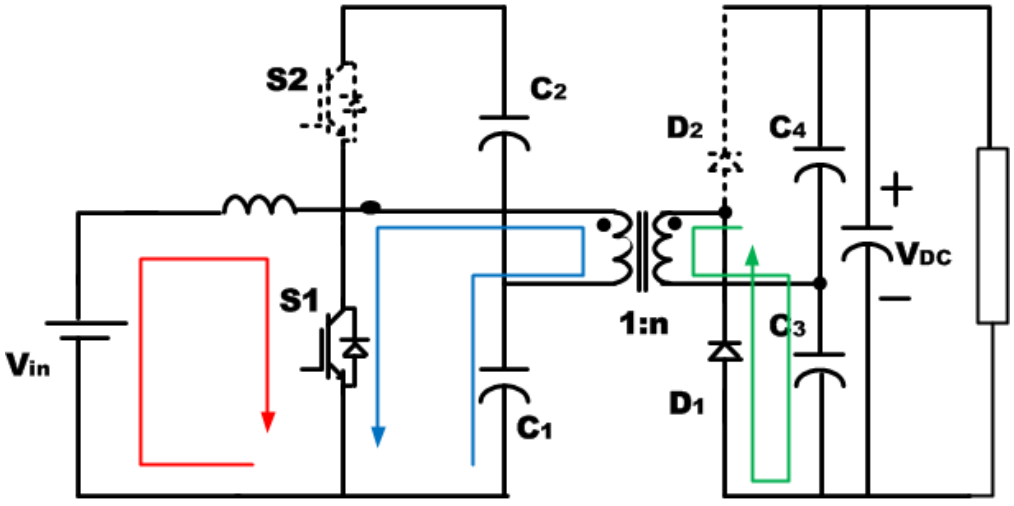

Fig. 2.3. Operation when Switch S1 is Turned ON

When switch S1 is OFF and S2 is turned ON, initially the inductor current flows through anti-parallel diode of switch S2 and through the capacitor bank for half of the ON-time of switch S2. During this interval, the current flowing through diode decreases and the current flowing through transformer primary increases. The path of the flow of current is shown in Fig. 2.4. As the current flowing through anti-parallel diode charges the capacitor bank, the reverse voltage across the diode increases and it turns OFF. Since, S2 is gated ON during this time, the capacitor C2 now discharges through switch S2 and transformer primary. During the ON gating pulse of switch S2, on the secondary side, diode D2 conducts to charge the capacitor C4. The path of current flow is shown in Fig 2.5.

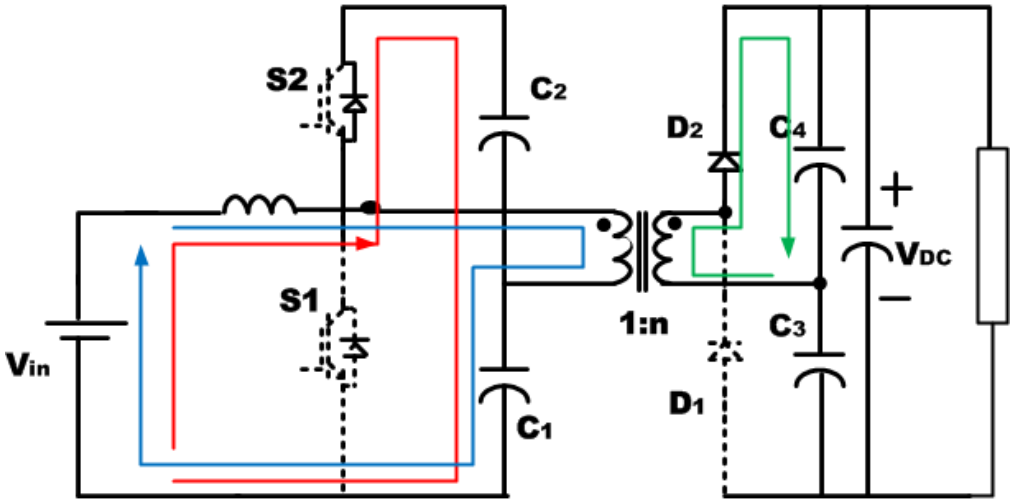

Fig. 2.4. Operation when Switch S2 is Turned ON, Charging the Capacitor Bank

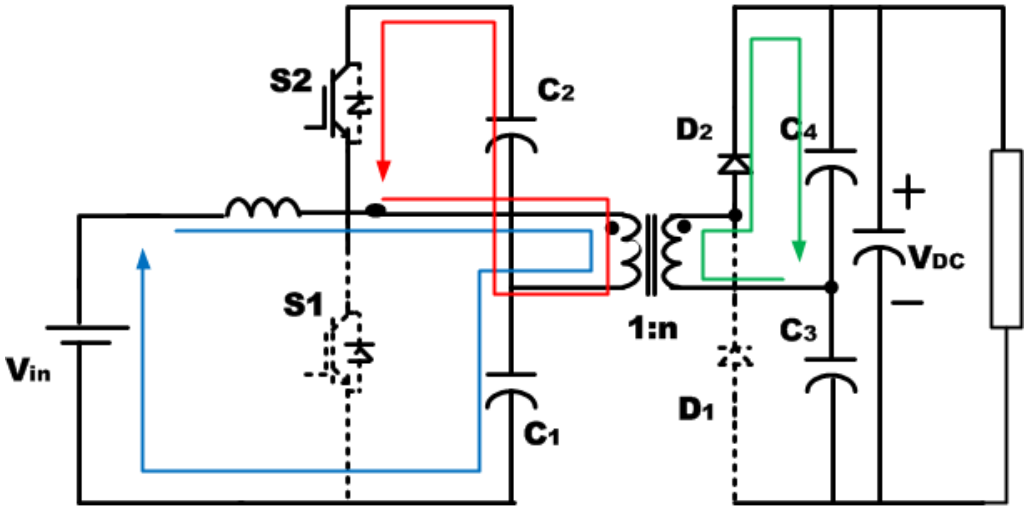

Fig. 2.5. Operation when Switch S2 is Turned ON, Capacitor C2 Discharging

The timing diagram for the operation of half bridge boost converter, as explained above is shown in Fig. 2.6. As can be observed from the plot of current through switch S2((e)I_top) in Fig. 2.6, during the time when S2 is gated ON, the inductor current initially flows through the anti-parallel diode to charge the capacitor bank and then after the diode is reverse biased, the capacitor C2 discharges through switch S2 and transformer primary.

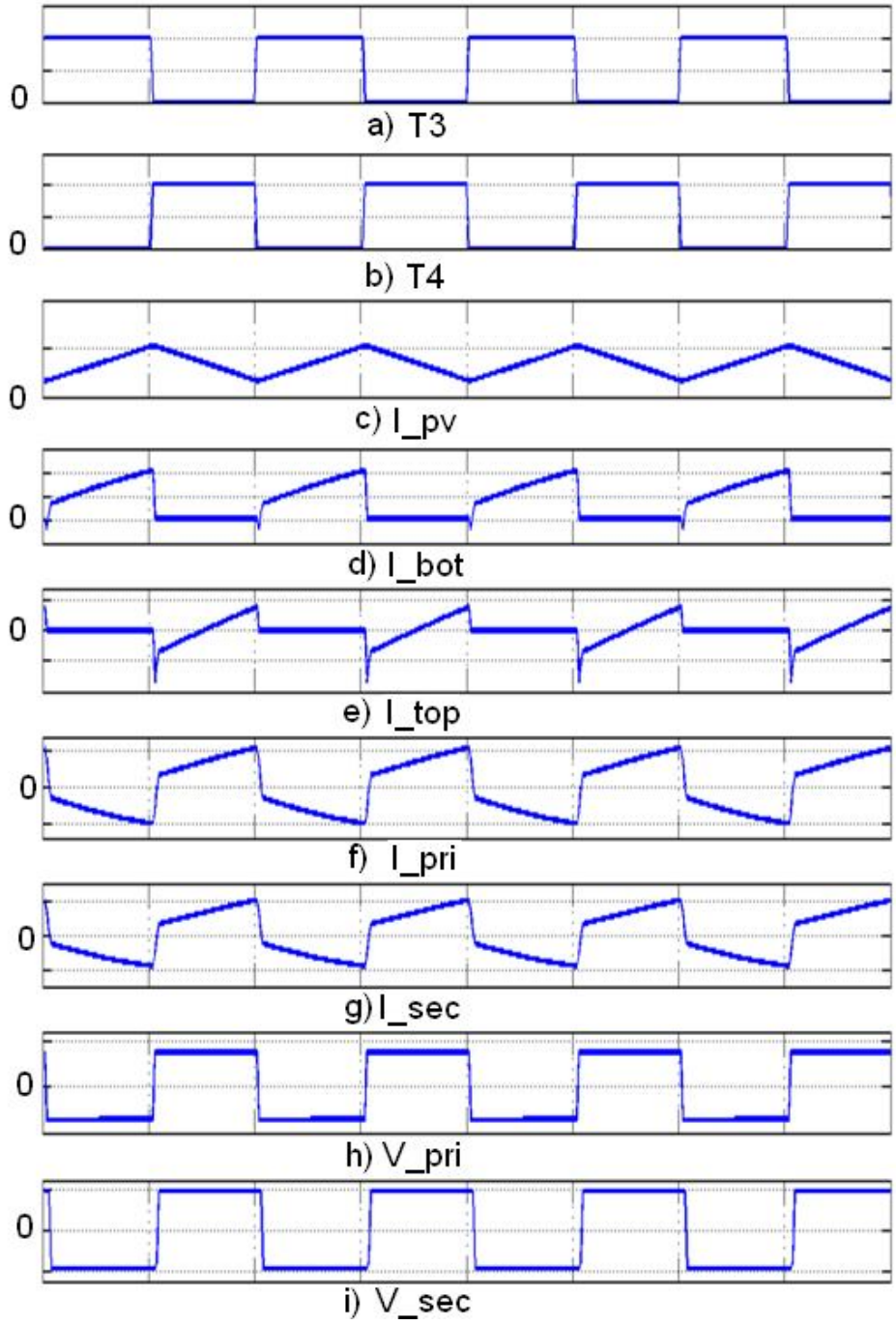

Fig. 2.6. Timing Diagram of Operation of Half-Bridge Boost Converter

When S1 ON, the primary voltage $V_P = -V_{C1}$. The secondary voltage $V_S = nV_p = -nV_{C1} = -V_{C3}$, or $V_{C3} = nV_{C1}$, for $0 < t < DT$, where D = duty cycle of switch S1; T = time period of switching. For S1 ON, voltage across primary inductor $L = V_{in}$.

When S1 is turned OFF and S2 turned ON, the inductor current first flows through the anti-parallel diode of S2 to charge the capacitor bank. As capacitor voltage rises, the anti-parallel diode across S2 becomes reverse biased and the capacitor C2 discharges through switch S2 and transformer primary. During this time, the primary voltage $V_p = V_{c2}$. Secondary voltage $V_s = nV_p = nV_{c2} = V_{C4}$, for $DT < t < T$. For S2 ON, voltage across primary inductor $L = V_{in} - (V_{C1} + V_{C2})$. Now for a switching cycle, the total volt-second across primary inductor should be zero, hence we get $(V_{C1} + V_{C2}) = \frac{Vin}{(1-D)}$; the capacitor voltages are considered constant under steady state, $V_{C3} = nV_{C1}$, $V_{C4} = nV_{C2}$. Hence the output voltage is given by $V_O = V_{C3} + V_{C4} = n\frac{Vin}{(1-D)}$. Hence the output voltage of the secondary side DC link is function of the duty cycle of the primary side converter and turns ratio of transformer.

2.2. Bidirectional DC-DC Buck-Boost Converter with Half Bridge Boost Converter

In the proposed configuration as shown in Fig. 2.1, a bidirectional buck-boost dc-dc converter is used for battery charging/discharging control. The schematic of the configuration is shown in Fig. 2.7.

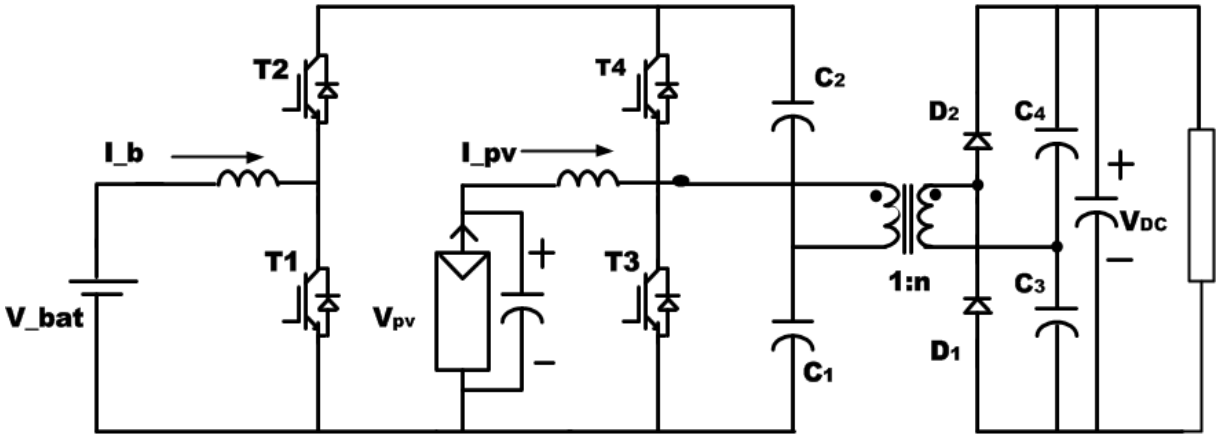

Fig. 2.7. Half-Bridge Boost Converter with Bidirectional DC-DC Buck-Boost Converter

In this configuration, the bidirectional converter is operated with band gap current control mode to limit the ripple band width of battery. The current I_b can be positive(discharging) as well as negative(charging). During discharging, the bidirectional converter charges the capacitor bank C2-C1. The half bridge boost converter operates in a slightly different manner from the way explained in section 2.1. Considering Fig. 2.7, during the ON time of T3, I_pv increases and capacitor C1 discharges through switch S1, same as that explained in section 2.1. However, during the ON time of S2, the duration of current flowing through anti-parallel diode of the inverter is lesser. This is pertained to the fact that as the bidirectional converter is already charging the capacitor bank C2-C1, so the capacitor bank voltage becomes high faster and the diode is reverse biased quickly. Since S2 is gated ON already, the capacitor C2 discharges the dumped energy on it through the switch S2 and transformer primary winding. The time duration of flow of current through collector-emitter of S2 is higher than time duration of current flowing through anti-parallel diode of S2. This can be verified from the plot of (e)I_top in timing diagram shown in Fig. 2.8.

During charging, the bidirectional converter maintains a negative battery current. During battery charging mode, the half bridge boost converter dumps additional energy on the capacitor bank C2-C1 and the battery converter takes the dumped energy from the capacitor bank. During the ON time of T3, I_pv increases and capacitor C1 discharges through switch S1. However, during the ON time of S2, the duration of current flowing through anti-parallel diode of the inverter is higher in this case. Since the bidirectional converter is discharging the capacitor bank C2-C1, so the capacitor bank voltage becomes lower and the diode is forward biased for higher duration. The capacitor bank is charged as long as the anti-parallel diode is forward biased. Once the diode becomes reverse biased, the excess energy dumped on capacitor bank flows through the collector-emitter of switch S2 and transformer primary winding. The time duration of flow of current through collector-emitter of S2 is lesser than time duration of current flowing through anti-parallel diode of S2. This can be verified from the plot of (e)I_top in timing diagram shown in Fig. 2.9.

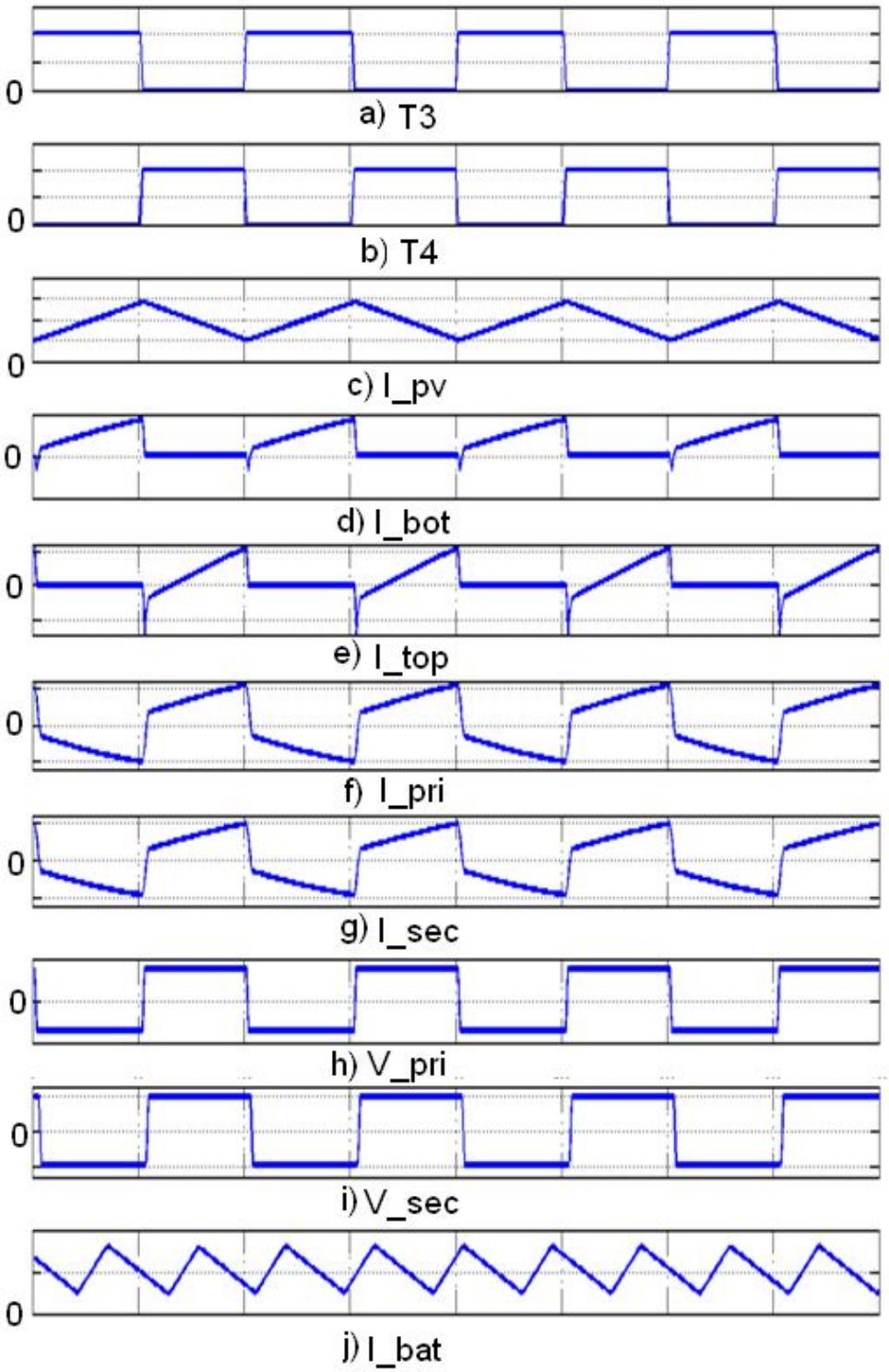

Fig. 2.8. Timing Diagram of Half-Bridge Boost Converter while Battery is discharging

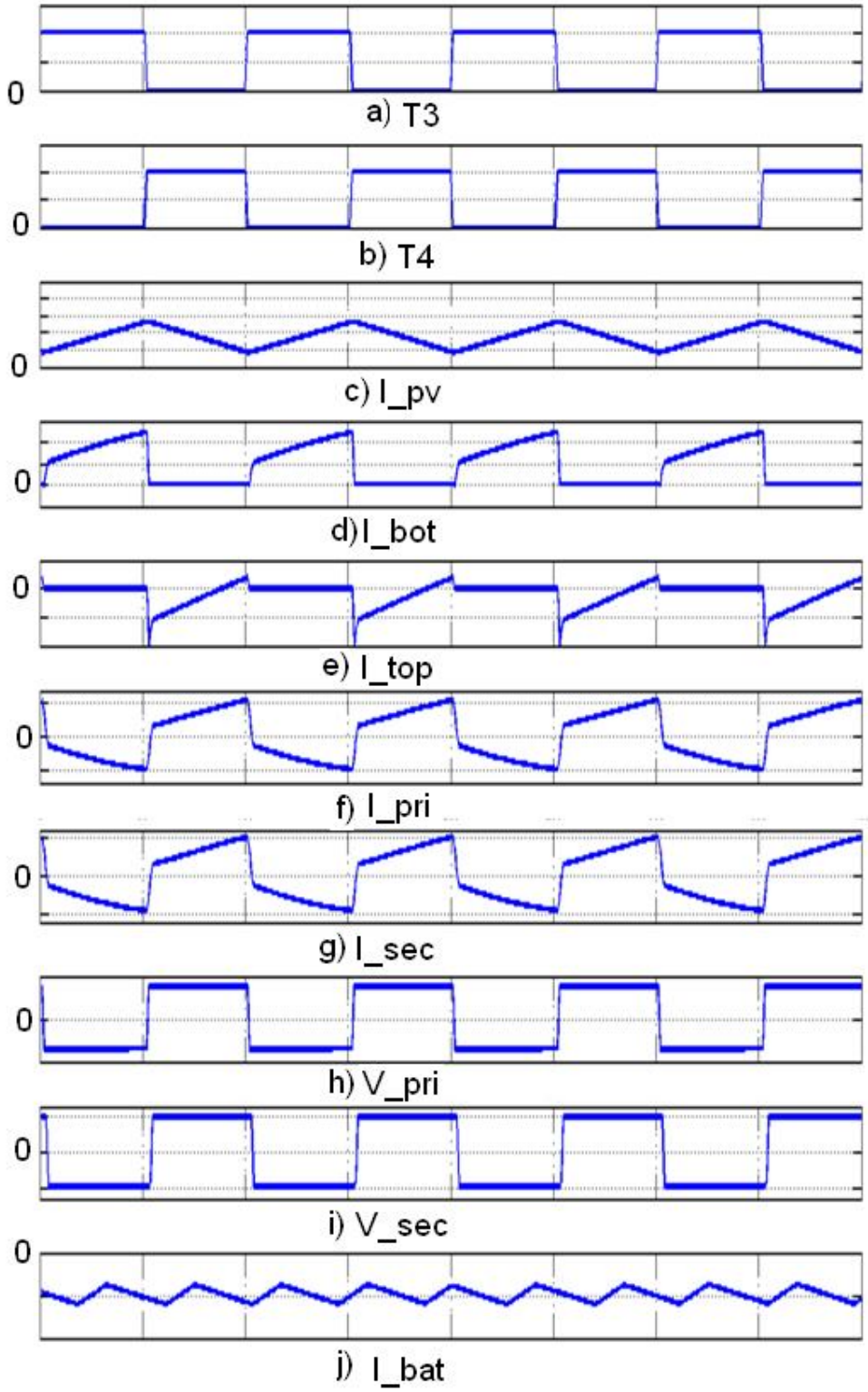

Fig. 2.9. Timing Diagram of Half-Bridge Boost Converter while Battery is charging

For the symbols used in Fig. 2.8 and 2.9,

T3 = switching pulse of bottom switch(T3)

T4 = switching pulse of top switch(T4)

I_pv = Current through the inductor connected to PV

I_bot = Current through the bottom switch T3

I_top = Current through the upper switch T4

I_pri = Current through the transformer primary

I_sec = Current through the transformer secondary

V_pri = Voltage across the transformer primary

V_sec = Voltage across the transformer secondary

I_bat = Current flowing out of the battery

2.3. Operation of the proposed configuration

The proposed configuration as shown in Fig. 2.10, has three converters and total 8 control switches and it has controllable converters for battery, PV and load.

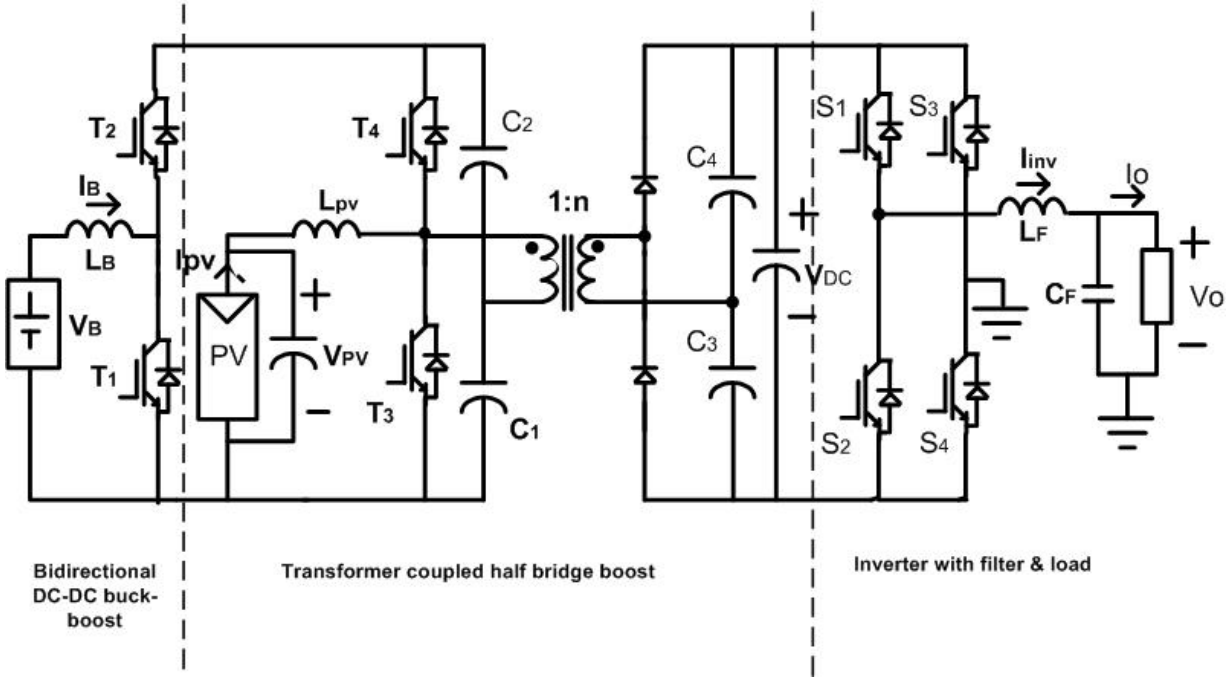

Fig. 2.10. Proposed Converter Configuration using Half-Bridge Boost Converter, Bidirectional Converter and Single Phase VSI.

Here the PV converter(half bridge boost converter) is operated under constant PWM switching scheme. The battery converter(bidirectional dc-dc buck-boost converter) is operated under band-gap control scheme to limit the current ripple of the battery current. The single phase VSI is operated under Sine-PWM technique with constant carrier frequency. The single phase VSI needs a 400V dc link for suitable operation for connecting to ac loads of 230V, 50 Hz rating. The dc link voltage V_{DC}, is 'n' times of primary side dc link voltage. However, the primary side dc link voltage can be controlled by half bridge boost converter or by bidirectional converter. The dc link voltage can be expressed as follows

$$V_{DC} = \frac{nV_{PV}}{(1 - D_{PV})} = \frac{nV_B}{(1 - D_B)}$$

where 'n' is the transformer turns ratio, V_B and V_{PV} are the battery and PV voltages respectively while D_B and D_{PV} are the duty cycle of the switches T1 and T3 in Fig. 2.10.

Chapter 3

Modelling and Sizing of PV Array and Battery

3.1 Mathematical Model of PV Module

In order to design a PV system it is necessary to select a PV module with high power capacity at MPP. For this thesis work, 36V, 280Wp solar module of BPSolar[17] has been selected. For simulation purpose, a mathematical model of solar module has been created. The mathematical model of the solar array has been built from the solar cell characteristics as depicted in [10],[11].The modeling of 36V, 280Wp solar array is given below

q = charge of an electron = 1.6×10^{-19} Coulomb

k = Boltzmann's Constant = 1.38×10^{-23} J/K

T_{aC} = ambient temperature = 25^{o}C

T_{aK} = operating temperature in K = 273 + T_{aC}

A = 1(ideality factor)

n = 1.2(diode quality factor)

T1 = standard operating temperature = 25^{o}C

T2 = maximum operating temperature = 75^{o}C

V_{oc_T1} = open circuit cell voltage at T1 = 44 V

I_{sc_T1} = short circuit current at T1 = 8.46 A

I_{sc_T2} = short circuit current at T2 = 8.70 A

S = solar radiation in kW/m^2

I_{ph} = photo generated current

I_s = cell saturation dark current

E_g = Band gap energy of an electron

The equivalent circuit of a PV array or module is shown in Fig 2.1.

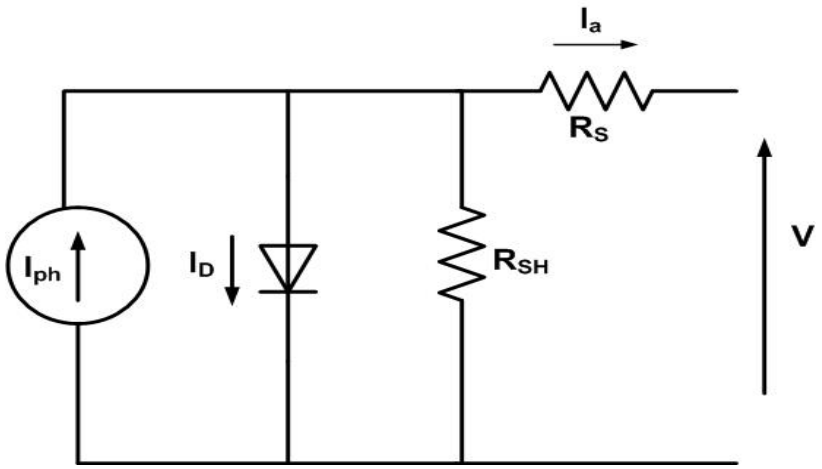

Fig. 3.1. Equivalent Circuit of a Solar Cell

V and I_a are the terminal voltage and current coming out of a solar module. The relation between V and I_a are expressed as follows

$I_a = I_{ph} - I_D - ((V + IR_s)/R_{sh})$ where I_D is expressed as $I_D = I_s[\exp(\frac{q(V+IR_s)}{nkA}) - 1]$;

I_{ph} is given by $I_{ph} = I_{ph\_T1} + K_i(T_{ak} - T_i)$ where $I_{ph\_T1} = I_{sc\_T1} * S$;

K_i is expressed as $K_i = (I_{sc\_T2} - I_{sc\_T1})/(T2 - T1)$;

I_s is expressed as

$$I_s = I_{s\_T1}\left(\frac{T_{ak}}{T1}\right)^{\frac{3}{n}} \exp\left(\left(q.\frac{E_g}{kA}\right)\left(\left(\frac{1}{T_{ak}}\right) - \left(\frac{1}{T1}\right)\right)\right)$$

I_{s_T1} is expressed as $I_{s\_T1} = I_{sc\_T1}/(\exp(qV_{oc\_T1}/(nkT1)) - 1)$

R_{SH} = shunt equivalent resistance = ∞

R_S = series equivalent resistance

$$= -\frac{dV}{dI_a}(\text{at } V = V_{oc}) - \frac{1}{X_v}$$

where X_v is expressed as

$$X_v = \frac{q\, I_{s\_T1}}{nkT1} \exp\left(q\frac{V_{oc\_T1}}{nkT1}\right)$$

The V-I and P-V characteristics of the modeled solar array at various values of solar insolation are shown in Fig 3.2 and 3.3, where $V_{pv} = V$ and $I_{pv} = I_a$.

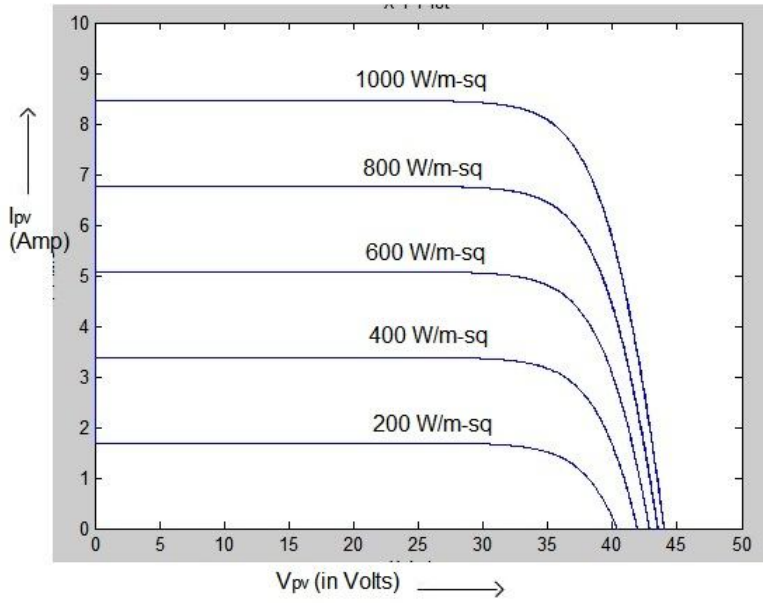

Fig. 3.2. I-V Characteristic of the Modeled Solar Module

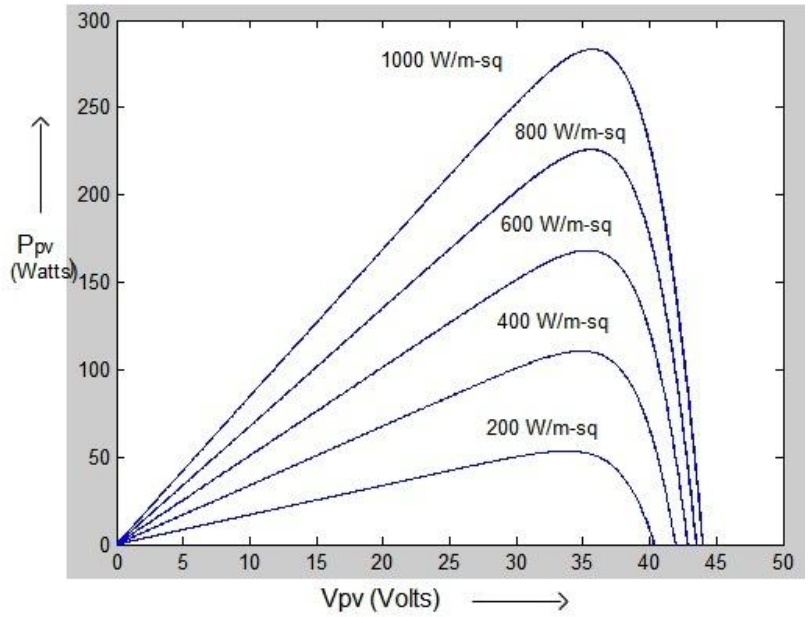

Fig. 3.3. P-V Characteristic of the Modeled Solar Module

3.2 Load Characteristics and PV Output Power Variation

In order to obtain an economic design of the system, a typical pattern of rural household load characteristics has been derived from the load characteristics presented in [10] for determining the PV and Battery sizing. In rural households, the load requirement is higher during night than during day time when the solar radiation is high. So optimum sizing necessitates the

energy discharged by the battery over a whole day should be returned to the battery by the PV modules during the daytime.

A typical load characteristic from [10] has been referred as a baseline for determining the load characteristics. The load characteristic explained in [10] has a maximum load of 3.8 kVA. For this PV power generating unit, the maximum load demand has been specified as 500 VA, hence an approximated scaled down version of the characteristic has been taken as shown in Fig. 3.4.

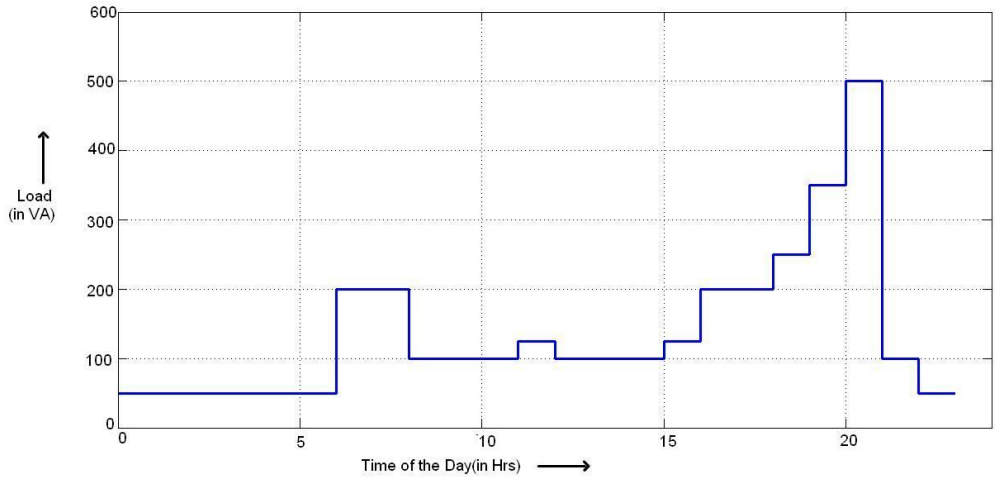

.

Fig. 3.4. Average Load Characteristics of a Day over 24 Hrs

While determining PV sizing, the worst month of the year having the lowest solar radiation needs to be considered. From [11], the solar radiation data over Mumbai for the month of August has been found to be lowest for the year. The variation of peak power variation over a day for 36V (mpp), 280Wp module from [17], for lowest radiation is shown in Fig. 3.5.

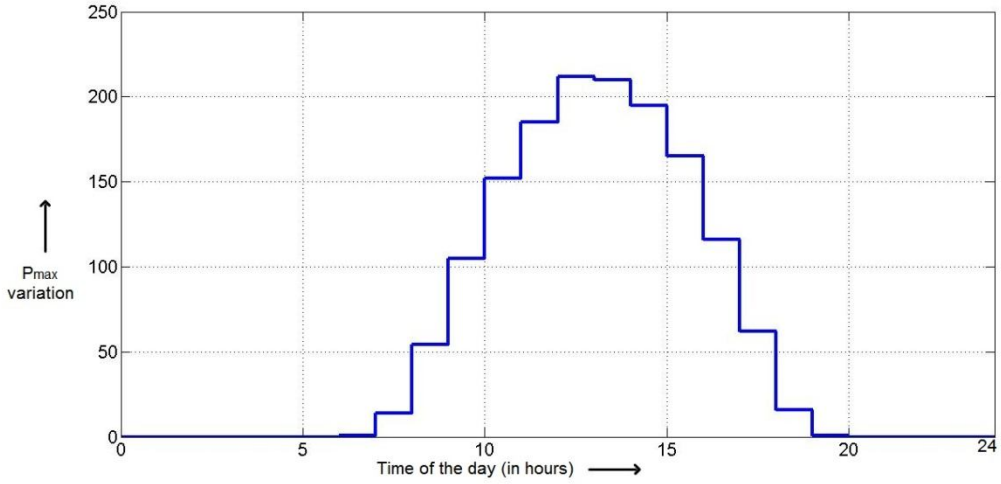

Fig. 3.5. Peak Power Variation of Solar Module over 24 Hrs

3.3. Determination of Number of PV modules

While determining the number of PV modules to be used, the total energy supplied by the PV modules over the day, should be sufficient enough to charge the battery for each day requirement. Let K be the number of PV modules required. The electrical circuit loss is considered to be 15% of the output power. The battery efficiency is considered to be 90%.

The following equation is used to determine the no of PV modules, considering all the losses in circuit and battery.

$$\int (KP_{pv} - P_{out} - P_{cir\_loss} - P_{b\_loss})dt = \int \Delta Q_b dt$$

K = number of PV modules

P_{out} = output power

$P_{cir\_loss} = 0.15 \times P_{out}$

$P_{b\_loss} = |(KP_{pv} - P_{out} - P_{cir\_loss})| \times 0.1$

ΔQ_b = correspond to change in battery energy level or SOC

The above integral over a 24 hr period must equate out to zero or greater for proper charging of the battery. By solving the above equation over the 24 hr variation of load and solar radiation as shown in Fig. 3.4. and Fig. 3.5, value of K=4 satisfies for $\int \Delta Q_b dt > 0$. Hence the

optimum value of K is equal to 4. The function $\int \Delta Q_b dt$ is plotted over a 24 hr scale as shown in Fig. 4.3.

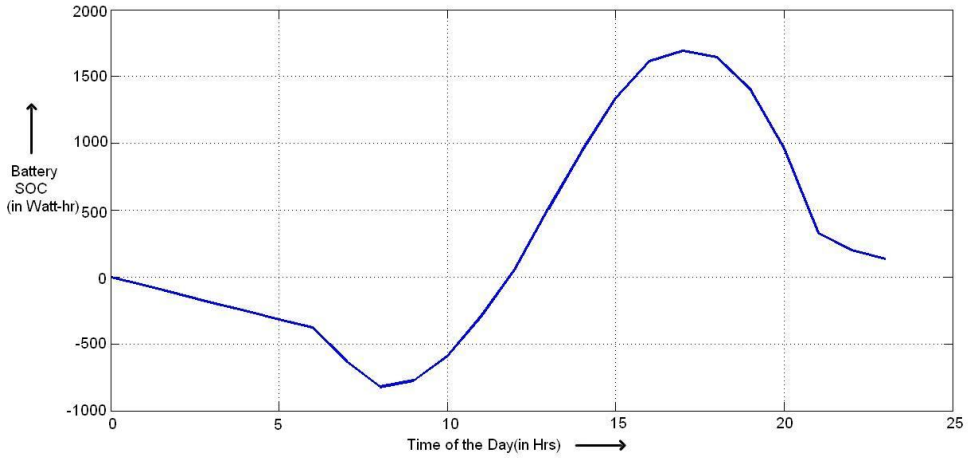

Fig. 3.6. Plot of Change in SOC(in Whr) Level of the Battery over 24 Hrs.

As evident from the plot of $\int \Delta Q_b dt$, there is a surplus of 75 Watt-hr of energy for the PV system designed. Hence the choice of K = 4, provides the optimum PV capacity to supply the Watt-hr requirement of the battery for a single day.

3.4. Determination of the Size of Battery

Stand alone PV based systems often require the battery capacity to sustain for extra few hours without solar radiation. To select an optimum size of battery an additional 6 hours of back up for the battery has been considered. Having lower battery voltage leads to higher current rating or higher Amp-hr rating. In the present case it is needed that the PV voltage and battery voltage be kept close to each other as they are connected to the same dc-link capacitor bank through boost converters (Fig.2.10). The battery nominal voltage is chosen to be 48 Volt. Considering 4 PV modules of 36V (mpp), 280Wp and the load characteristic as depicted in Fig. 10, the battery discharge requirement is 2500 Watt-hr(daily) and having 6 hours of backup(around 700 Watt-hr). The Amp-Hr discharge requirement is given as follows

Amp-Hr discharge requirement =

$$\frac{(\text{discharge requirement in Whr})}{(\text{nominal voltage of battery} = 48\text{V})}$$

The Amp-hr requirement comes out to be 67 Amp-hr. The regular Lead-Acid Batteries can be discharged till 50% of SOC. Hence using a regular battery, the Amp-hr requirement of the battery is (67/0.5) = 134 Amp-hr. The efficiency of the battery is considered to be 90%, which gives Amp-hr rating of 148 Amp-hr. For convenience, we can choose a battery of 150 Amp-hr rating.

Chapter 4

Control Schemes for PV, Battery and Inverter

4.1. DC Side Control for PV and Battery

In PV based power generation with battery as an energy storage element, it is required to supply the load demand by controlling the power sharing between PV and Battery. To extract maximum power from PV, PV must be operated at Maximum Power Point and the battery is to be controlled to supply extra load demand if needed, or get charged if the load requirement is less than that supplied by PV. Battery charging/discharging requires the battery to be charged or discharged in a way that the battery current is within its permissible limit. Efficient battery operation requires the battery to be charged with a constant current with a very small amount of ripple(2%). Hence hysteresis current control is employed for the battery. However, PV can be controlled using PWM control.

The dc link voltage can be controlled either by the battery or by the PV(chapter 2). The PV and Battery should control the power sharing between them in such a way that the load demand is met by controlling the dc link voltage V_{dc}, and by controlling the battery current. Moreover, during charging, battery current should not exceed its maximum limits specified by SOC controller. The PV and Battery can be operated in two ways, MPPT mode of operation and Non-MPPT mode of operation. In MPPT mode of operation, PV is controlled to deliver maximum power while the battery charges/discharges to control the DC link voltage, while in Non-MPPT mode of operation, PV charges the battery with a constant load current and maintains the DC-link voltage.

4.1.1. MPPT Mode of Operation

In MPPT mode of operation, the load demand is met by the power delivered by the PV and battery, as expressed in the following equation

$$P\_pv + P\_bat = P\_load$$

where P_pv = Power supplied by PV at MPP

P_bat = Power supplied(+ve) or taken (-ve) by battery

P_load = Power taken by load

In this mode, P_bat is –ve when power delivered by PV is higher than that required by the load. The battery takes a charging current in this mode, provided that the battery current doesn't exceed its reference value specified by SOC controller. P_bat is +ve when battery is discharging to meet the load demand. During very low radiation or night time, battery supplies the entire load demand. The control scheme for MPPT mode is depicted in Fig. 4.1.

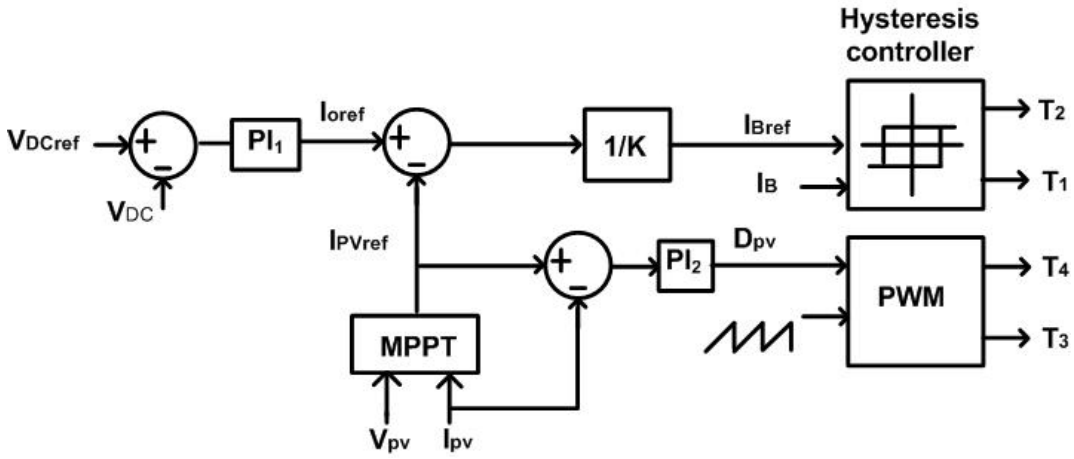

Fig. 4.1. Block Diagram for MPPT Control Mode Operation

Here, $I_{Bref} = (I_{Oref} - I_{PVref})/K$;where K=1.2.

I_{oref} indicates the load component of current reflected to PV. The value K indicates the ratio of battery voltage and PV voltage to reflect the battery current on the PV side. Here PV current follows the reference from MPPT controller and battery current follows the reference from the difference of I_{Oref} and $I_{PVref.}$. The battery is given the responsibility to maintain the dc link voltage V_{DC} for any change in load demand. The system operates in MPPT mode, as long as battery current I_B is less than the maximum value specified by SOC of the battery. In this scheme if load demand increases, a change in I_{Oref} takes place which prompts the I_{Bref} to adjust to a new value depending upon I_{PVref}, specified by the MPPT controller.

4.1.2. Non-MPPT Mode of Operation

In Non-MPPT mode also the relation P_pv + P_bat = P_load follows where P_bat is negative and the battery charging current is maintained at its reference value. PV is having excess power in this case if operated at Maximum Power Point, hence PV is operated at some other operating point(on the decreasing slope of P vs V characteristic) to supply the load demand and charge the battery with full charging current. The control scheme for Non-MPPT mode is given as Fig. 4.2.

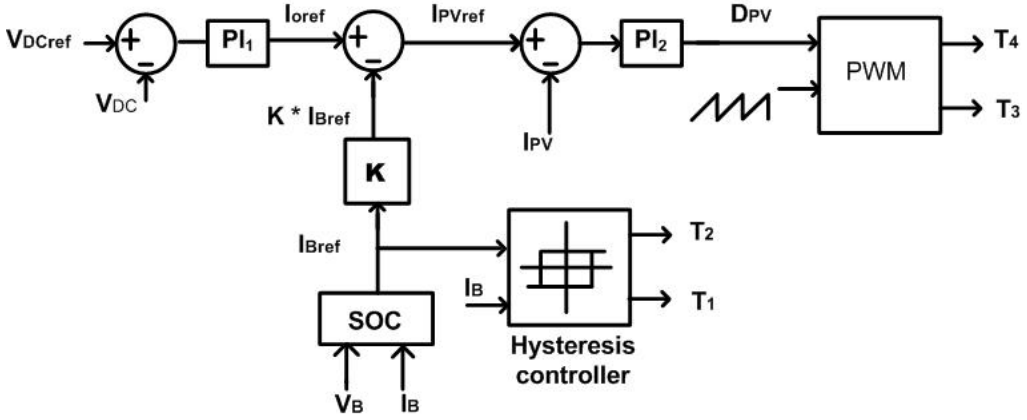

Fig. 4.2. Block diagram for Non-MPPT Control Mode Operation

Here, $I_{PVref} = I_{Oref} - K \times I_{Bref}$, where K=1.2. In this mode Battery current follows the reference from SOC controller and PV maintains the V_{DC} by following the current reference from the difference of I_{Oref} and $K \times I_{Bref.}$. Any small change in load demand is handled by PV in this mode. The system operates in the Non-MPPT mode, as long as the operating point doesn't cross the Maximum operating point ($\frac{di}{dv} < 0$) or V_{DC} doesn't fall below some specific value(360V). The check in V_{DC} is provided to give the battery a faster control. Any drastic change in load will cause V_{DC} to fall below 380, the controller will shift from Non-MPPT mode to MPPT mode giving the battery the responsibility to maintain V_{DC}.

4.1.3. Transition between MPPT and Non-MPPT Mode of Operation

Efficient operation of the system requires the two conditions for MPPT mode and Non-MPPT mode, to be checked consistently and shift the operating mode from one to the other and disabling the other mode. This is achieved by generating two control signals M1 and M2(complimentary to each other) as shown in Fig. 4.3.

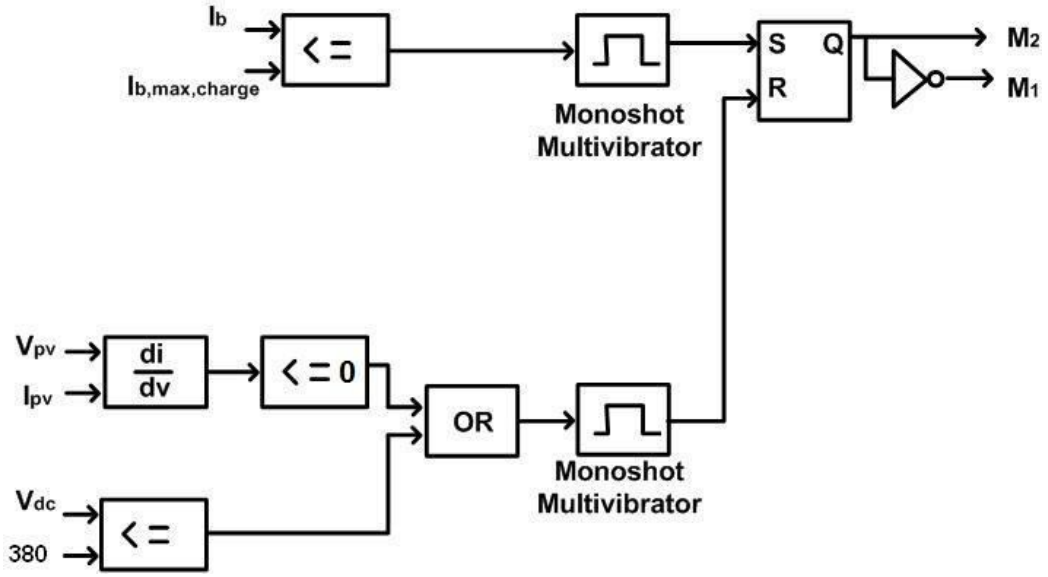

Fig. 4.3. Generation of Signals M1, M2 for Control Mode Changes

Using these two signals the controller shifts from one mode of control to another mode as depicted in Fig. 4.4. The two complementary signals decide which mode to be selected by the controller. For M1=1, M2=0, the controller operates the PV in MPPT mode and battery is given the responsibility to maintain the dc link. If load reduces or solar radiation increases, I_B hits I_{Bmax} from SOC, and M2 is set to 1, M1 is set to 0. The controller then operates the battery in constant current mode as specified by I_{Bmax} and gives PV the responsibility to maintain V_{DC}. The switching actions for PV and battery controlled by hysteresis current controller and constant frequency PWM is shown in Fig. 4.5.

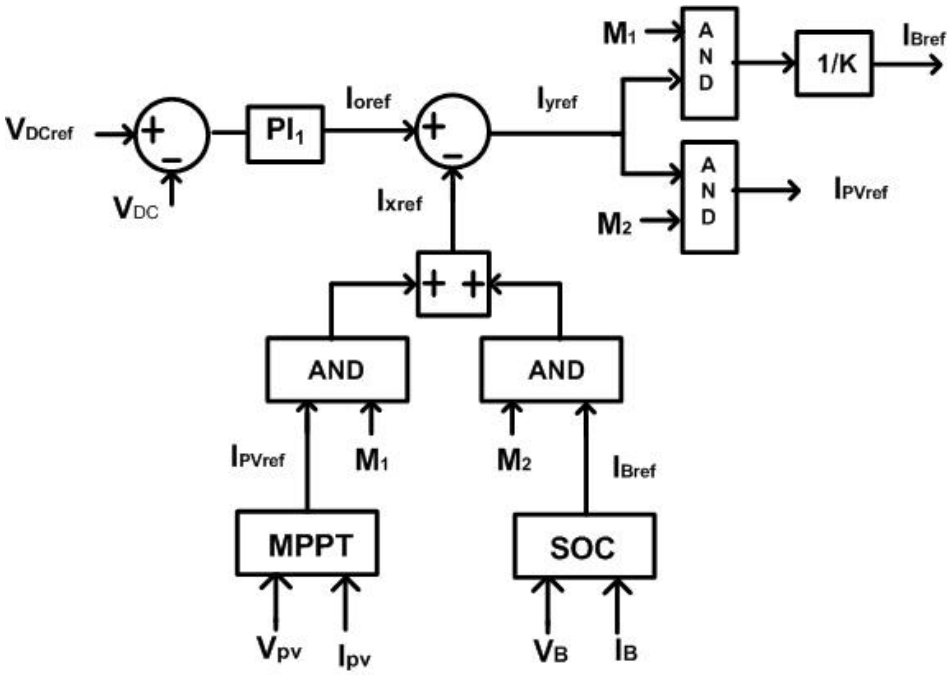

Fig. 4.4. Full Control Scheme for Operating in the MPPT and Non-MPPT Modes

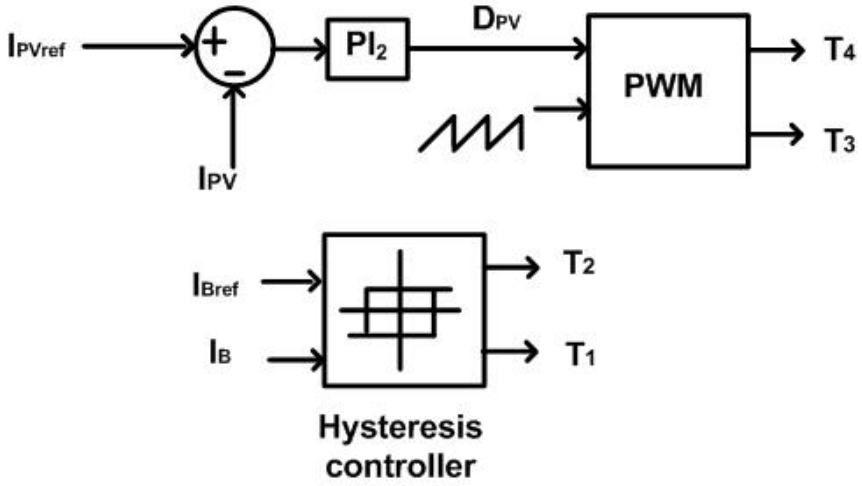

Fig. 4.5. Controlled Switching of Switches T1,T2 and T3,T4.

4.2. AC side control for Single Phase VSI

Stand alone systems for AC loads require fast output voltage control. A D-Q reference frame approach[14] has been used for controlling output voltage of the single phase inverter. D-Q reference frame approach is utilized here by using the output voltage reference as the rotating α component and taking zero as reference for rotating β component. The α-β components are transformed into d-q components on synchronously rotating D-Q reference frame.

$V_\alpha = V_m * \sin\omega t$ and $V_\beta = 0$

The α-β components are transformed to rotating d-q axes as follows.

$$\begin{pmatrix} V\_d \\ V\_q \end{pmatrix} = \begin{pmatrix} \cos\omega t & \sin\omega t \\ -\sin\omega t & \cos\omega t \end{pmatrix} \begin{pmatrix} V\_\alpha \\ V\_\beta \end{pmatrix}$$

The reverse transformation from d-q to α-β components is given as follows

$$\begin{pmatrix} V\_\alpha \\ V\_\beta \end{pmatrix} = \begin{pmatrix} \cos\omega t & -\sin\omega t \\ \sin\omega t & \cos\omega t \end{pmatrix} \begin{pmatrix} V\_d \\ V\_q \end{pmatrix}$$

The block diagram control scheme using D-Q reference frame controller is shown in Fig. 5.6.

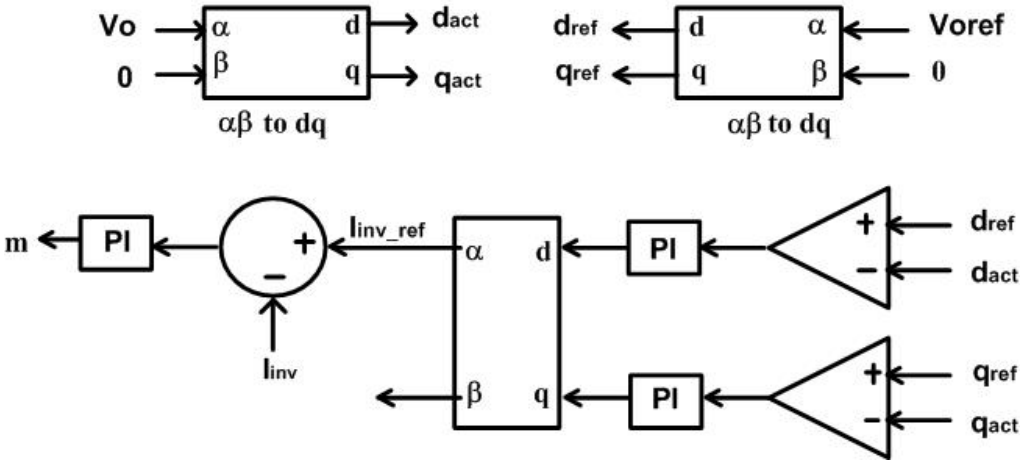

Fig. 4.6. Control Scheme for Inverter Output Voltage Control

The PI control action forces the β component to attain zero value and the output voltage Vo to follow the reference. The advantage of this method is that the input to the first two PI controllers are varying DC, which causes the PI control action to be faster than conventional methods of voltage control for single phase VSI.

4.3. MPPT Algorithm- Incremental Conductance

The MPPT algorithm that is being used for generating current reference for PV is incremental conductance[16], which has been found to perform faster than other methods. In this method, the slope of the conductance(-dI/dV) is checked and a current reference is generated for the PV converter. The logic diagram explaining the method for determining the current reference is shown in Fig. 4.7.

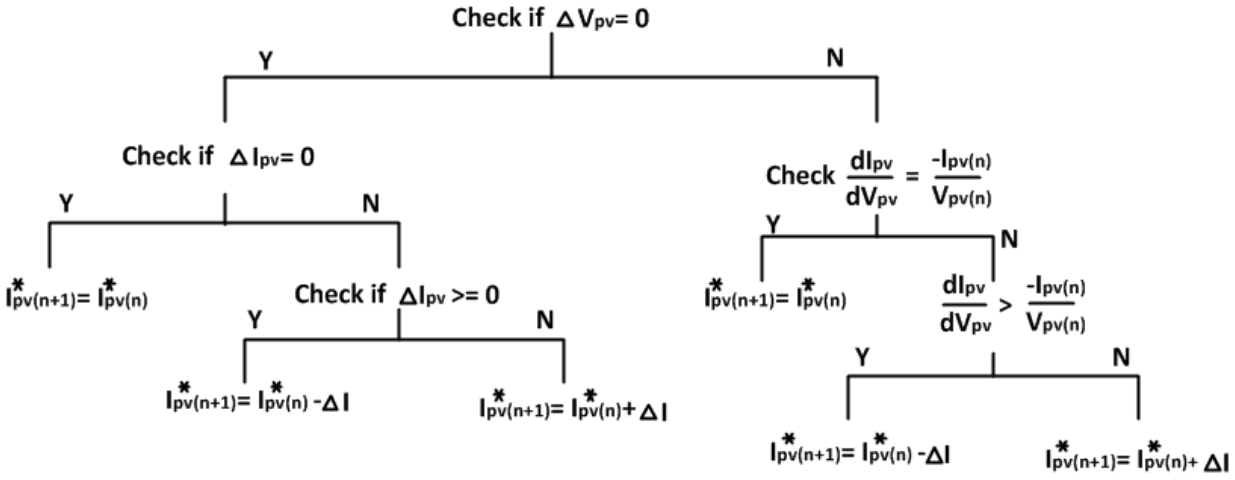

Fig. 4.7. Logic for Incremental Conductance Method

Chapter 5

Hardware Implementation

A laboratory prototype of the proposed system consisting of a half bridge boost converter, bidirectional dc-dc converter and single phase VSI has been developed to validate the viability of the scheme. Implementation of hardware prototype requires selection of proper hardware components. Sizing and design issues pertaining to major components of the prototype are presented below.

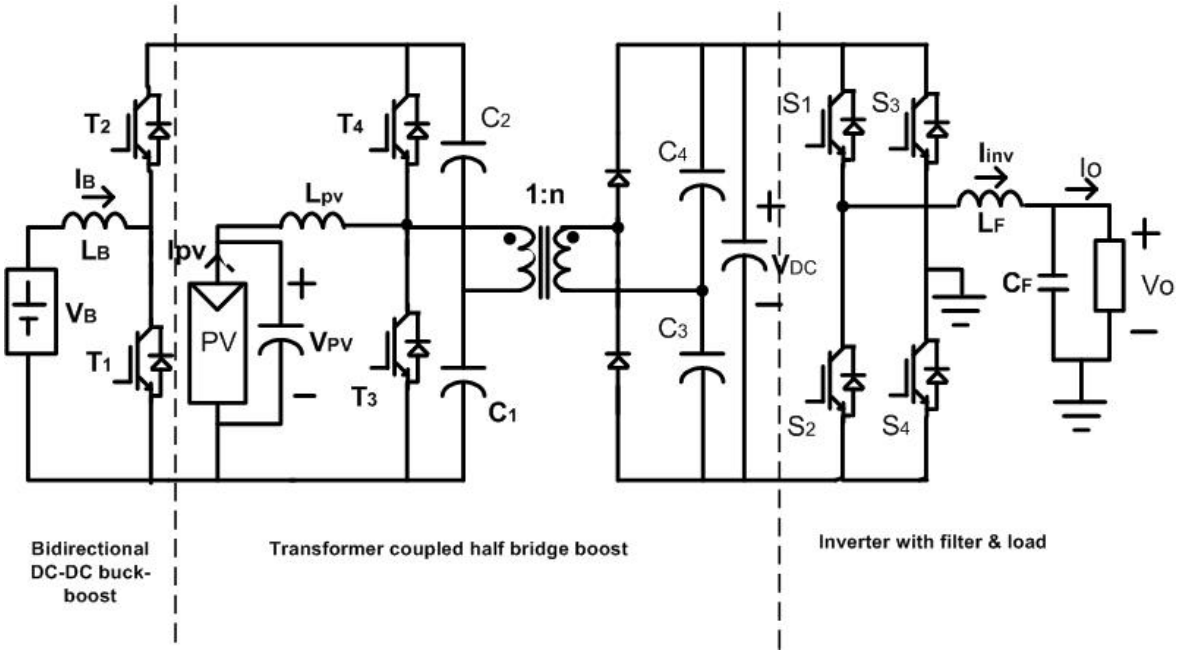

Fig. 5.1. Proposed Configuration for PV, Battery and AC loads

5.1. DSP Controller

The hardware prototype built needs to perform various computing, sensing of input signals and generation of output signals. For the scheme presented in the thesis work requires sensing of voltages and currents in the power circuit, performing MPPT check through an algorithm, computation of different PI loop outputs, generation of PWM signals, performing a band gap control of current sensed through the input signals etc. Implementation of all these functions necessitates the use of a DSP controller. For convenience, TI DSP TMS320F28335 is

chosen which has 16 ADC input pins and 12 PWM signals, 150 MHz clock frequency. Higher clock frequency of 150 MHz range can be easily used to perform control actions for 10 kHz switching frequency signals, band gap control of current, MPPT checking which is generally performed at an interval of 0.2-0.5 seconds and control of output voltage of frequency 50 Hz. The overall schematic diagram of the hardware prototype which is controlled by DSP is presented below.

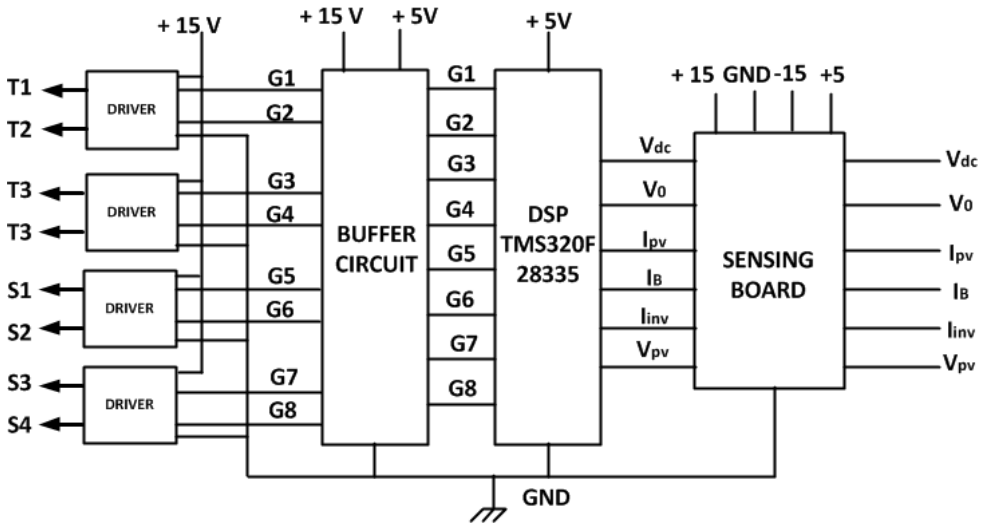

Fig. 5.2. Overall Control Schematic

The programmable timers in the DSP are utilized to generate interrupt signals at intervals of 50 µseconds. The C program is executed at an interval of the 50 µseconds. At every timer interrupt, the DSP takes the ADC signals as its input variables, performs the PI control loop calculations and generates the PWM signals for the gate drivers. For performing calculations of MPPT algorithm, a second timer is used to generate interrupts at an interval of 0.4 seconds. At every interrupt of this timer, the DSP executes the code for MPPT algorithm and generates a current reference for PV current I_{pv}. For sensing the input ADC signals, the ports A0-A2 and B0-B2 are used. For generating the PWM signals at a fixed frequency of 10 kHz, the GPIO pins 00-05 are programmed and for generating switching signals for battery converter switches, which are controlled using a band gap current control technique, pins 06-07 are used.

5.2. Selection of Transformer

The DC link voltage V_{DC}, is required to be maintained at 400V. The half bridge boost converter can give a maximum practical boost of 2-2.5 times on the primary side DC link. PV MPP voltage is 36V. Hence considering a boost factor of 2, primary side DC link voltage is 72. Since, the DC link voltage at secondary side is 'n' times the DC link voltage at primary side. Hence 'n' turns out to be 5.55. Now, considering voltage drops at transformer primary and secondary sides, the turns ratio is chosen to be 6. The PV voltage varies between 36-44V. During ON/OFF operation of switches T_3 and T_4(Fig. 5.1.), each of the capacitors appear across the transformer primary winding. Since, primary side DC-link voltage is around 2×36V =72V(minimum) and 44V×2 = 88V(maximum), the capacitors C_3,C_4 will also experience a voltage of 36V to 44V on each of them. Hence, the transformer primary voltage is chosen to be 50V, higher than the voltage across the transformer primary. The secondary voltage rating is thus 6×50V = 300V. The transformer chosen has a capacity of 1 kVA.

5.3. Selection of Inductors

The choice of inductor is influenced by current ripple allowance, switching frequency, operating voltage and duty cycle. Since the primary side of half-bridge boost converters is a boost converter essentially, hence the inductance value can be found from the following expression,

$$L = \frac{DV_{pv}}{f_s \, \Delta I}$$

Considering 10 kHz switching frequency, current limit to be 2% of PV operating current, PV MPP voltage of 36V and D-0.5 at MPP operation, we get a L value of 0.5 mH.

The inductor present in the bidirectional converter connected to battery, operates as an inductor of a boost converter while battery is in discharging mode and operates as the inductor of a buck converter while the battery is in charging mode. Hence, the value of the inductor for a buck boost converter can also be found out from the above equation. The battery current ripple is chosen fixed at 0.5A. To keep the frequency at 10 kHz with a battery voltage of 48V and to maintain the primary side dc link voltage around 72V, we get a L value of 3.2 mH.

The inductors considered are made of ferrite core material with operating frequency of 10 kHz approx.

5.4. Selection of Capacitors

The values of the capacitors chosen are based on the allowable voltage ripple and voltage that they have to withstand. The dc link capacitor maintains a voltage of 400V. With a safety factor of 2, the voltage rating is chosen to be 2×400 = 800V. The primary side split capacitors each can experience a maximum voltage of 44V. With a safety factor of 2, the voltage rating is chosen to be around 100V. Similarly, the secondary split capacitors have a rating of around 400V. To decide the capacitance value of summing capacitor of dc link, a high value capacitance of value 2000 μF is chosen. The voltage ripple is of around 1%. Similarly, for the primary side and secondary side split capacitors, capacitance value of 500 μF is chosen to have minimal ripple(less than 1%).

5.5. Selection of Switches

To determine the rating of the switches, on-state maximum current and off-state voltage are considered. For inverter switches(S1-S4), off-state voltage is around 400V. On-state peak current for a load of 500VA, can go upto 3.1A, with a safety factor of 2 the minimum voltage and current ratings are chosen to be 800V and 6.5A.

For PV switches(T3,T4), maximum current can be around 30A and off state voltage is around 72V. For the lower PV switch, during on-state, the capacitor C_2 also discharges through the transformer primary winding and switch T3. The current that is delivered by the capacitor C2 while discharging depends upon the leakage inductance of the transformer. From simulation studies, for a 500 VA load, the discharging current of capacitor C2 can be upto 20A(peak) since capacitor voltage is around 36V-44V. For the top PV switch, maximum current that can flow through anti-parallel diode and collector-emitter path is around 32A. Lower PV switch has a peak current rating of 32 + 20 = 52A. To maintain symmetry of the switches, the same switch at bottom(T3) is considered for the upper position(T4) also. With a safety factor of 2, the minimum voltage and current rating is chosen to be 144V, 100A.

The maximum charging or discharging current for a 48V, 150 Ahr battery can be 15A. The off state voltage for the battery converter switches T1 and T2 is around 72V. While the peak current that can pass through them is around 15A. Applying a safety factor of 2, the minimum rating for PV switches is considered to be 144V, 30A.

5.6. PV Simulator, Battery and Loads

PV panel output is realized using Agilient Technologies Solar Array Simulator E4360A. Battery used is four 12.7 volt, 7.2 Ahr battery from Quanta. Load is realized using rheostats and bulb loads.

5.7. Selection of Drivers

For IGBTs, with a operating frequency of 10kHZ, Semikron Drivers SKHI 22AR is found to be suitable with in-built protection and blanking time of 4 µseonds between switching of top and bottom switches. The drivers have a maximum operating frequency of 50 kHz with 8 mA of output current rating.

5.8. Designing of Sensing Circuit

For performing, closed loop control of the system, sensing the voltages and currents are necessary. In view of this, a sensing circuit with galvanic isolation between power circuit and sensing circuit is developed. For providing isolation in voltage sensing, ISO122P is used which provides galvanic isolation between primary and secondary side voltage. For primary side voltage, the voltage is stepped down using a resistor-divider circuit with op-amp as shown in Fig. 5.3, provided the input voltage to DSP does not exceed 3.3V. For PV voltage(V_{pv}) sensing, R1= 67kΩ, R2 = 15kΩ. For secondary dc link voltage(V_{DC}) sensing, R1 = 1MΩ, R2 = 22kΩ.

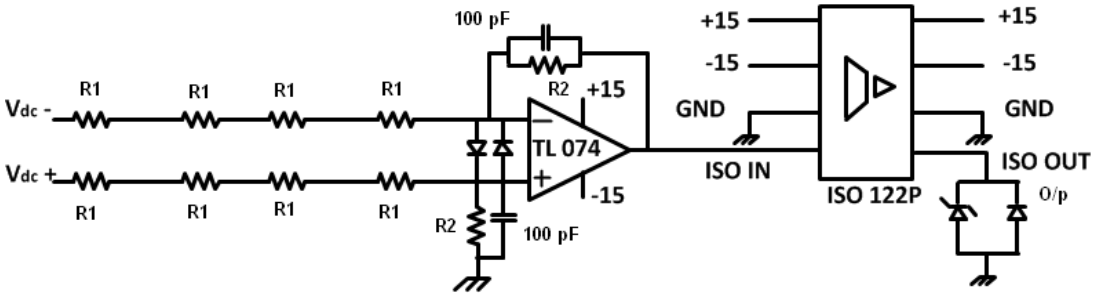

Fig. 5.3. Sensing Circuit for DC voltages

For ac output voltage sensing, a positive voltage shift of 1.5V using IC LM317 is given to the output of ISO122P, as DSPs can only take positive voltages as input. The feedback resistances of LM317 are adjusted to give 1.5V output, which is then added to the stepped down ac voltage through an op-amp resistor divider circuit. The schematic diagram is shown in Fig. 5.4. Here, for output load voltage sensing, R1 = 1MΩ, R2 = 12kΩ, R3 = 1kΩ, R4 = 330Ω, R5 = 68Ω.

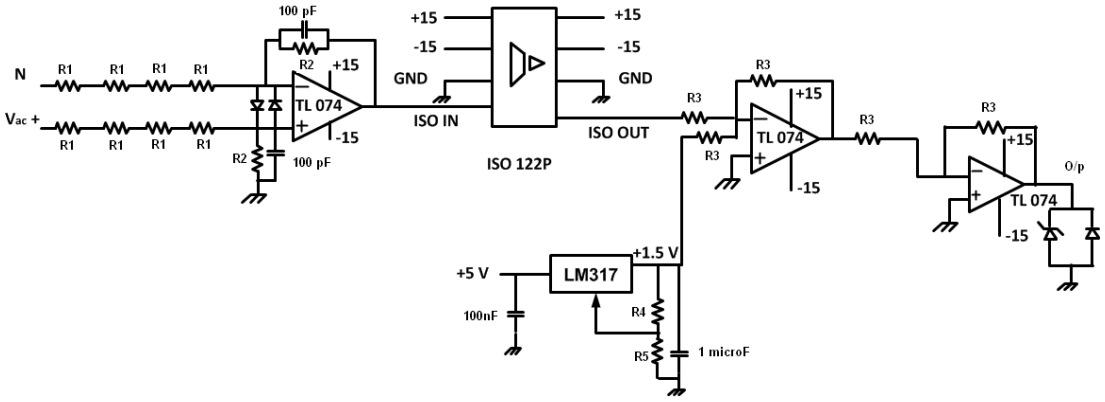

Fig. 5.4. Sensing Circuit for AC voltages

For current sensing, LEM current sensors HAS 100-S and LEM 55-P is used. PV current is unidirectional, hence 1.5 V shift is not required. However, Battery and inverter output current are bidirectional. Hence 1.5 V shifts using LM317 are necessary. The sensing circuit diagrams for unidirectional and bidirectional currents are shown in Fig. 5.5 and 5.6. For PV current(I_{pv}) sensing, R_L = 1kΩ, R1 = 510kΩ, R2 = 1MΩ.

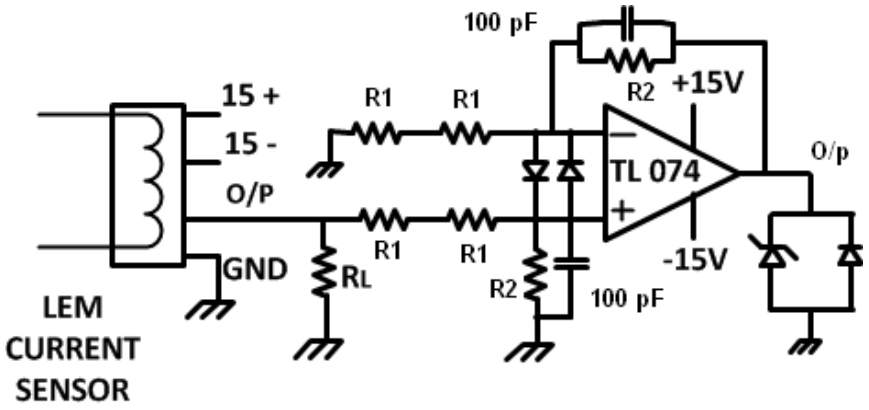

Fig. 5.5. Sensing Circuit for DC Currents

For sensing battery and inverter output currents, the schematic diagram shown in Fig. 5.6 is used. For battery current sensing, R_L = 1kΩ, R1 = R2 = 1MΩ, R3 = 1kΩ, R4 = 330Ω, R5 = 68Ω.

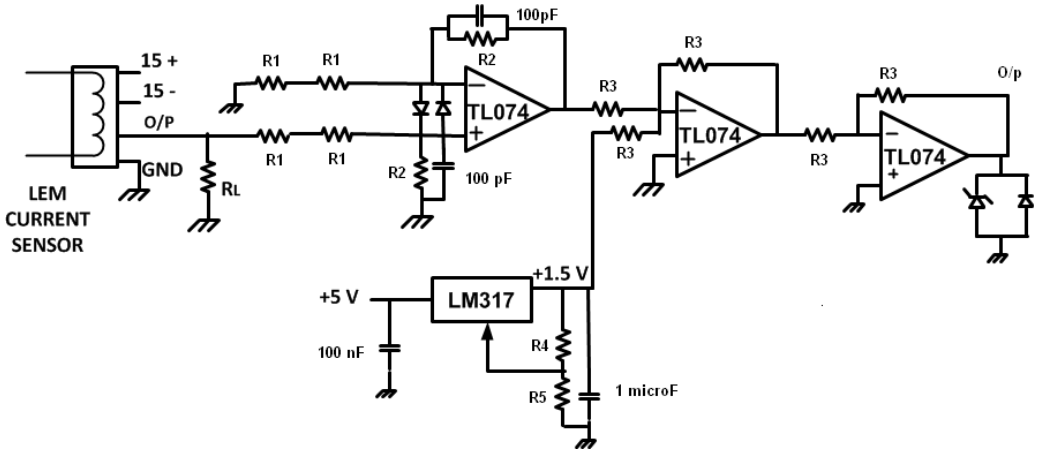

Fig. 5.6. Sensing Circuit for AC Currents

5.9. Designing of Buffer Circuit

The PWM signals generated through DSP TMS320F28335 has a voltage rating of 3.3V. SKHI 22AR drivers require 15V of input pulses. Hence, a step-up buffer circuit is required. The schematic of the buffer circuit designed is shown in Fig. 5.7.

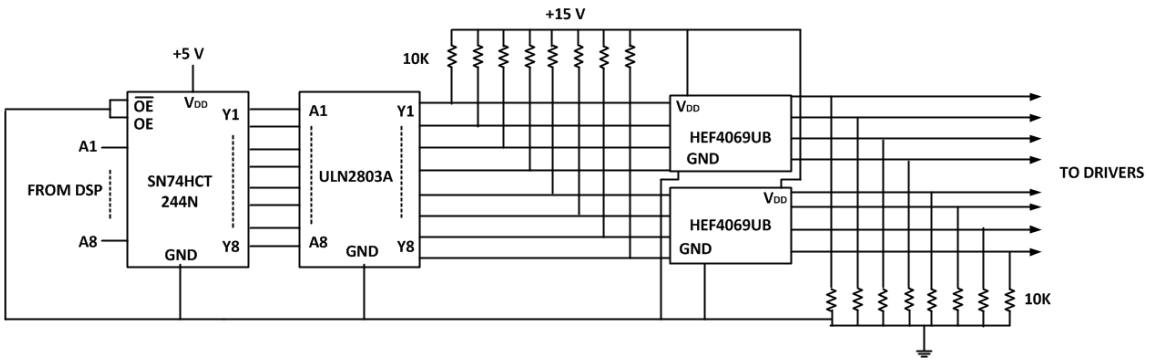

Fig. 5.7. Buffer Circuit Schematic

5.10. Designing of Auxiliary power Supplies

Sensing boards, buffer circuits, drivers require uninterrupted +/-15 volts and 5 volts supply which require minimal amount of current. This dc power supplies can be designed using linear regulators which can provide the required current. The schematic for such +/- 15 volt and +5 volt supplies are shown in Fig. 5.8 and 5.9.

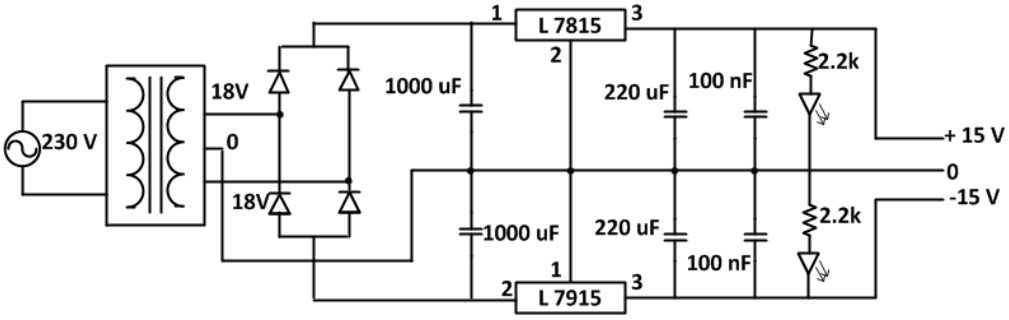

Fig. 5.8. Power Supply of +/-15 volts

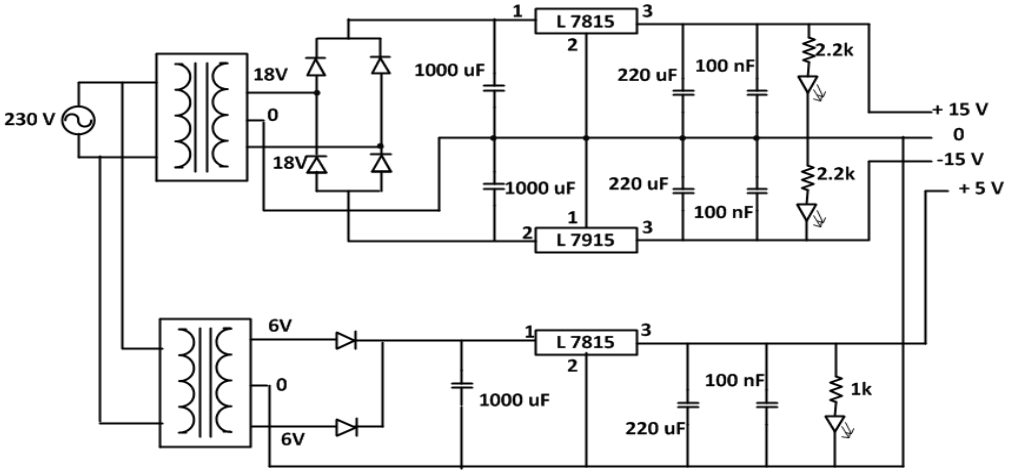

Fig. 5.9. Power Supply of +/-15 volts and +5 volts

5.11. Hardware Prototype Pictures

Various pictures depicting the hardware prototype developed are shown in Pictures for the hardware prototype developed, are shown in Fig. 5.10, 5.11 and 5.12.

Fig. 5.10. PV Simulator, Battery and Bulb Loads

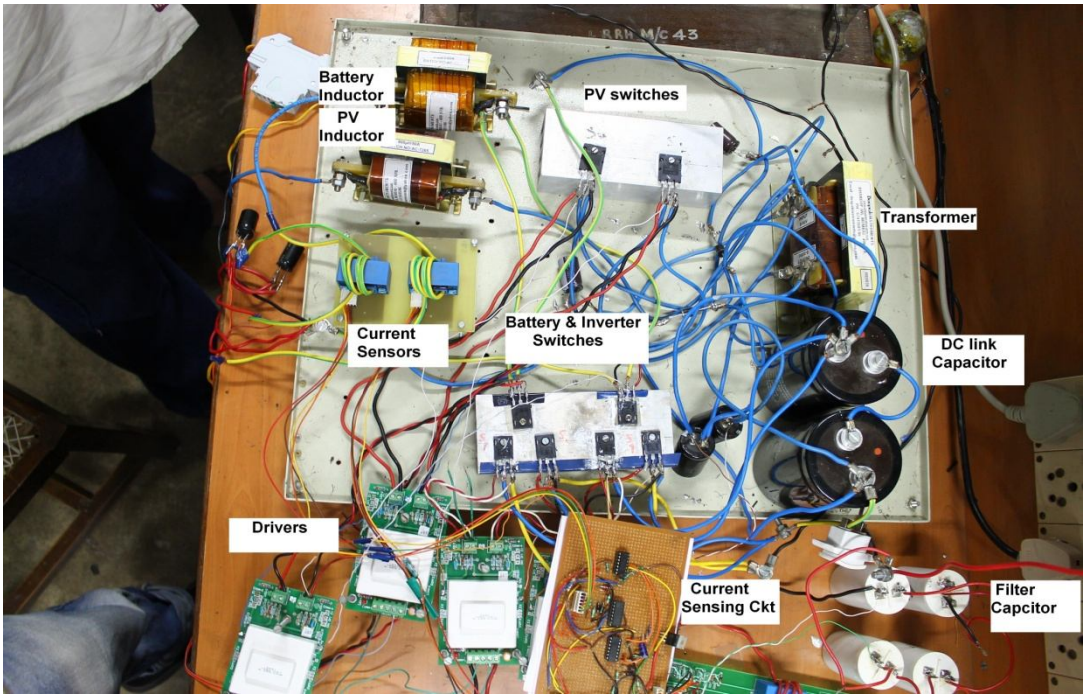

Fig. 5.11. Power Circuit Setup

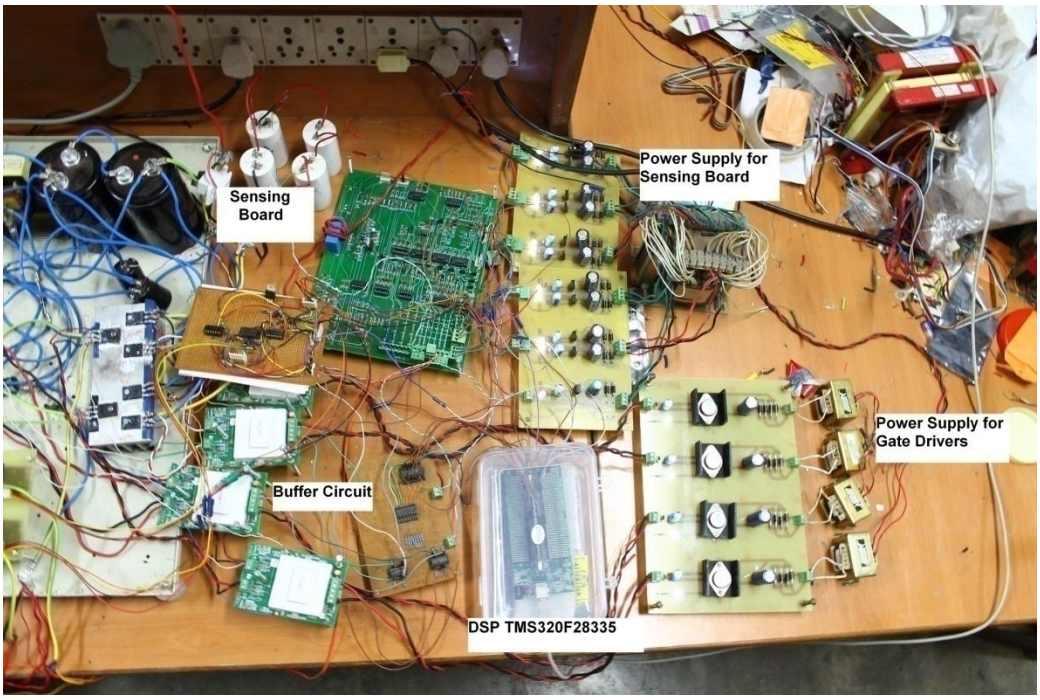

Fig. 5.12. Control and Sensing Circuit Setup

Chapter 6

Results

Detailed simulation studies are carried out to confirm the validity of the proposed sche,e. Subsequently the viability of the scheme is verified by performing detailed experimental studies on the laboratory prototype developed for the purpose. Simulation for the above system is carried out in MATLAB/SIMULINK to emulate different operating conditions.

6.1. Simulation Results

6.1.1. Case 1: MPPT Mode of Operation

In this mode, PV operates at MPP, delivering maximum power and DC link is maintained by battery by taking a charging current less than that specified by SOC. PV operates at 0.5 kW/m^2 with current at MPP I_{mpp} = 15.5A. load connected is 300W, 50VAr. The maximum battery charging current is taken as 8 Amps.

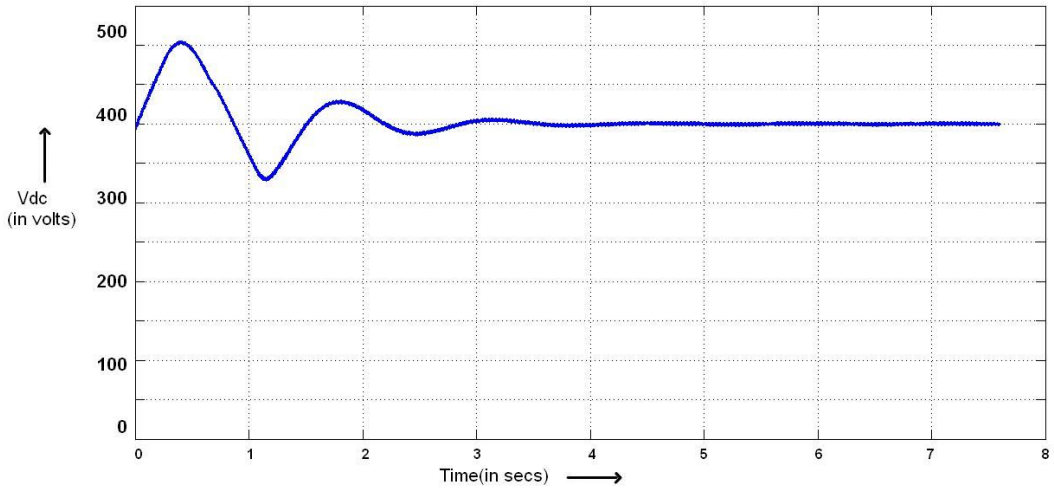

Fig. 6.1. DC link voltage at MPPT

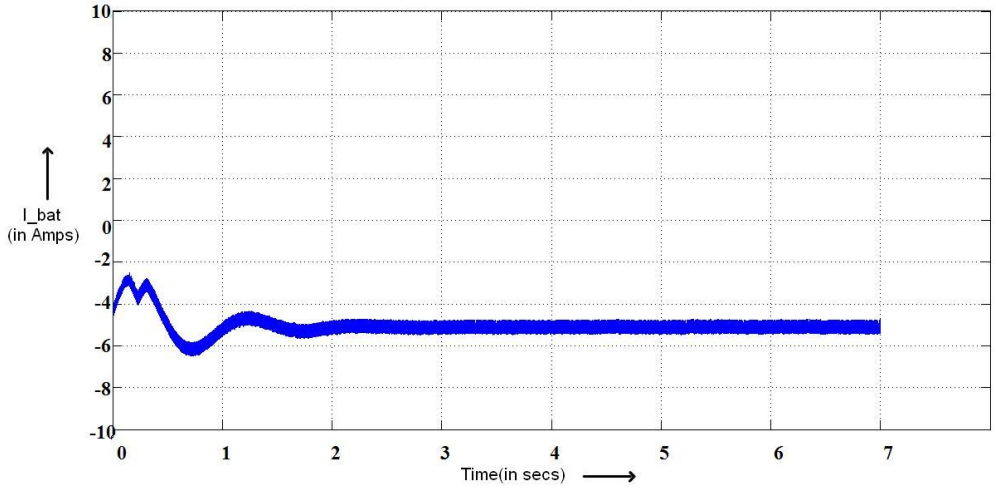

Fig. 6.2. Battery Current at MPPT

In mppt mode of operation, the dc link voltage Vdc stabilizes at 400V(Fig. 6.1) due to the control action performed by the battery converter. As total power developed by PV is higher than that required for load, the battery takes a charging current(Fig. 6.2) of 5.5A, which is less than that specified by SOC controller(8A). This validates the controller scheme proposed for MPPT mode of operation.

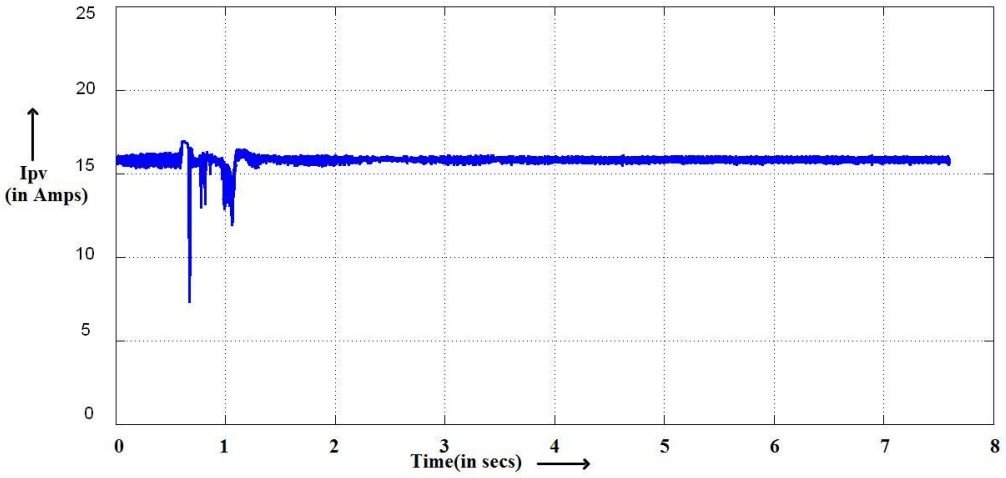

Fig. 6.3. PV Current at MPPT

From Fig 6.3, it can be inferred that PV operates to deliver maximum power at solar insolation of 0.5 kW/m^2 with I_{mpp} = 15.5A, while Fig. 6.1 and 6.2 show that the dc link voltage is maintained at 400V, by control action performed by the battery converter.

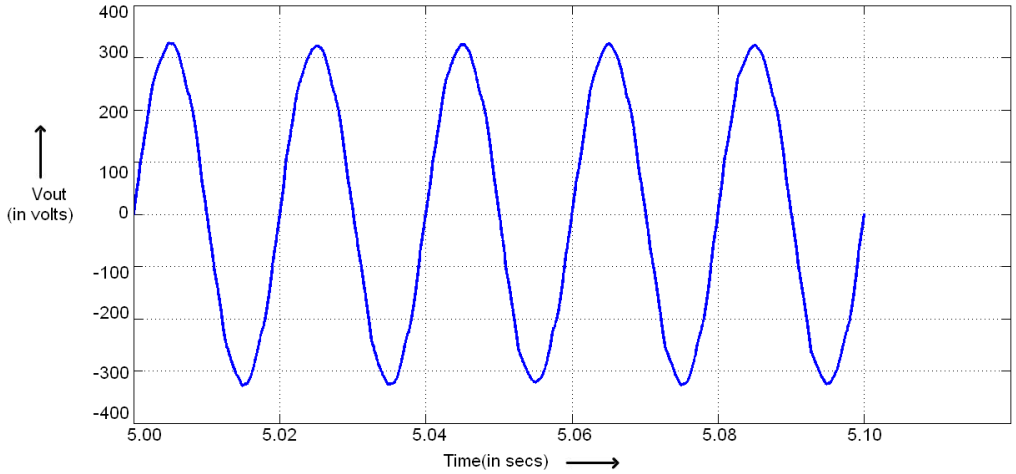

Fig. 6.4. Output Voltage Shape at MPPT

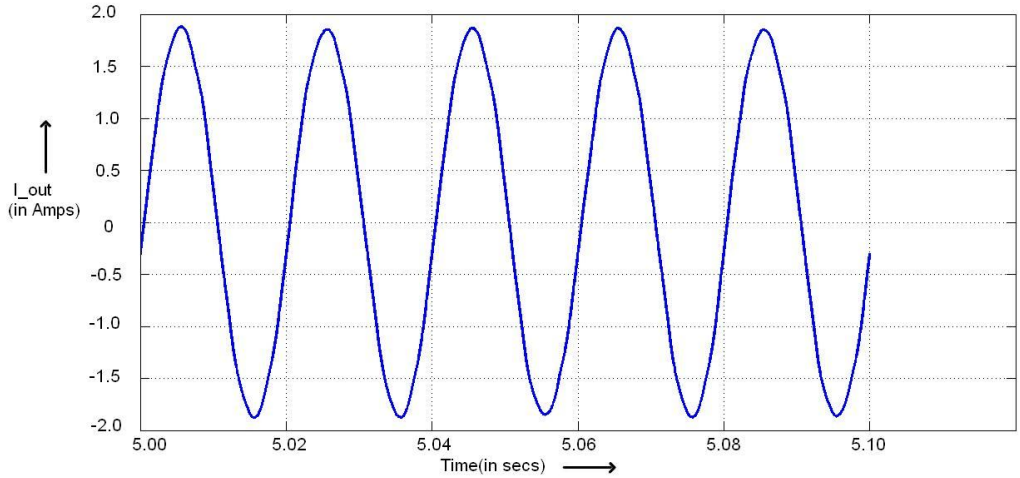

Fig. 6.5. Output Current Shape at MPPT

Fig. 6.4 and Fig. 6.5 gives the steady state output voltage and current waveforms. This justifies the fact that the output voltage and current are maintained sinusoidal by the control action performed of the single phase inverter.

6.1.2. Case 2: Step Change in Load in MPPT Mode of Operation

In this mode, PV operates at MPP at 0.4 kW/m^2 solar insolation with I_{mpp} = 13A, delivering maximum power and the battery converter maintains the DC link voltage by taking a charging current less than that specified by SOC controller(8A). During initial transient period of

5 seconds, battery maximum charging current is maintained at 20A so that the system settles down at MPPT. An increment in load of 200W, 50VAr takes place at 8 second and the load is disconnected around 17 second.

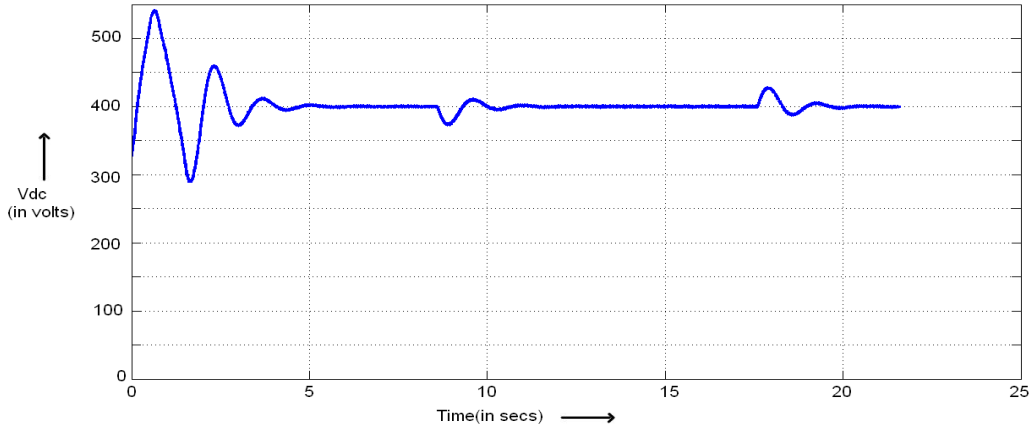

Fig. 6.6. DC Link Voltage Variation under Load Changes

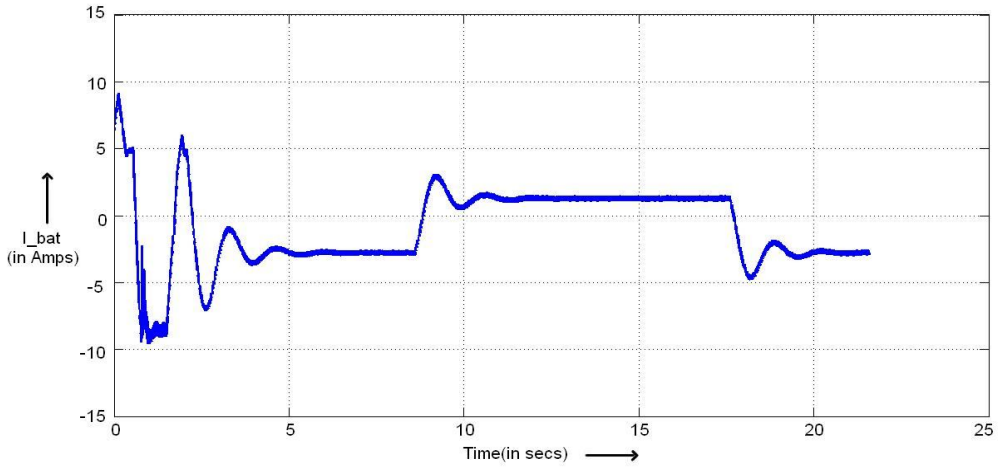

Fig. 6.7. Battery Current at MPPT Operation under Load Changes

Initially, the dc link voltage stabilizes at 400V by the control action performed by the battery converter which takes in a charging current of 2.5A while PV continues to operate at MPP with I_{mpp} of 13A. At 8 second, an increment in load takes place, which causes a fall in dc link voltage(Fig. 6.6). As battery converter is controlling the dc link voltage, a fall in dc link voltage triggers the battery current to increase(Fig. 6.7) for supplying the extra load demand by restoring the dc link voltage at 400V. Removal of the same load occurs at 17 second, which causes the dc link voltage to swell up. Increase in dc link voltage causes the power delivered by

to fall. The current delivered by battery falls and finally it stabilizes at some point by taking in a charging current of 2.5A. This supports the control scheme proposed for MPPT mode of operation that dc link voltage changes can be handled by the control action of battery converter.

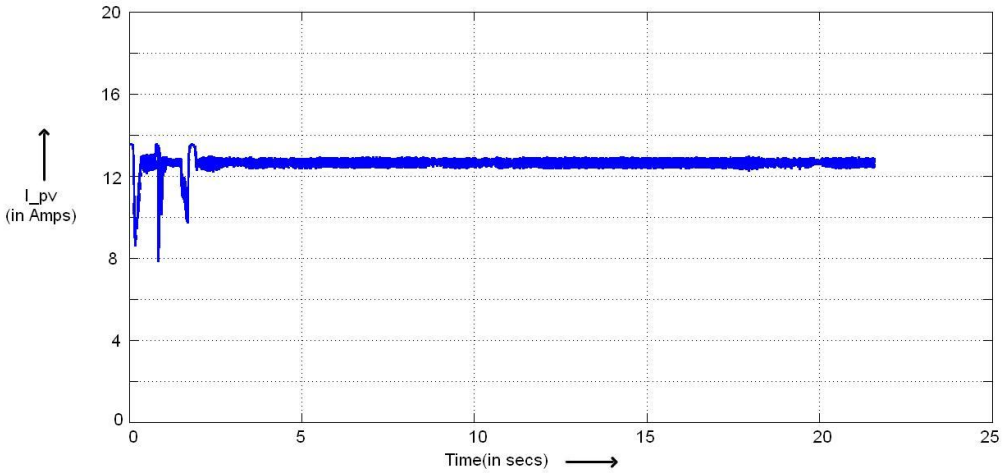

Fig. 6.8. PV Operating at MPPT and Delivering Constant Current

From Fig. 6.8, it can be inferred that the PV converter continues to operate at MPPT, regardless of load changes taking place.

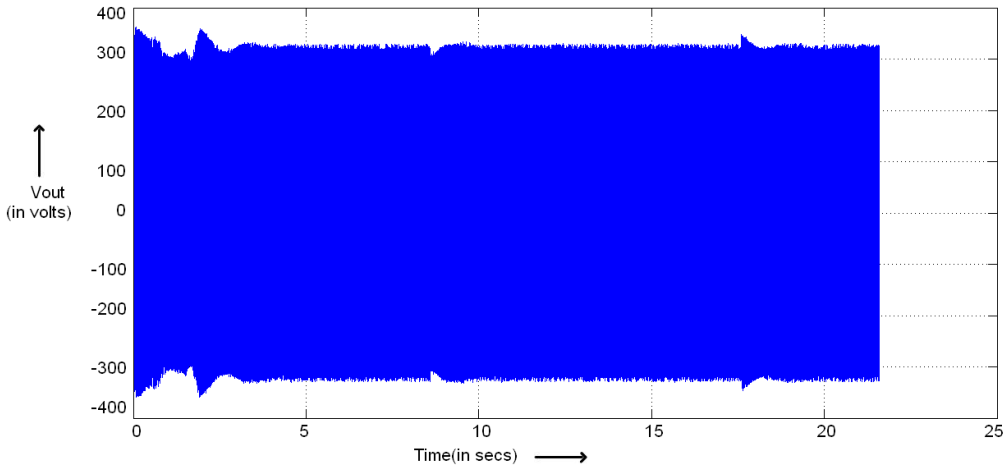

Fig. 6.9. Output Voltage under Load Changes

Fig 6.9 and Fig. 6.10 show the output voltage and current changes respectively. The load voltage falls at an increment of load at 8 second, but is quickly restored due to the fast control

action of inverter and battery controller(Fig. 6.9).The load current increases at 8 second due to addition of load and falls at 11 second due to removal of load(Fig. 6.10).

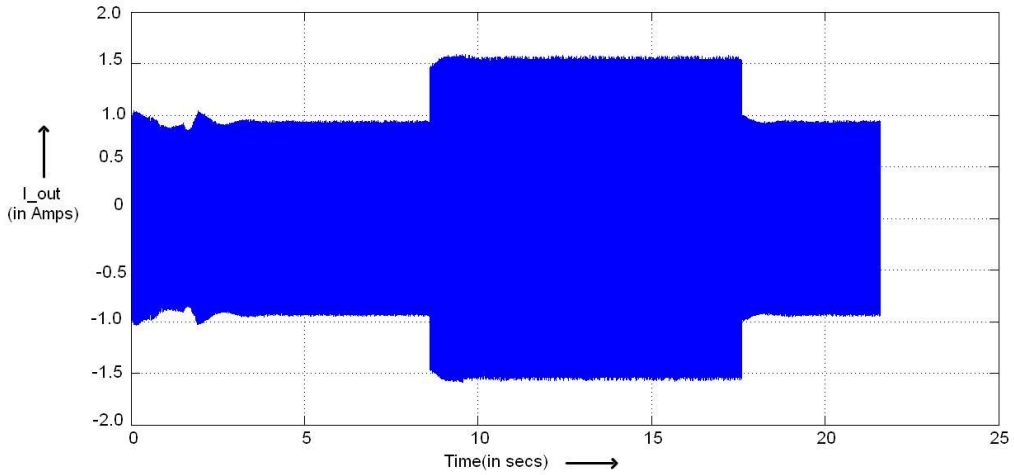

Fig. 6.10. Changes in Load Current

6.1.3. Case 3: Non-MPPT Mode of Operation

In this mode, PV operates at a operating point other than MPP, delivering the power required by load and charges the battery with a constant current specified by SOC. PV operates at 0.4 kW/m^2 and the load connected is 200W, 50VAr. PV maximum power point current I_{mpp} is 13 A. The maximum battery charging current is taken as 4 Amps.

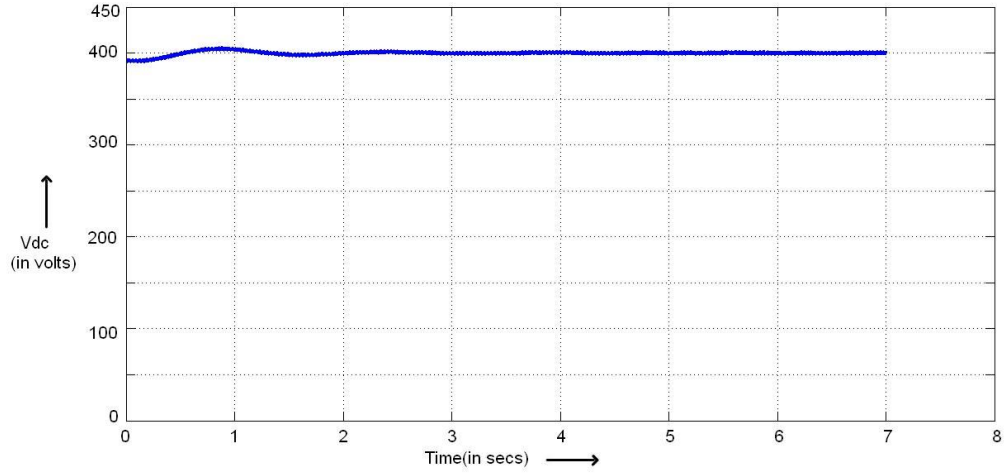

Fig. 6.11. DC Link Voltage at Non-MPPT Mode

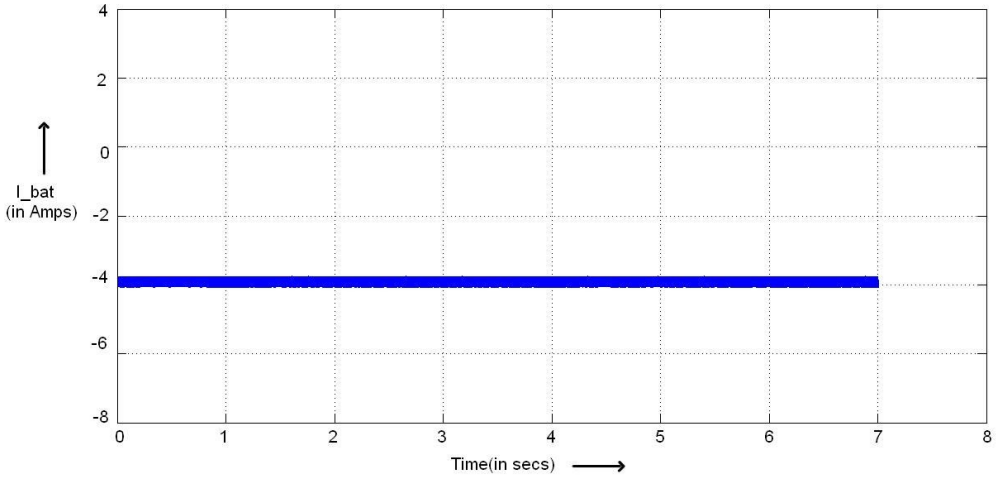

Fig. 6.12. Battery Charging Current at Non-MPPT Mode

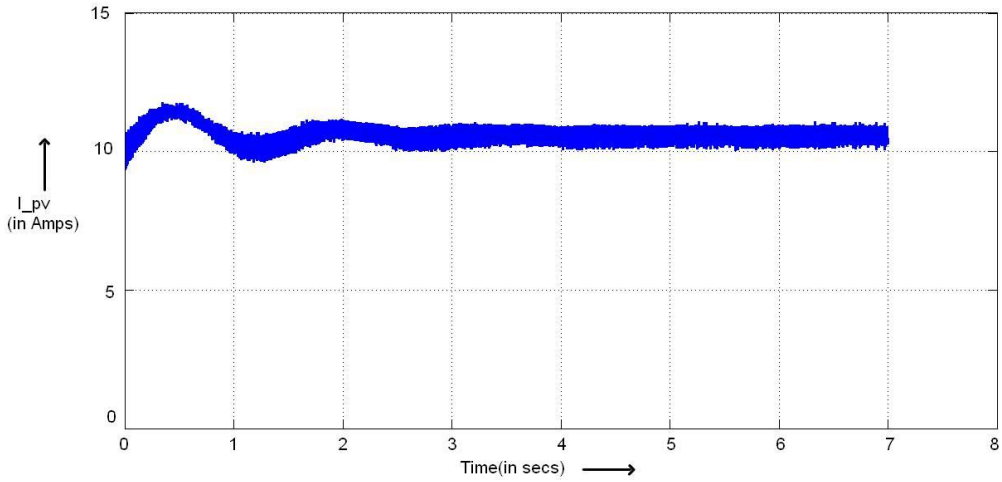

Fig. 6.13. PV Current at Non-MPPT Mode

From Fig. 6.11, 6.12 and 6.13, it can be seen that PV converter maintains the dc link voltage at 400V, while the battery converter maintains the charging current at 4A, as specified by the controller. PV operates at a current of 10A, which is lower than the current I_{mpp} = 13A\. These figures justify the control scheme of charging the battery with a constant current and maintaining the dc link voltage by the PV converter.

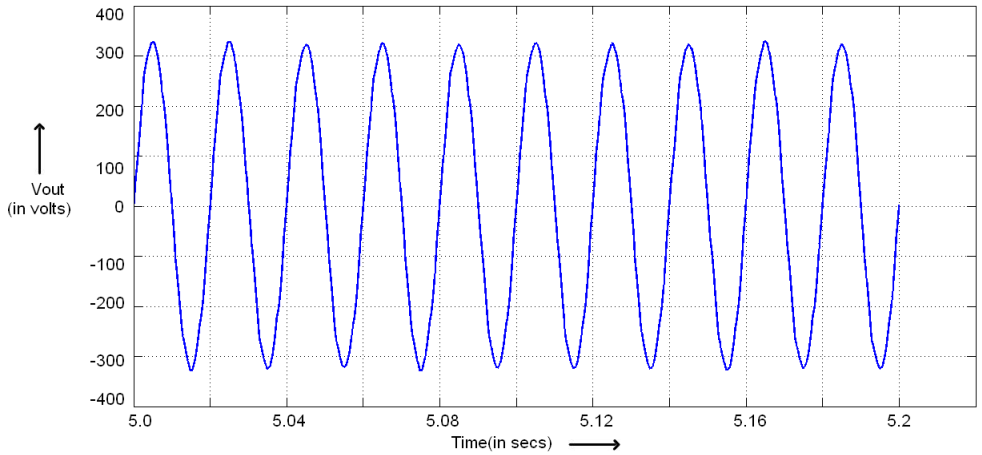

Fig. 6.14. Output Voltage Shape at Non-MPPT Mode

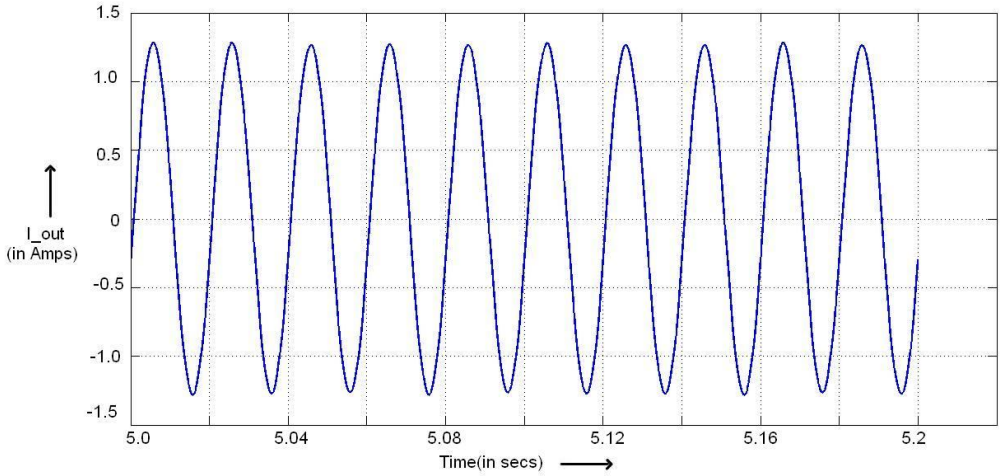

Fig. 6.15. Output Current Shape at Non-MPPT Mode

The output voltage and current shapes at Non-MPPT mode of operation can be seen from Fig. 6.14 and Fig. 6.15.

6.1.4. Case 4: Step Change in Load in Non-MPPT Mode of Operation

In this mode, initially PV operates in Non-MPPT mode with 0.5 kW/m^2 solar insolation. The PV MPP current is I_{mpp} = 15.5A. The battery charging current is 4A and the load connected is a 200W, 50VAr load. A 100 watt load is added at 2.5 second and the same load is withdrawn at 6 second.

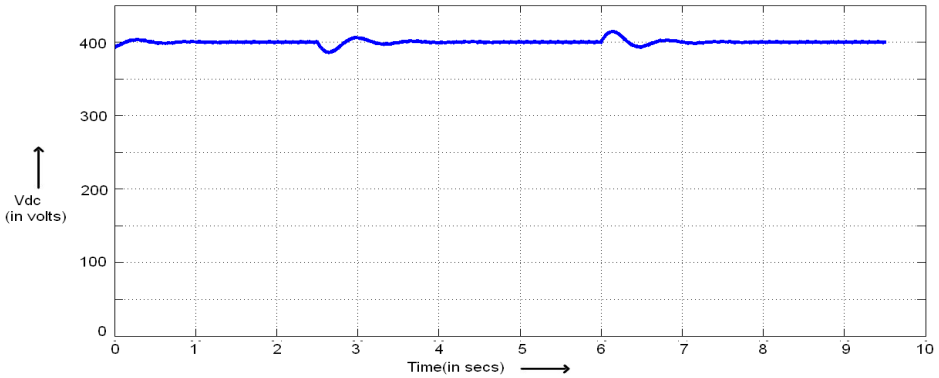

Fig. 6.16. DC Link Voltage Variation under Non-MPPT Mode

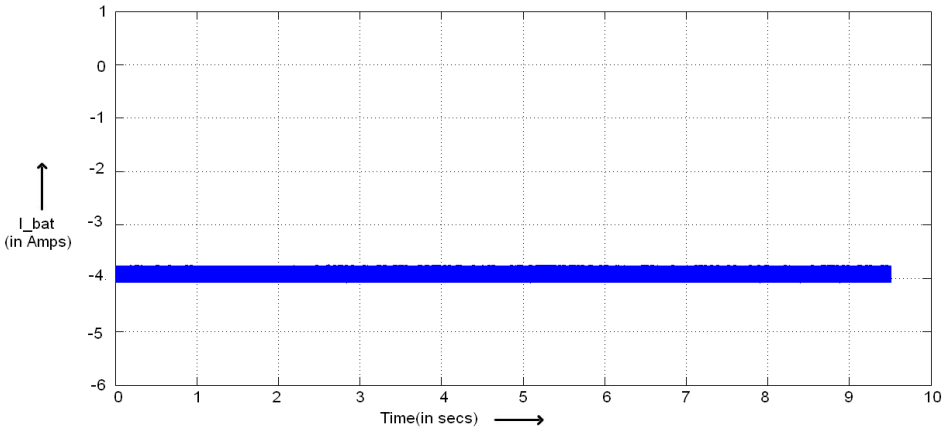

Fig. 6.17. Constant Battery Charging current

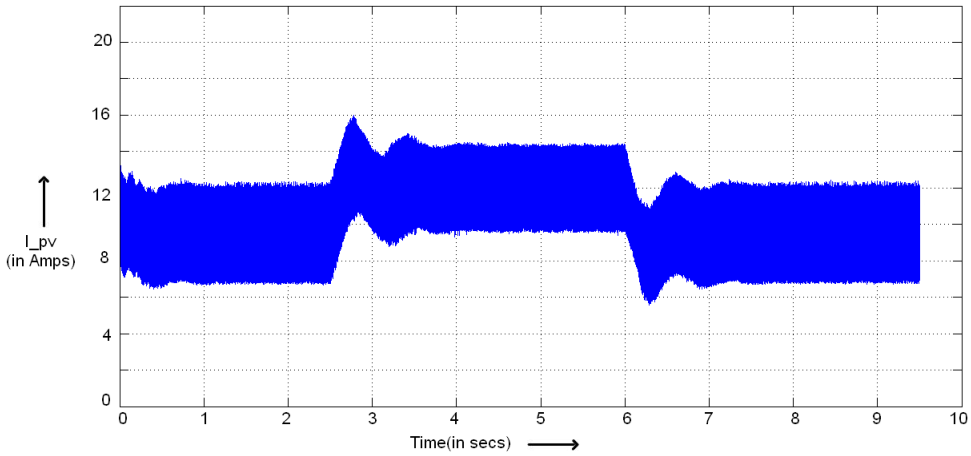

Fig. 6.18. PV Current Variation with Load Changes in Non-MPPT Mode

In this case, initially PV operates at current of 10A(Fig. 6.18), and the battery charging current is maintained at 4A(specified by SOC). At 2.5 seconds, a load change of 100W takes place, which causes the dc link voltage to fall(Fig. 6.16). As PV is maintaining the dc link voltage, with fall of dc link voltage PV current increases(Fig. 6.17) to a new value to restore the dc link voltage. At 6 sec, the same load is withdrawn, dc link voltage swells up which causes the PV current to decrease to restore the dc link voltage. These changes in load and subsequent changes in dc link voltage and its restoration justifies the control scheme for Non-MPPT mode of operation, where PV supplies the power required to charge the battery and to supply the load demand.

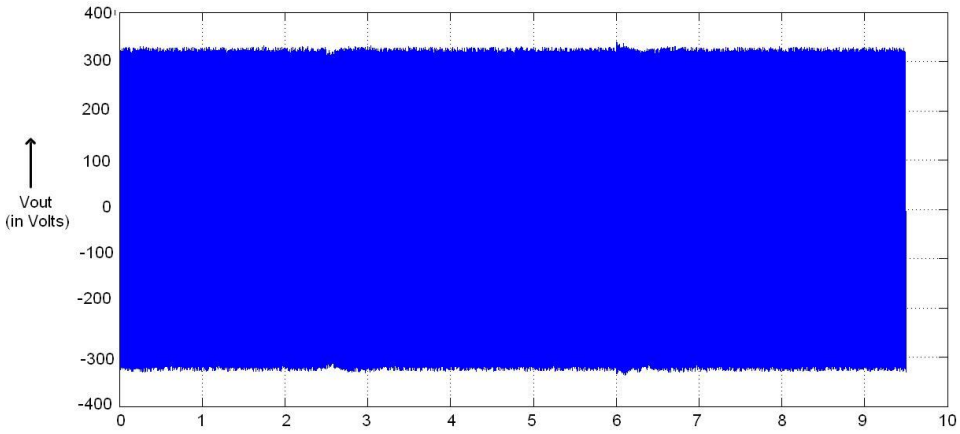

Fig. 6.19. Output Voltage under Load Variation

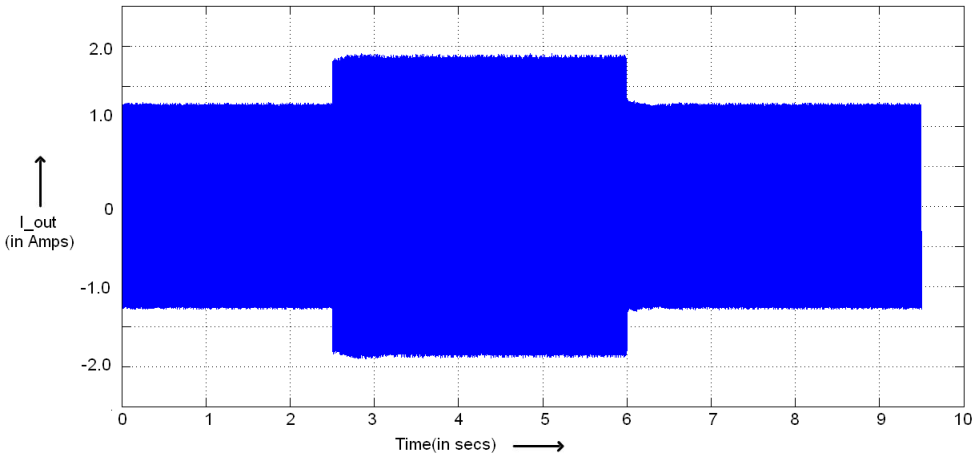

Fig. 6.20. Output Load Current Variation under Load Changes

The changes in output voltage and output current can be seen from Fig. 6.19 and Fig. 6.20, where the output voltage momentarily falls due to increment in load, and it again is restored by the controller, while the load current increases. Similarly, for removal of load, the output voltage momentarily swells up but again is restored by the controller, while the load current decreases.

6.1.5. Case 5: Change in Mode of Operation from MPPT to Non-MPPT caused by Step Change in Load

In this case, PV initially operates at MPP with solar insolation of 0.8 kW/m^2 at I_{mpp} = 22A, drawing a charging current less than the maximum charging current specified at 8 Amps. The load connected is 400W, 50 VAr. At 5 second, a load of 200W, 30 VAr is withdrawn. At 14 second, a load of 100W is added.

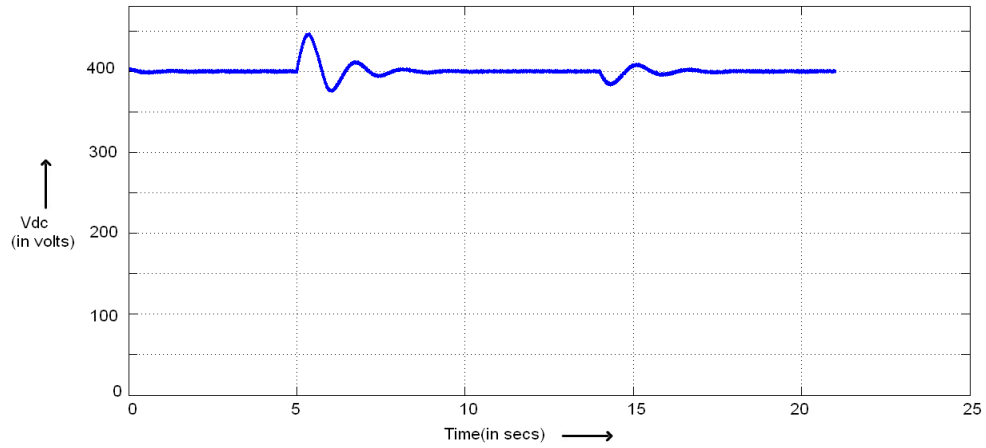

Fig. 6.21. DC Link Voltage Variation under Load Changes

In this case the dc link voltage initially was maintained at 400V. At 5 second, due to removal of a load, the dc link voltage swells up(Fig. 6.21), which is restored by the controller to 400V again. At 14 second, addition of a load occurs, which causes the dc link voltage to fall, which is restored again by controller at 400V.

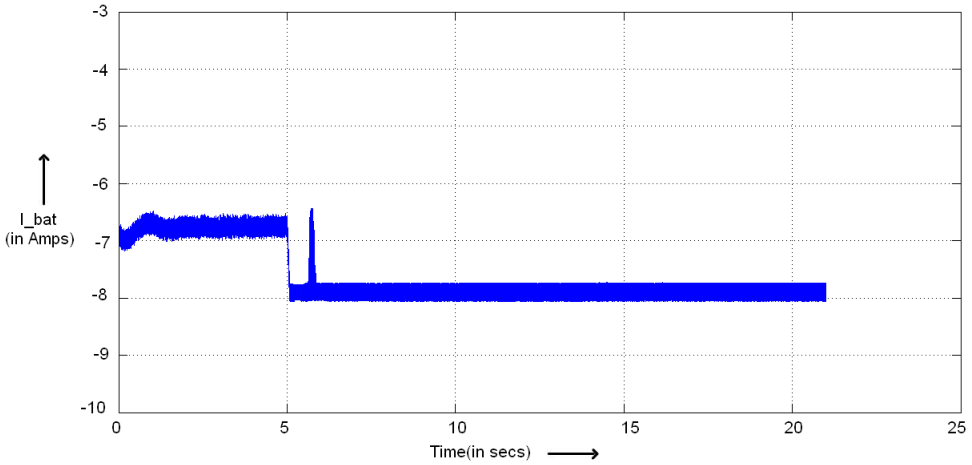

Fig. 6.22. Battery Current Variation under Load Changes

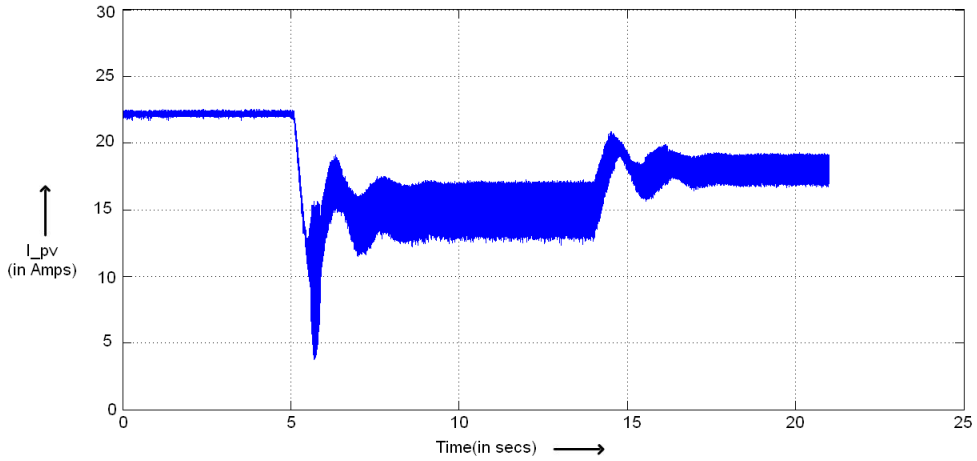

Fig. 6.23. PV Current Variation under Load Changes

Here initially the system was operating at MPPT, with battery maintaining the dc link voltage by taking a charging current of 7A which is less than the maximum charging current specified by the SOC. PV was delivering maximum power while operating at a current of 22A. At 5 second, step removal of 200W of load causes the dc link voltage to swell. As dc link voltage increases, the battery controller start taking in more current(Fig. 6.22) to restore the dc link. As battery current hits the limit of 8A, the controller shifts the action to Non-MPPT mode of operation. PV current now starts falling(Fig. 6.23) while battery current is maintained at 8A. PV current now stabilizes at 15A, charging the battery with a current of 8A and maintaining the dc link voltage by supplying the required load demand. At 14 second, 100W of load is added, which causes the dc link voltage to fall and the PV controller starts restoring the dc link voltage by

increasing the PV current which ultimately stabilizes at 18A(Fig. 6.23). During this time, the battery current remains unaffected as the controller still continues to work in Non-MPPT mode(Fig. 6.22).

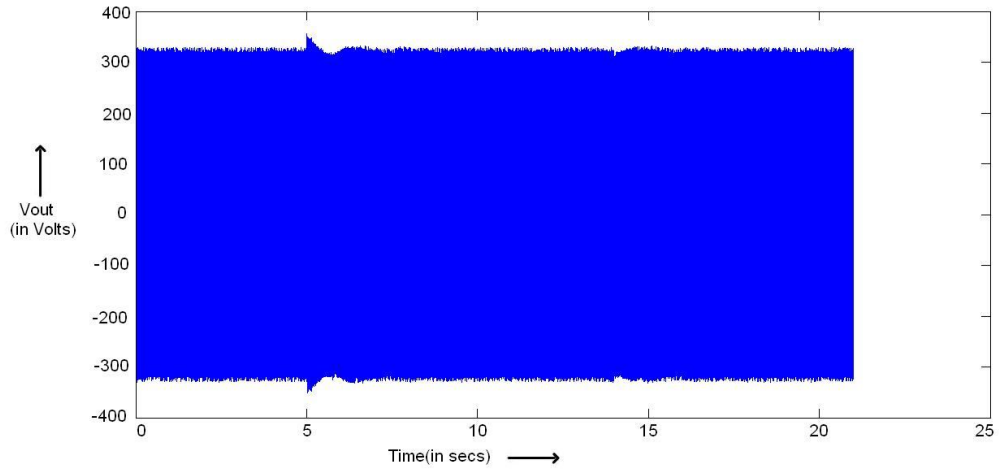

Fig. 6.24. Load Voltage Variation under Load Changes

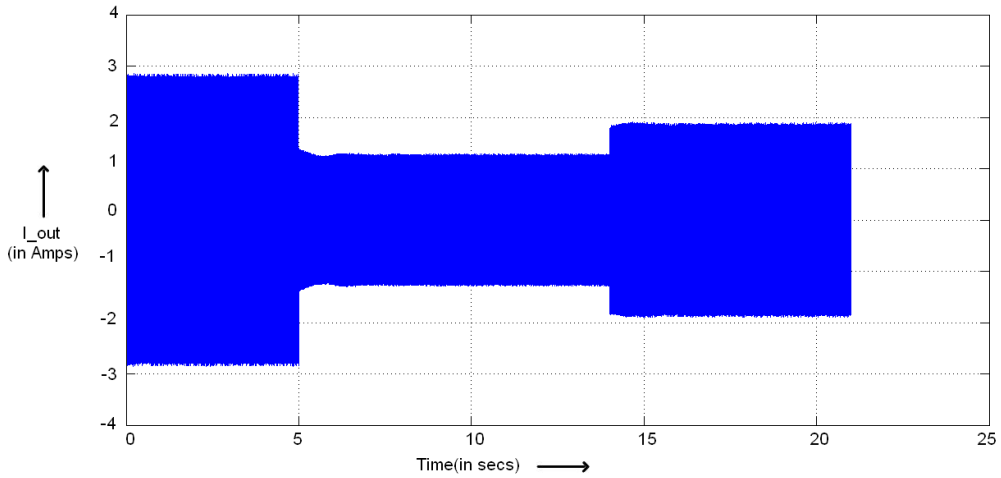

Fig. 6.25. Load Current Variation under Load Changes

Figures 6.24 and 6.25 shows the load voltage and load current variation under these mode of operation. As can be seen, the load voltage variation is very quickly restored by the d-q control action of the inverter, compared to the time required for restoration in DC link votage.

6.1.6. Case 6: Change in Operating Mode from MPPT to Non-MPPT Mode and back caused by Step Change in Solar Insolation

In this mode, initially PV operates in MPPT mode at 0.5 kW/m^2 with I_{mpp} = 15.5A. The load connected is a 300W, 50 MVAr load. The battery takes a charging current of 5A, which is less than the maximum charging current of 8A. While an increase in solar insolation at 9 second causes change in operating mode from MPPT to Non-MPPT. At 9 second, solar irradiation changes to 0.9 kW/m^2. The system enters Non-MPPT mode of operation. At 17 second, solar insolation decreases to 0.55 kW/m^2. The system again comes back to MPPT mode. During initial transient mode of 5 second, battery charging current reference is taken higher so that the system settles down at MPPT operation.

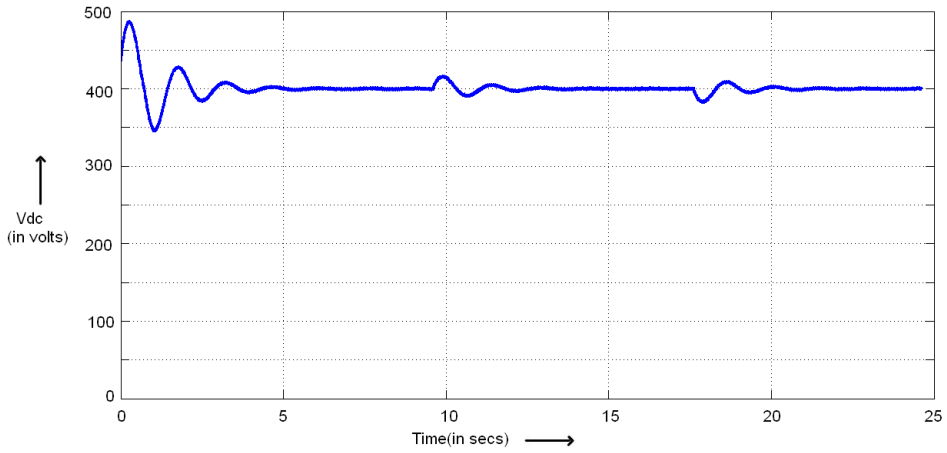

Fig. 6.26. DC link voltage Variation under Solar Insolation Changes

The dc link voltage is initially maintained by the battery converter at 400V. At 9 second solar insolation gets a step change to 0.9 kW/m^2, which changes the operating mode to Non-MPPT mode of operation as the PV MPPT power at this level of insolation is higher than that required. The dc link voltage is now maintained by the PV converter. At 17 seond, the solar insolation level comes down to 0.55 kW/m^2. The controller now again restores the DC link and moves into Non-MPPT mode of operation.

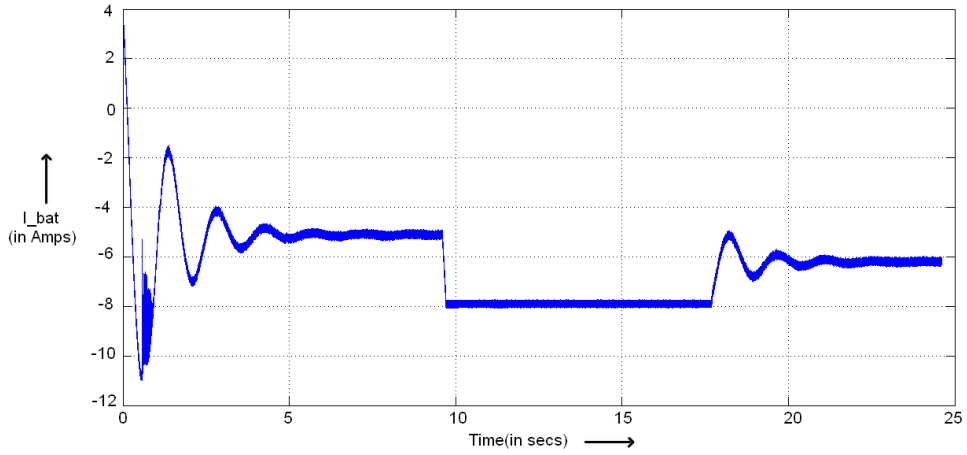

Fig. 6.27. Battery Current Variation under Solar Insolation Changes

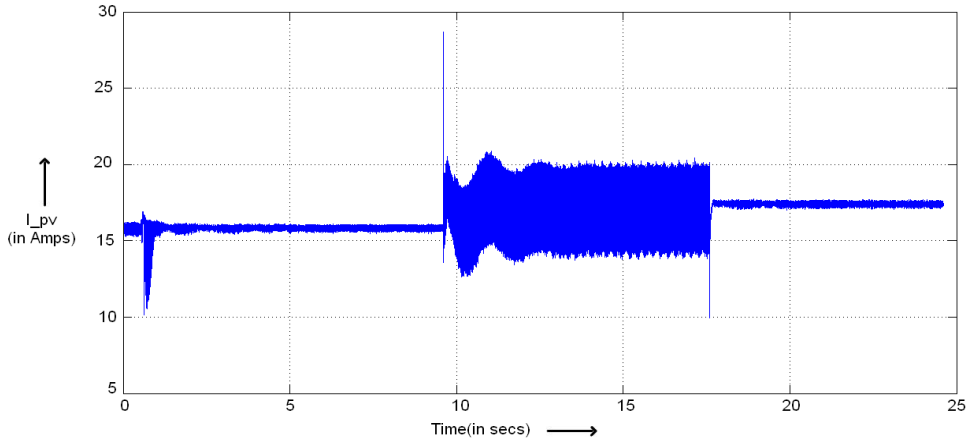

Fig. 6.28. PV Current Variation under Solar Insolation Changes

Initially, the battery converter was maintaining the dc link voltage by taking a charging current of 5A at MPPT mode. At 9 second, step change in solar insolation, causes the battery charging current to increase. As the battery charging current increases and hits the limit of 8A, the controller shifts the operating mode to Non-MPPT mode of operation. PV now supplies the power required to charge the battery with 8A current and supplies the power to maintain dc link. PV current now stabilizes at 16A. At 17 second, the solar insolation level falls to 0.55 kW/m^2, the controller now shifts to MPPT mode of operation as dc link voltage touches the limit of 380V. Battery now comes out of charging mode and now stabilizes at a lower charging current of 6A. PV converter now maintains the current at I_{mpp} = 17A.

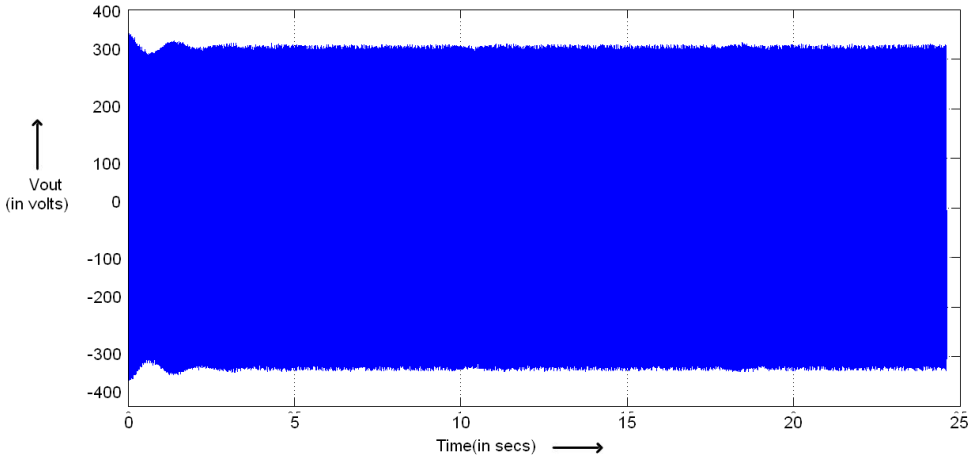

Fig. 6.29. Load Voltage Variation under Solar Insolation Changes

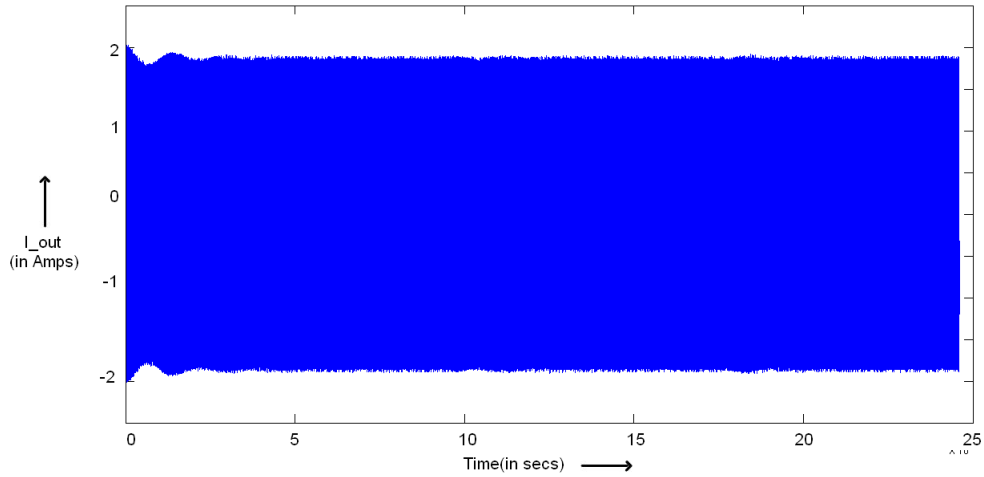

Fig. 6.30. Load Current variation under Solar Insolation Changes

The load voltage and load current variation under the changes in mode of operation are shown in Fig. 6.29 and Fig. 6.30. It can be observed that the load voltage variation is very marginal and is quickly restored by the d-q control action of the inverter, compared to the time required for restoration in DC link votage. Load current remains constant throughout as no change in load takes place.

6.2 Experimental Validation

Testing of the prototype is done with the PV simulator, a battery and connected loads. The PV simulator is set according to the solar model described in chapter 2. V_{oc} = 44 V, V_{mpp} = 36.5V. The simulator has a maximum current rating of 6.4 Amps. The I_{sc} and I_{mpp} are chosen as follows. I_{sc} = 6.2 Amps, I_{mpp} = 5.2 Amps.

6.2.1. Case 1: MPPT Mode of Operation

In this mode, PV is operated at MPPT and battery is given the responsibility to maintain the DC link voltage. The load connected takes around 70 watts for 230V ac voltage.

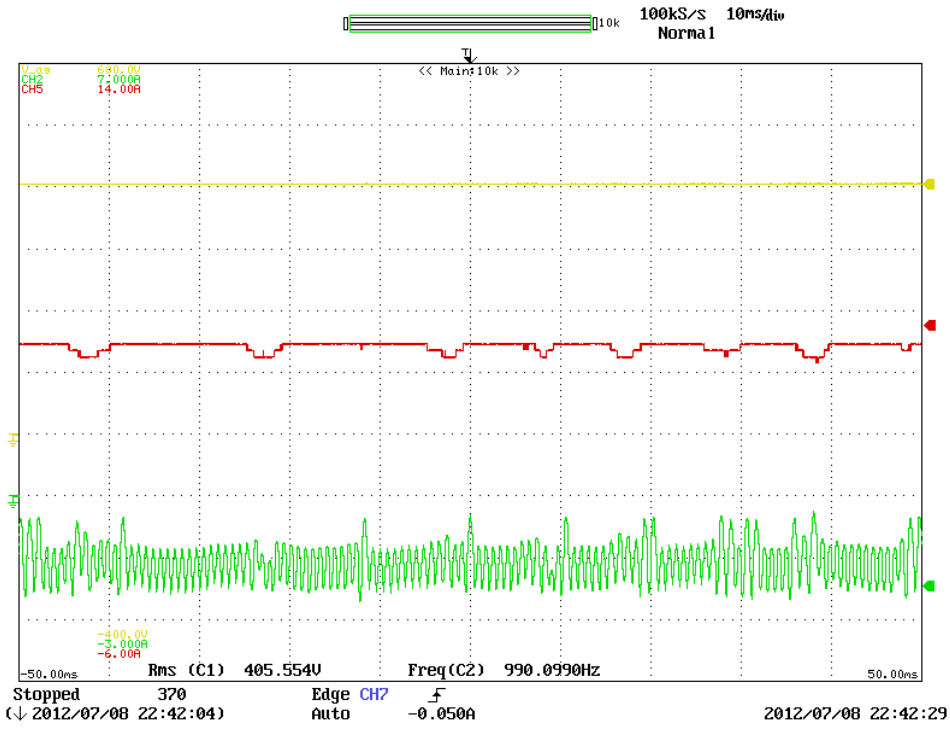

Fig. 6.31. Steady State Response of the proposed scheme. (TR:1) dc link voltage (V_{dc}; 100V/div). (TR:2) PV Current (I_{pv}; 2A/div). (TR:3) Battery Current (I_b; 1A/div). Time Scale: 10ms/div.

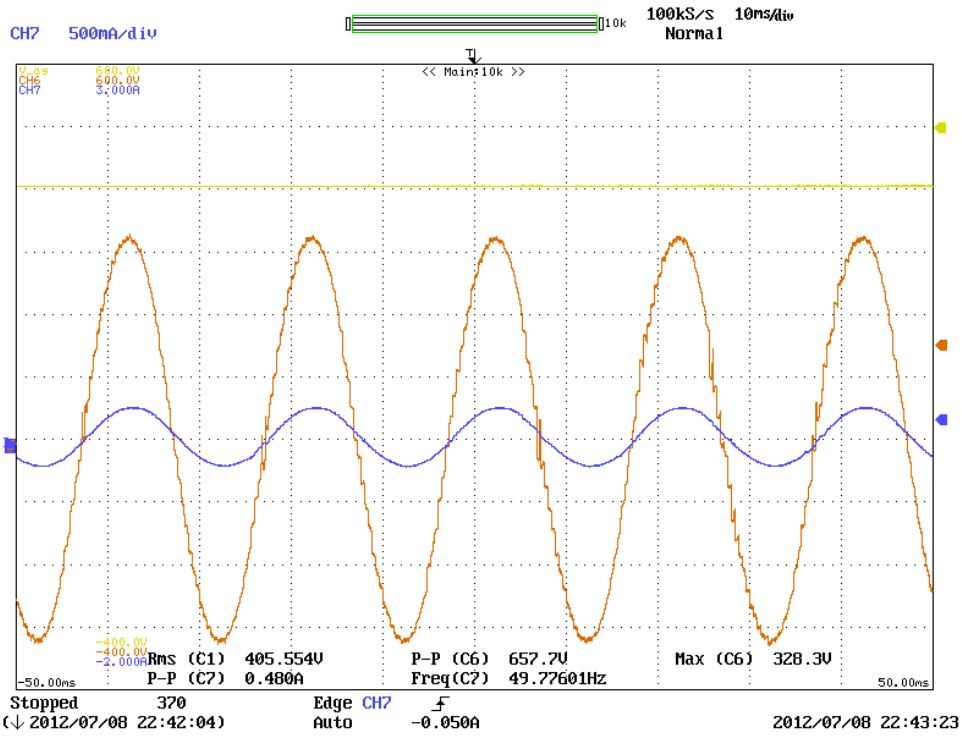

Fig.6.32. Steady State Response of the proposed scheme. (TR:1) dc link voltage (V_{dc}; 100V/div). (TR:2) Load Voltage (V_o; 100V/div). (TR:3) Load Current (I_o; 500mA/div). Time Scale: 10ms/div.

From the above figures, it can be observed that PV is operating at a current of 5.5A, which is its current Impp at maximum power point. The load connected takes 70 watts at 230V, 50Hz , while the battery controller which is maintaining the dc link voltage at 400V takes a charging current of around 1A as the power supplied by PV is higher than that required by the load.

6.2.2. Case 2: Step Change in Load in MPPT Mode of Operation

A step change in load of 50 watts takes place while PV is operating in MPPT mode as in case 1. As explained in chapter 4, battery which maintains the dc link voltage in MPPT mode, adjusts its current to maintain the dc link at MPPT. PV simulator is set same as in case 1. V_{oc} = 44 V, V_{mpp} = 36.5V. Each panel on the simulator has a maximum current rating of 6.2 Amps. The I_{sc} and I_{mpp} are chosen as I_{sc} = 6.2 Amps, I_{mpp} = 5.5 Amps.

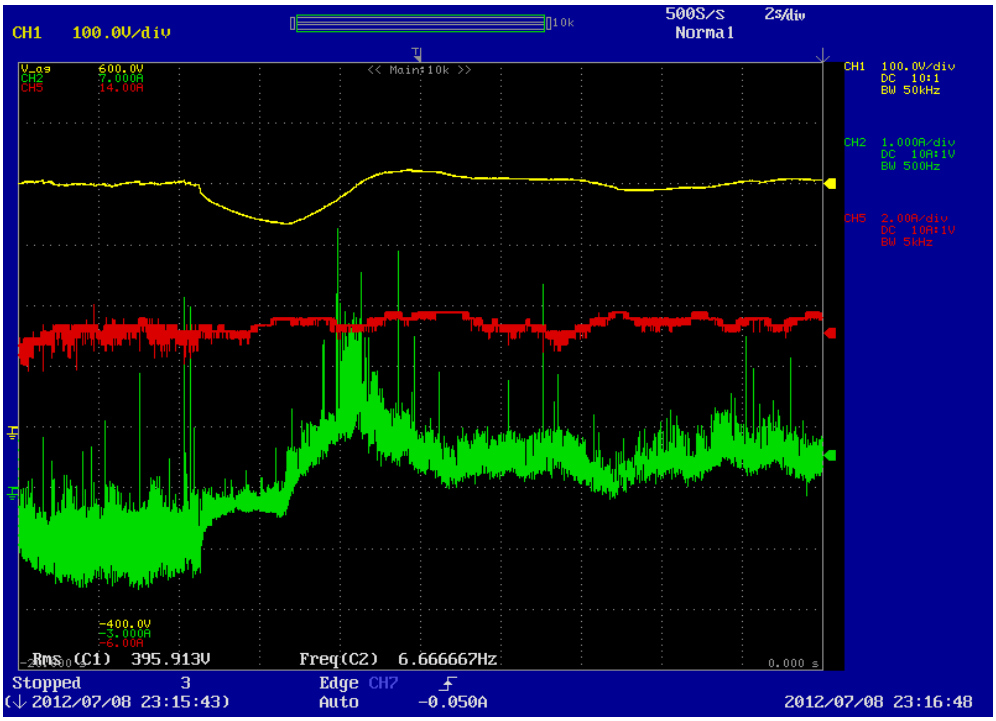

Fig.6.33. Response of the Scheme in MPPT Mode under Step Change in 50 watts of Load. (TR:1) dc link voltage (V_{dc}; 100V/div). (TR:2) PV Current (I_{pv}; 2A/div). (TR:3) Battery Current (I_o; 1A/div). Time Scale: 2s/div.

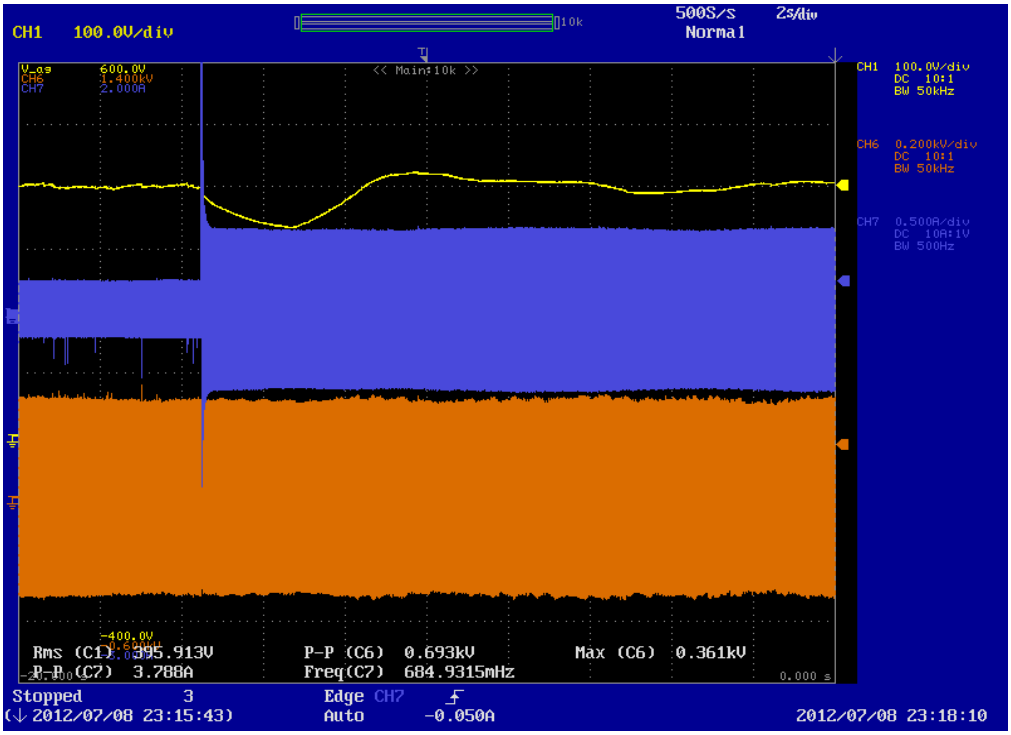

Fig.6.34. Response of the Scheme in MPPT Mode under Step Change in 50 watts of Load. (TR:1) dc link voltage (V_{dc}; 100V/div). (TR:2) Load Current (I_{pv}; 0.5A/div). (TR:3) Load Voltage (I_o; 200V/div). Time Scale: 2s/div.

From the above figures Fig 6.33 and Fig. 6.34, it can be observed that initially PV was operating at a current of 5.5A, which is its current I_{mpp} at maximum power point. The initial load connected takes 70 watts at 230V, 50Hz , When a step change in 50 watts of load takes place, the dc link voltage falls and the battery current ramps up to restore the dc link voltage(Fig. 6.33). The PV current remains undisturbed and continues operation at MPPT. The change in load voltage is less as the inverter control action is faster enough to adjust the load voltage to 325V(peak). The change in load current can also be seen from Fig. 6.34.

Now, the 50 watts of load is removed from the output and the dynamics are observed as shown below.

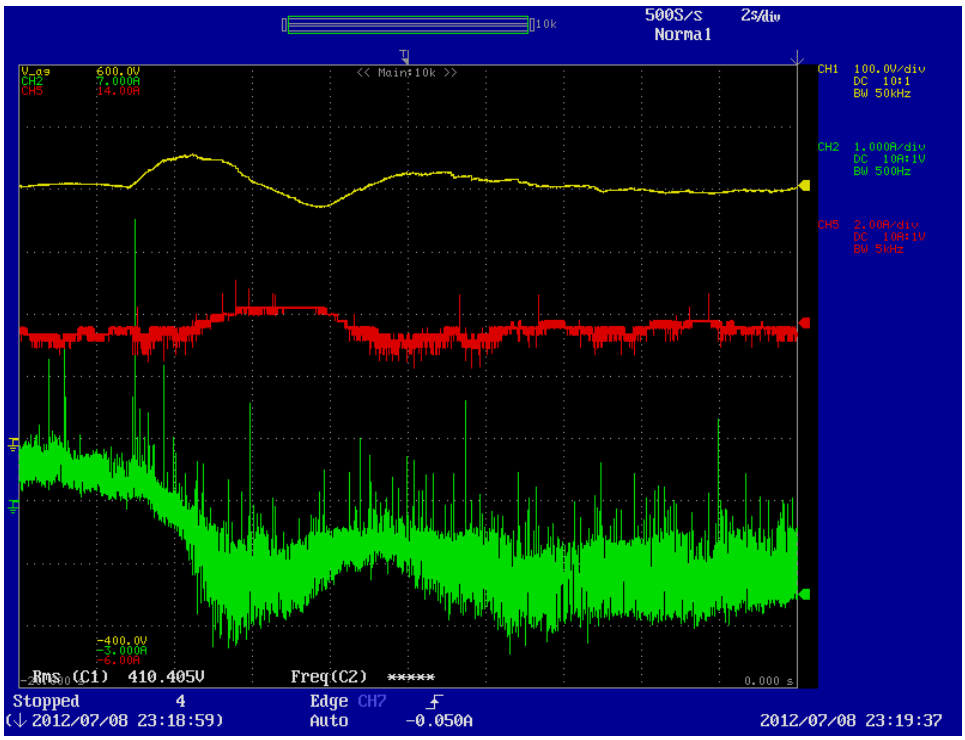

Fig.6.35. Response of the Scheme in MPPT Mode under Step Change in 50 watts of Load. (TR:1) dc link voltage (V_{dc}; 100V/div). (TR:2) PV Current (I_{pv}; 2A/div). (TR:3) Battery Current (I_o; 1A/div). Time Scale: 2s/div.

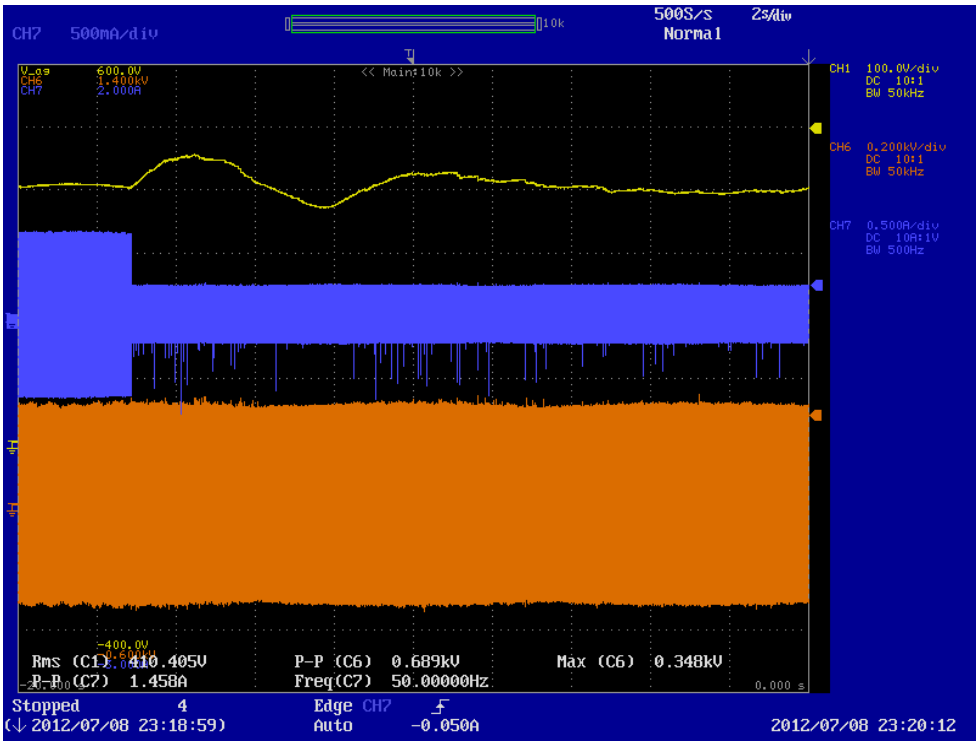

Fig.6.36. Response of the scheme in MPPT mode under Step Change in 50 Watts of Load. (TR:1) dc link voltage (V_{dc}; 100V/div). (TR:2) Load Current (I_{pv}; 0.5A/div). (TR:3) Load Voltage (I_o; 200V/div). Time Scale: 2s/div.

On removal of the 50 watts of load, the dc link voltage increases, but as battery controller is maintaining the dc link voltage, its current reference changes and it moves into charging mode as before. The PV current experiences some momentary disturbances but continues to operate in MPPT mode. The changes in load voltage and load current can be observed form Fig. 6.36. It can be observed that the battery controller is able to maintain the dc link voltage from the control actions mentioned in chapter 4. The output load voltage controller is also fast enough to maintain 230V(rms) at load terminal.

Next a change in 100 watts of load is realized and the dynamics of the controller are observed. The operating conditions of PV simulator, initial load all are kept unchanged.

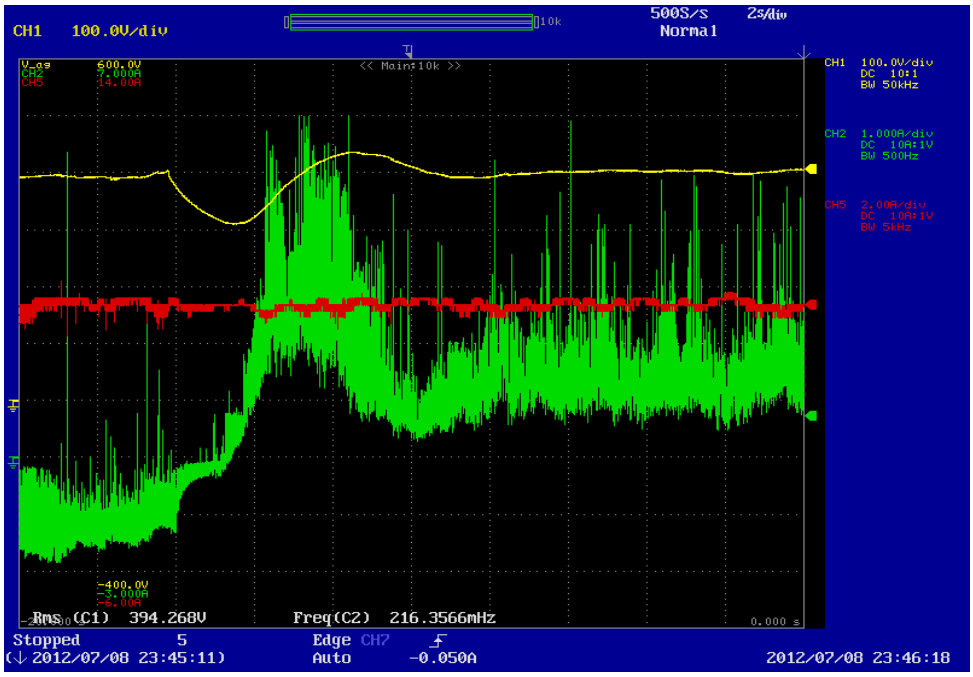

Fig.6.37. Response of the scheme in MPPT mode under step change in 100 watts of load. (TR:1) dc link voltage (V_{dc}; 100V/div). (TR:2) PV Current (I_{pv}; 2A/div). (TR:3) Battery Current (I_o; 1A/div). Time Scale: 2s/div.

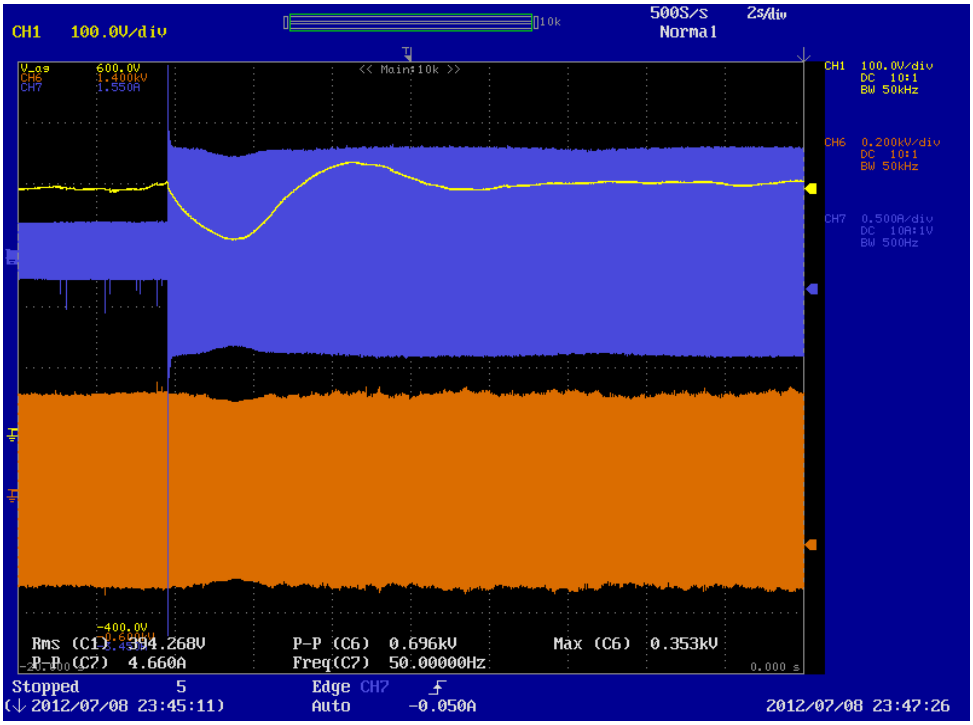

Fig.6.38. Response of the scheme in MPPT mode under step change in 100 watts of load. (TR:1) dc link voltage (V_{dc}; 100V/div). (TR:2) Load Current (I_{pv}; 0.5A/div). (TR:3) Load Voltage (I_o; 200V/div). Time Scale: 2s/div.

As can be observed from Fig. 6.37 and 6.38, the proposed scheme for MPPT mode of operation is robust enough to handle a change in 100W of load. The battery controller acts in a robust manner to restore the dc link voltage to 400V under high value of load changes. Next, the 100W of load is now removed to observe the dynamics.

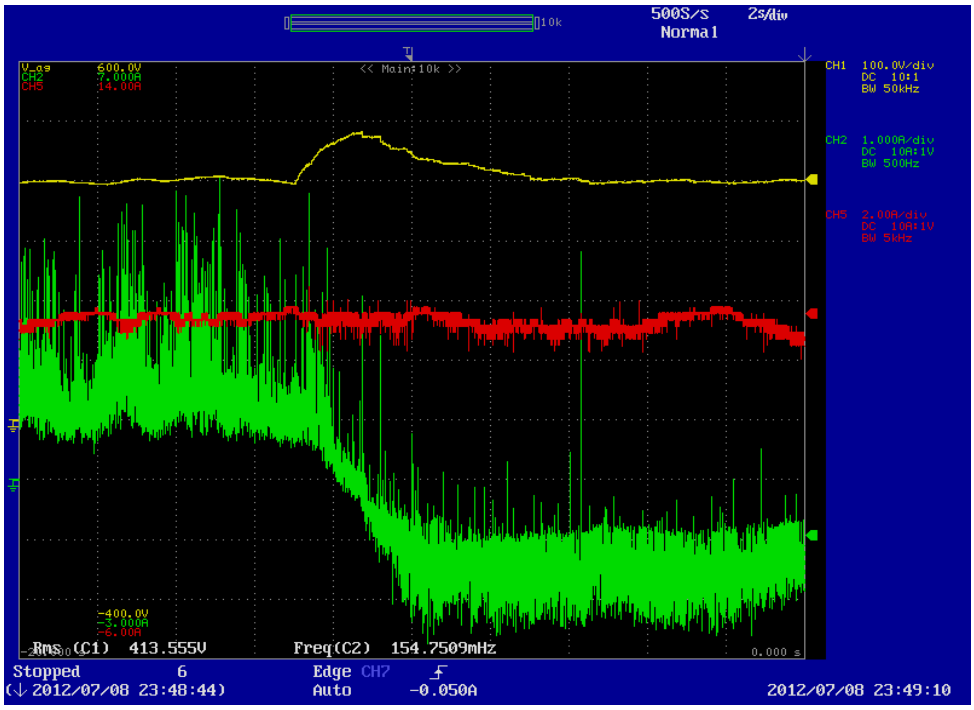

Fig.6.39. Response of the scheme in MPPT mode under step change in 100 watts of load. (TR:1) dc link voltage (V_{dc}; 100V/div). (TR:2) PV Current (I_{pv}; 2A/div). (TR:3) Battery Current (I_o; 1A/div). Time Scale: 2s/div.

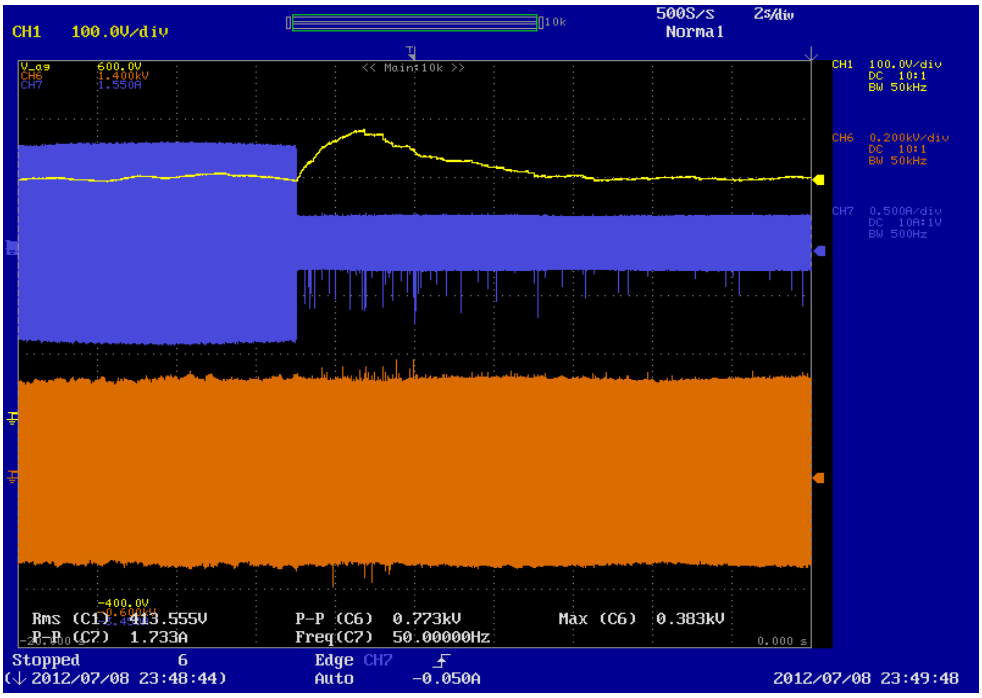

Fig.6.40. Response of the scheme in MPPT mode under step change in 100 watts of load. (TR:1) dc link voltage (V_{dc}; 100V/div). (TR:2) Load Current (I_{pv}; 0.5A/div). (TR:3) Load Voltage (I_o; 200V/div). Time Scale: 2s/div.

As can be seen in Fig. 6.39, the step change in load by removing the 100W of load causes an increment in dc link voltage, which causes the battery current reference to fall and eventually the battery takes a charging current to stabilize the dc link voltage. From Fig 6.40, the changes in dc link voltage and load current are observed.

6.2.3. Case 3: Non-MPPT Mode of Operation

In this mode of operation, PV operates at some point other than MPPT, not delivering maximum power. In this mode, the dc link is controlled by the PV converter as explained in chapter 4. The battery is charged with a constant current. PV in this mode of operation supplies both the power required for the load and for charging the battery. Each panel on the simulator has a maximum current rating of 6.2 Amps. Two panels are connected in parallel to give current rating of I_{sc} and I_{mpp} as follows I_{sc} = 12.4A, I_{mpp} = 11A. The battery charging current reference is taken as 1.25A. The load connected takes around 70 watts of power at 230V rms voltage. First, the operation of the scheme under constant load condition is observed and then load changes are taken place to observe the dynamics of the controller.

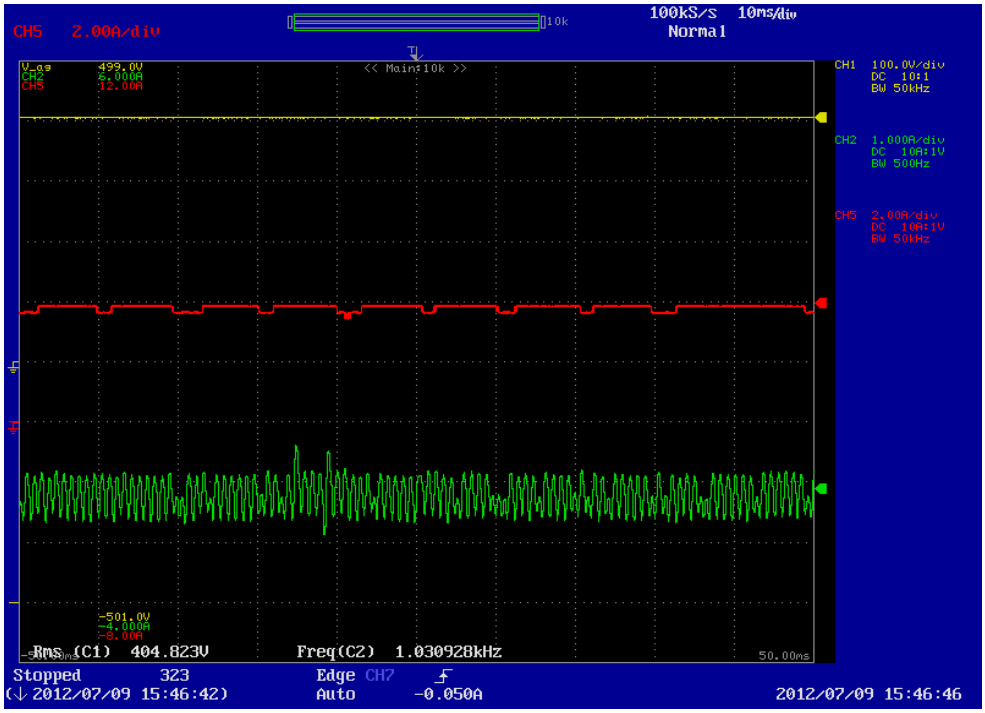

Fig.6.41. Response of the scheme in Non-MPPT mode. (TR:1) dc link voltage (V_{dc}; 100V/div). (TR:2) PV Current (I_{pv}; 2A/div). (TR:3) Battery Current (I_o; 1A/div). Time Scale: 10ms/div.

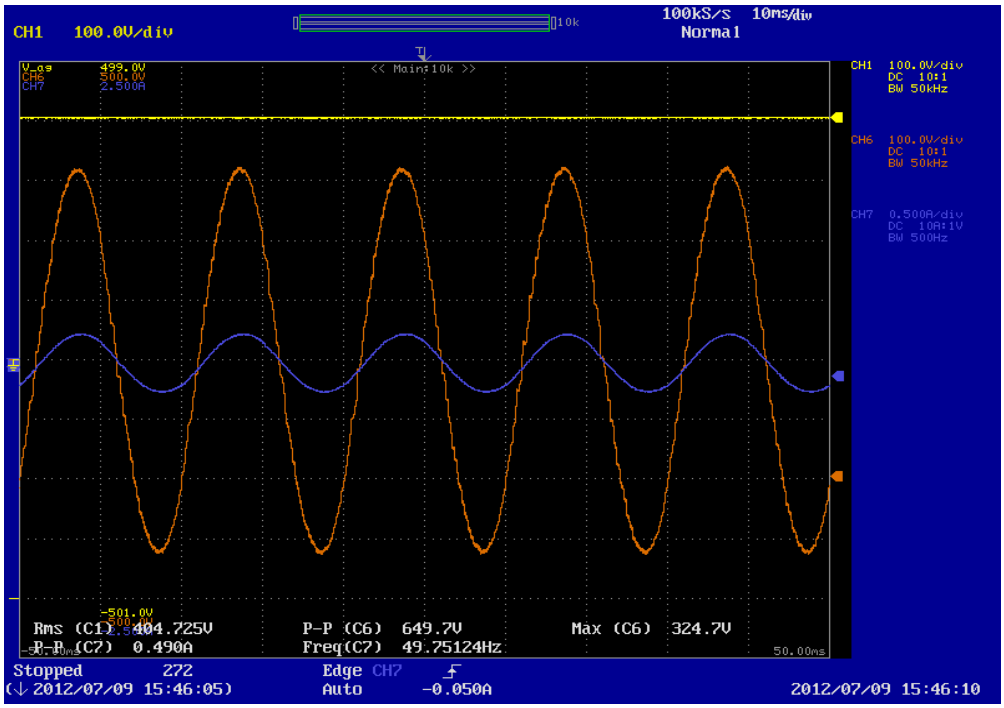

Fig.6.42. Response of the scheme in Non-MPPT mode. (TR:1) dc link voltage (V_{dc}; 100V/div). (TR:2) Load Voltage (V_o; 2A/div). (TR:3) Load Current (I_o; 500mA/div). Time Scale: 10ms/div.

From the figure it can be observed that the PV current and battery charging current are maintained at 3.9A and 1.25A. PV converter is maintaining the load demand and the power required to charge the battery. The load voltage waveform is maintained sinusoidal by the inverter and filter.

6.2.4. Case 4: Step Change in Load in Non-MPPT Mode of Operation

A step change in load of 50 watts takes place while PV is operating in Non-MPPT mode. As explained in chapter 4, in Non-MPPT mode PV maintains the dc link voltage in Non-MPPT mode, adjusts its current to maintain the dc link. PV simulator is set same as in case 3. Two panels are connected in parallel to give current rating of I_{sc} and I_{mpp} as follows I_{sc} = 12.4A, I_{mpp} = 11A. The battery charging current reference is taken as 1.25A. The initial load connected takes around 70 watts of power at 230V rms voltage. The dynamics of the system are observed after the load change takes place.

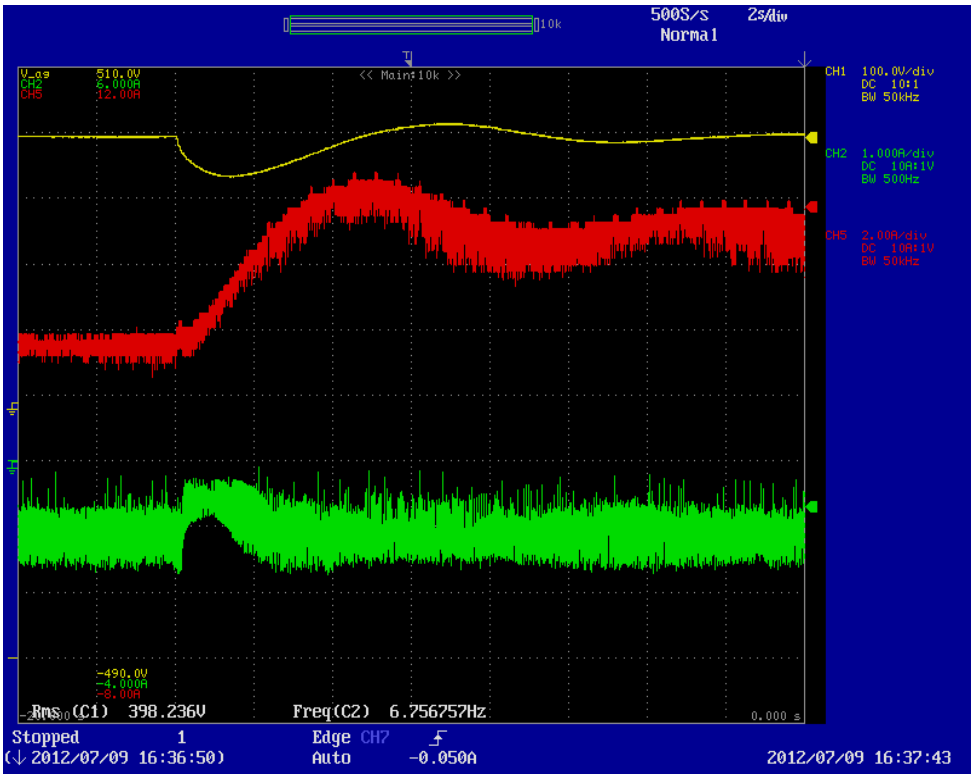

Fig.6.43. Response of the scheme in Non-MPPT mode under step change in 50 watts of load. (TR:1) dc link voltage (V_{dc}; 100V/div). (TR:2) PV Current (I_{pv}; 2A/div). (TR:3) Battery Current (I_o; 1A/div). Time Scale: 2s/div.

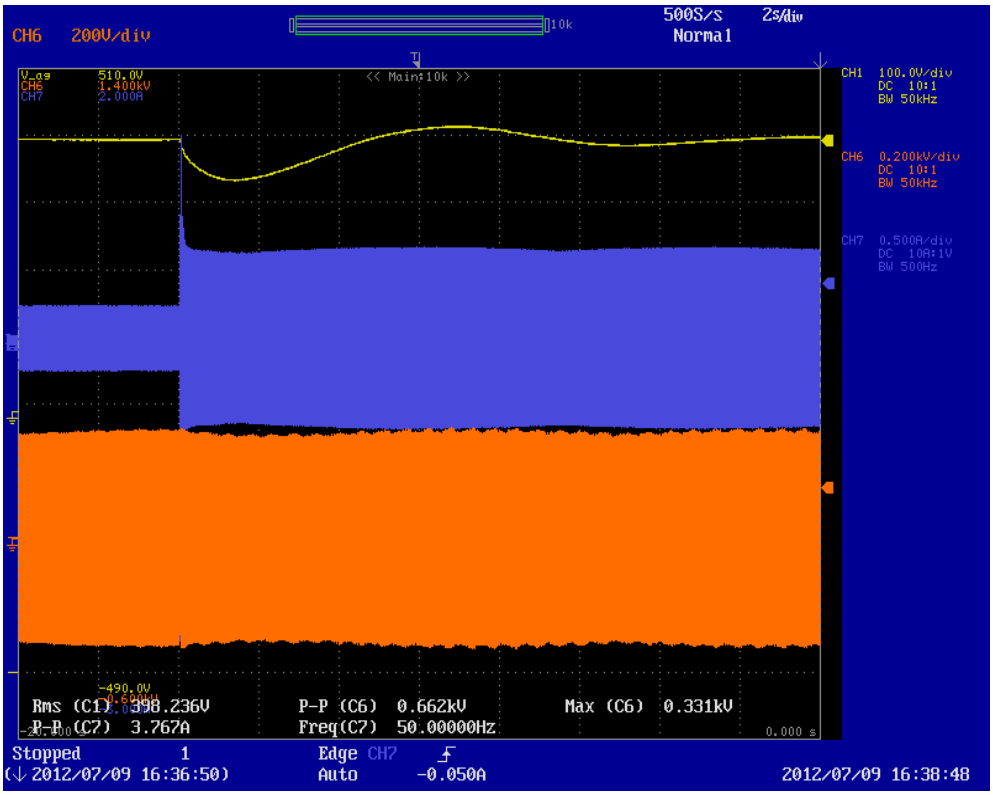

Fig.6.44. Response of the scheme in Non-MPPT mode under step change in 50 watts of load. (TR:1) dc link voltage (V_{dc}; 100V/div). (TR:2) Load Current (I_{pv}; 0.5A/div). (TR:3) Load Voltage (I_o; 200V/div). Time Scale: 2s/div.

From the above figures Fig 6.43 and Fig. 6.44, it can be observed that initially PV was operating at a current of 4A. The initial load connected takes 70 watts at 230V, 50Hz , When a step change in 50 watts of load takes place, the dc link voltage falls and the PV current increases to restore the dc link voltage(Fig. 6.43). The Battery current experiences momentary disturbance and continues charging at a current of 1.25A. The change in load voltage is less as the inverter control action is faster enough to adjust the load voltage to 325V(peak). The change in load current can also be seen from Fig. 6.44. Next, the 50 watts of load is withdrawn and the dynamics of the system are observed.

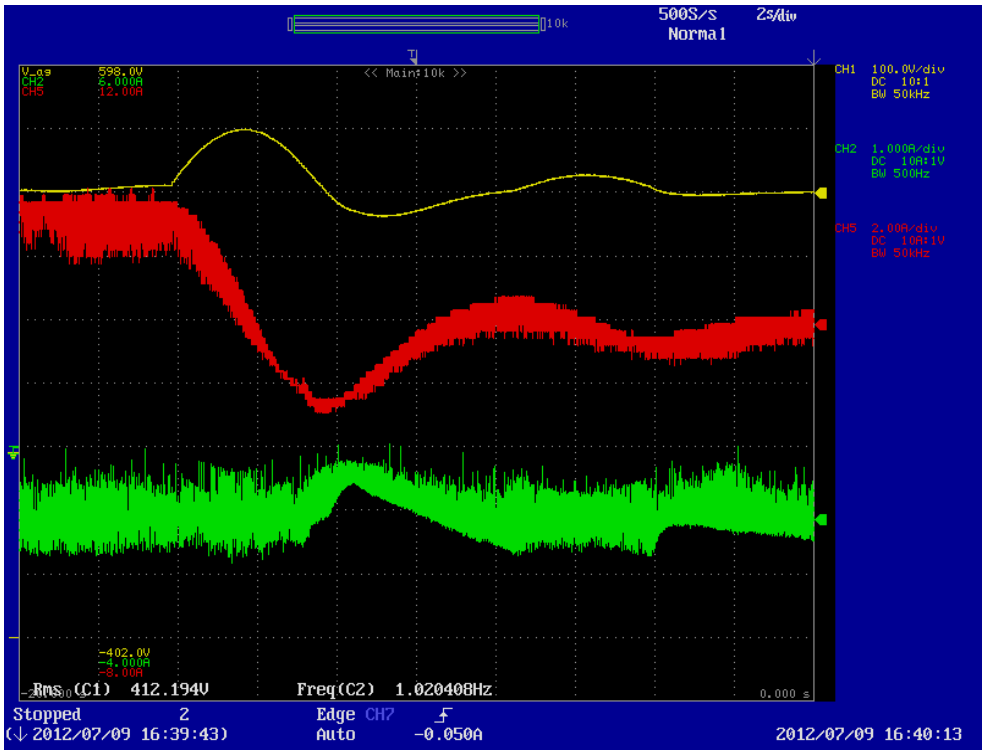

Fig.6.45. Response of the scheme in Non-MPPT mode under step change in 50 watts of load. (TR:1) dc link voltage (V_{dc}; 100V/div). (TR:2) PV Current (I_{pv}; 2A/div). (TR:3) Battery Current (I_o; 1A/div). Time Scale: 2s/div.

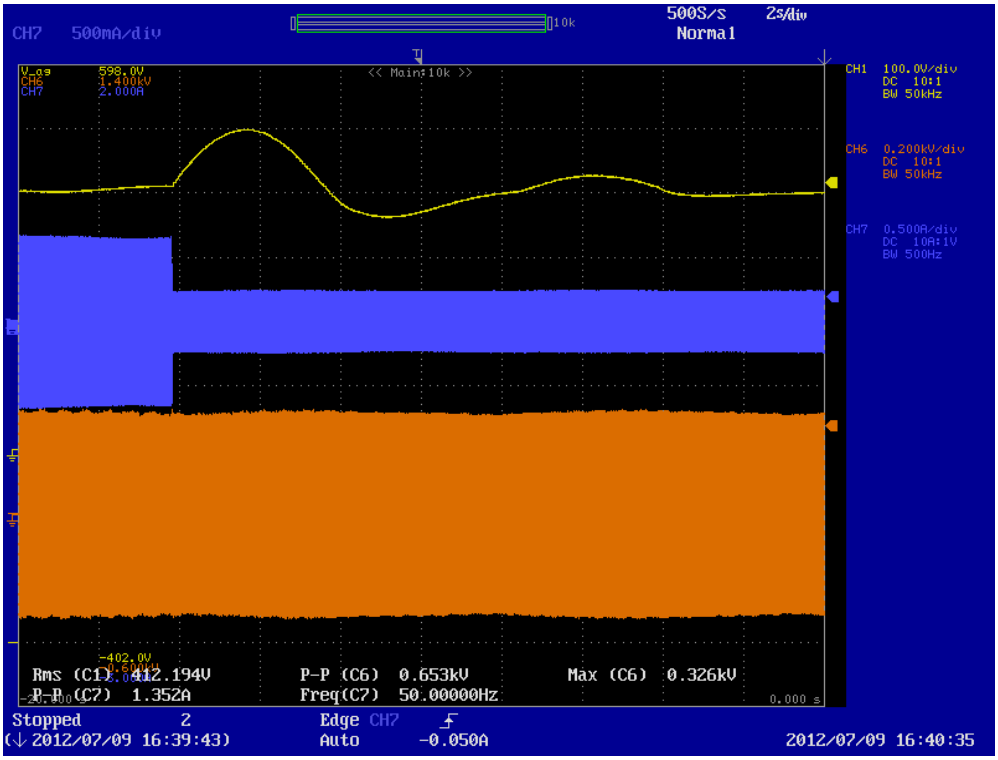

Fig.6.46. Response of the scheme in Non-MPPT mode under step change in 50 watts of load. (TR:1) dc link voltage (V_{dc}; 100V/div). (TR:2) Load Current (I_{pv}; 0.5A/div). (TR:3) Load Voltage (I_o; 200V/div). Time Scale: 2s/div.

From the above figures Fig 6.45 and Fig. 6.46, it can be observed that initially PV was operating at a current of 7A. When the 50 watts of load is removed, the dc link voltage swells up and the PV current decreases to restore the dc link voltage(Fig. 6.45). The Battery current experiences momentary disturbance and continues charging at a current of 1.25A. The change in load voltage is less as the inverter control action is faster enough to adjust the load voltage to 325V(peak). The change in load current can also be seen from Fig. 6.46.

Chapter 7
Conclusion and Future Work

7.1 Conclusions

The task of this master thesis is to develop a reliable, efficient and reduced stage configuration for PV based stand alone power generating unit with a control method for the proposed configuration. From the above chapters and from the results of the simulation and experimental studies, it can be observed that the proposed configuration, with some reduction in the number of controlled switches and the control method, has the ability to operate successfully under different operating conditions. In MPPT mode of operation, the half bridge boost converter has the ability to operate the PV at MPPT successfully while the battery converter is capable of responding quickly to maintain the dc link voltage. In non-MPPT mode of operation, the battery converter charges the battery with a constant current while PV maintains the load demand by maintaining the dc link voltage and by supplying the power necessary to charge the battery with a constant current. The control method proposed has successfully performed under various load change and solar insolation level changes. Observation of these results depict that the control method is robust enough to maintain the dc link voltage for the inverter while controlling the battery charging/discharging in a reliable manner. From the ananlysis of the hardware results, calculated efficiency of the system is found to be around 70% from the primary test results of the experimental studies.

7.2 Future Work

There are some areas of improvements which can be taken up as next few steps for this project. First of all, some improvement of efficiency in the hardware prototype is necessary. Calculations of power sharing and load demand reveal that most of the losses taking place are in the magnetic part of the prototype, transformers and high frequency inductors. Efficient designing of the high frequency transformer and inductors using soft magnetic material and low

resistive conductors, can be one of the important future tasks. Currently, hard switching technique for the IGBTs has been employed at operating frequency of 10 kHz. Secondly, reduction of switching frequency(down to 5 kHz), and soft switching techniques for the IGBTs can be implemented using ZVS or ZCS techniques, that can provide some improvement of efficiency. Thirdly, the control mechanism of shifting the operating mode between MPPT and Non_MPPT mode of operation also has to be implemented. Next, ripple in the battery current can also be minimized using smaller time steps. However, DSPs generally perform efficiently at a sampling rate of 50 μseconds. Hence, to improve the battery current ripple, implementation of analog control is also feasible. Another feasible scope is to use MOSFETs in place of IGBTs and determine the efficiency for the prototype developed.

References

[1] Hong Wang, Donglai Zhang, "*The Stand-alone PV Generation System with Parallel Battery Charger*",Electrical and Control Engineering(ICECE), 2010 International Conference, Publication Year: 2010, Page(s): 4450 – 4453.

[2] R. Gules, Pacheco De Pellegrin, H.L. Hey, J. Imhoff, "*A Maximum Power Point Tracking System with Parallell Connection for PV Stand Alone Applications*", IEEE Transactions on Industrial Electronics, Publication Year: 2008, Volume: 55, Issue: 7, Page(s): 2674 – 2683.

[3] D. B. Candido, J.R.R. Zientarski, R.C. Beltrame, J.R. Pinheiro, H.L. Hey, "*Implementation of a Stand Alone Photovoltaic System Based on Decentralized DC-DC Converters*", Brazilian Power Electronics Conference, 2009. COBEP'09. Publication year: 2009, Page(s): 2674 – 2683.

[4] Liu Shengyong, Zhang Xing, Guo Haibin, Xie Jun, "*Multiport DC/DC Converter for Stand-Alone Photovoltaic Lighting System with Battery Storage*", International Conference on Electrical and Control Engineering(ICECE), 2010. Publication Year: 2010, Page(s): 3894 – 3897.

[5] Chen Yaow-Ming, Liu Yuan-Chuan, Wu Feng-Yu, "*Multi-input DC/DC Converter Based on the Multiwinding Transformer for Renewable Energy Applications*", IEEE Transactions on Industry Applications, Publication year: 2002, Page(s): 1096 – 1104.

[6] M.J.V. Vazquez, J.M.A Marquez, F.S. Manzano, "*A Methodology for Optimizing Stand-Alone PV System Size Using Parallel Connected DC/DC converters*", IEEE Transactions on Industrial Electronics, Publication Year: 2008, Issue: 7, Pages(s): 2664 – 2673.

[7] R.O. Caceres, I. Barbi, "*A Boost DC–AC Converter: Analysis, Design, and Experimentation*", IEEE Transaction on Power Electronics, Publication Year: 1999, Vol: 14, Issue: 1, Page(s): 134 – 141.

[8] Fathy Khairy; Woo Lee Hyun; T. Mishima; M. Nakaokal, "*Boost-Half Bridge Single Power Stage PWM DC-DC Converter for Small Scale Fuel Cell Stack*", IEEE International Power and Energy Conference, 2006. PECon'06.Publication Year: 2006, Page(s): 426 – 431.

[9] F.Z. Peng, Li Hui, Su Gui-Jia, J.S. Lawler, "*A New ZVS Bidirectional DC–DC Converter for Fuel Cell and Battery Application*", IEEE Transaction on Power Electronics, Publication Year: 2004, Volume: 19, Issue: 1, Page(s): 54-65.

[10] Tsai Huan-Liang, Tu Ci-Siang, Su Yi-Jie, "*Development of Generalized Photovoltaic Module Using MATLAB/SIMULINK*", Proceedings of the World Congress on Engineering and Computer Science 2008, WCECS 2008, October 22 - 24, 2008, San Francisco, USA.

[11] J.A. Gow, C.D. Manning, "*Development of a photovoltaic array model for use in power-electronics simulation studies*", IEE Proceedings – Electric Power Applications, Publication Year: 1999, Volume: 146, Issue: 2, Page(s) 193 – 200.

[12] E.S. Sreeraj, Kishore Chatterjee, Santanu Bandyopadhyay, "*Design of isolated renewable hybrid power systems*", Solar Energy, Vol. 84, Issue 7, pp. 1124-1136, July 2010.

[13] Anna Mani, S. Rangarajan, "*Handbook of Solar Radiation over India*", Allied Pub. 1982.

[14] Dong Dong, "*Modeling and Control Design of a Bidirectional PWM Converter for Single-phase Energy Systems*", Thesis submitted to the Faculty of Virginia Polytechnic Institute and State University, May 6,2009.

[15] David Linden, Editor; Thomas B. Reddy, Editor, "*Handbook of Batteries*", McGraw-Hill Publication.

[16] Zhou Xuesong, Song Daichun, Ma Youjie, Cheng Deshu, "*The simulation and design for MPPT of PV system Based on Incremental Conductance Method*", Information Engineering (ICIE), 2010 WASE International Conference, Vol.2, Publication Year: 2010, Page(s) 314-317.

[17] *www.bpsolar.com*